

**Development and Mechanistic Studies of
Palladium-Catalyzed Ligand-Directed C–H Bond
Functionalization Reactions**

by

Kate Butler McMurtrey

A dissertation submitted in partial fulfillment
of the requirements for the degree of
Doctor of Philosophy
(Chemistry)
in the University of Michigan
2014

Doctoral Committee:

Professor Melanie S. Sanford, Chair
Assistant Professor Kenichi Kuroda
Associate Professor Anne J. McNeil
Professor John P. Wolfe

© Kate B. McMurtrey 2014

ACKNOWLEDGEMENTS

I am so blessed to have had the opportunity to come to the University of Michigan for my graduate studies and learn from so many talented and wonderful people. I knew very little about the chemistry world especially who the key people were and what I would enjoy studying. Therefore, I feel very fortunate to have been able to work for Melanie, where I have enjoyed the exceptional chemistry and hardworking people, especially Melanie herself. Your lab has been a place where I have not only been able to develop as a chemist but also feel included and encouraged. Your optimism is contagious and has helped to push me through challenging times. Your expectations helped me to be confident in myself as a chemist. I have learned to be an improved presenter, researcher, problem solver, teacher, writer, and thinker, as well as a better chemist over all. Melanie, your kindness and patience have been appreciated along the way, especially when I've lacked in knowledge and confidence. I have enjoyed teaching with you and have learned a lot from your example. Over the years, I have come to recognize your care of your students and truly wanting what is best for them. This is a rare characteristic among advisors, especially those as busy and successful as you are. Also, I am grateful for your acceptance and support with my unconventional last year of graduate school while being pregnant, having William, and writing my dissertation from afar. Thank you for assisting me as I try to take on too much! It hasn't been the easiest, but I am happy to be where I am today, thanks to the help from you, Melanie, and many others.

Next I would like to thank Dr. McCusker for his support on our photochemistry studies and allowing the use of his instruments and time through our collaboration. I would especially like to acknowledge Dani for her endless help as she taught me all I know about photochemistry including how to answer our questions and the experiments we would need to perform. She answered limitless questions and was there every step of

the way, even when I couldn't be there. Thank you for adding your excitement to the work. Science!

I would also like to thank my dissertation committee for their time and support as I have progressed throughout the years. Anne, thank you for letting me rotate in your group. I learned so much as I started off, awkwardly trying to balance graduate school life. You are always excited about good chemistry and cute babies too, so it's been fun to converse over our common interests. Professor Wolfe, thank you for all of your helpful suggestions over the years. Professor Kuroda, I appreciate all of your time as you've served on my committee, especially as my chemistry turned out to not be very materials related. I'd also like to thank Tracy Stevenson and Chris Peters who have dealt with our safety issues, especially fires, over the years. I'm grateful to others who keep the chemistry building and the department running smoothly Laurie MacDonald, Jon Boyd, Margarita Bekiares, and the many who have dealt with our chemical ordering issues.

I have enjoyed my time working with everyone in the Sanford Lab. Andrew, thank you for mentoring me even though my project was very different from yours. I knew so little and appreciated all you taught me during my first year at Michigan. Anna, thanks for being there by my side as we stressed about first year problems such as classes, rotations, and the pending doom of candidacy. Amanda Hickman, thank you for taking me in as I joined Club Palladium. You helped me to really feel connected in the lab as you taught me, encouraged me, helped me to not stress about graduate school pressures, and just talked with me about life. Joy, thanks for being my friend and not just my sister's. When I started, I loved coming to the lab and seeing a familiar face. I was happy I could really get to know you and your fun you had to share. Dipa, I am so grateful I was able to work on such an interesting project with you that I carried on after you left. Thank you for all you taught me and your patience with me. Amanda Cook, I'm so grateful for your friendship over the past two and a half years. Thank you for letting me share the details of my life and be part of yours as well. I appreciated being able to talk about chemistry and get your help with my many questions. Monica, Chelsea, Sharon, and Naoko, thank you for your help, encouragement, friendship, and always being there to talk. Sydonie, Zac, and Aakash, thank you for your hard work and

patience as I learned to be a better mentor. I'd like to give additional thanks to Naoko, Pablo, Amanda, and Dani for editing thesis chapters.

Also I want to thank a number of people from outside of Michigan who have helped me get to where I am today. I was fortunate to have talented teachers and professors, before coming to Michigan, who were instrumental in my scientific growth. Mr. Shelton, thank you for enjoyable chemistry classes and encouragement to excel in chemistry. Dr. Nerz, thank you for being inspiring, kind, and overall a great organic chemistry professor. Dr. Mallory, working in your lab was such a wonderful experience for me. My love for research started in your lab, and I learned so much from the research as well as in class. I am so grateful for that opportunity to study under you. Sally, thank you for your assistance in the lab, for all you taught me, and the continued friendship with both of you. Amber, thanks for studying orgo with me and for your continued friendship no matter the distance.

Finally, none of this would be possible without the love, support, and encouragement of my family—my sisters, Annie (and family) and Ellen, my parents, Wendy and Lee, my grandpa, Eliot, my husband, Mike, and many others. Annie, thank you for all the chemistry help along the way, including answering questions and proofreading. It's been fun and so convenient to have a sister in chemistry. Ellen, I'm happy you've gone with the family trend of loving chemistry. Mom and dad, thank you for all you've taught me and the encouragement you've given me to do great things. And thank you for teaching me how to be a hard worker and to do all I can do. Grandpa, thank you for letting me work with you and teaching me all along the way. Your love for reading, learning, working, thinking, and chemistry inspired me in all I do. Mike, thank you for your love, support, encouragement, and jokes that got me through the hard days. Thank you for making our time in Ann Arbor enjoyable and happy. My son, William, probably only hindered the process, but I love you more each day.

TABLE OF CONTENTS

ACKNOWLEDGEMENTS	ii
LIST OF SCHEMES	viii
LIST OF FIGURES	x
LIST OF TABLES	xiii
LIST OF ABBREVIATIONS	xiv
ABSTRACT	xvi
CHAPTER 1 Introduction	1
1.1 C–H Functionalization	1
1.2 Site-Selectivity for C–H Functionalization Reactions	3
1.3 Palladium Catalysis for C–H Functionalization Reactions	5
1.4 Challenges and Objective	7
1.5 References	10
CHAPTER 2 Palladium-Catalyzed C–H Fluorination using Nucleophilic Fluoride	11
2.1 Background and Significance	11
2.2 Reaction Optimization	17
2.3 Substrate Scope	20
2.4 Fluorination Using CsF	24
2.5 Rapid Fluorination for Positron Emission Tomography (PET)	25
2.6 Mechanistic Insights	26
2.7 Conclusions	30

2.8	Experimental Procedures and Characterization of Data.....	32
2.9	References	47
CHAPTER 3 Room-Temperature C–H Arylation by Palladium-Catalysis and Visible-Light Photocatalysis.....		49
3.1	Background and Significance.....	49
3.2	Reaction Optimization.....	56
3.3	Substrate Scope of 2-Arylpyridine Derivatives.....	60
3.4	Directing Group Scope	64
3.5	Scope of Aryldiazonium Salts.....	68
3.6	Background Reaction	72
3.7	Proposed Mechanism	73
3.8	Conclusions	75
3.9	Experimental Procedures and Characterization of Data.....	76
3.10	References	97
CHAPTER 4 Mechanistic Investigation of C–H Arylation with Diaryliodonium Salts by Palladium-Catalysis and Visible-Light Photocatalysis		99
4.1	Background and Significance.....	99
4.2	Methodology and Comparison	102
4.3	Radical Mechanism	107
4.4	Kinetic Studies	108
4.4.1	Hammett Studies.....	108
4.4.2	Kinetic Isotope Effect Studies	110
4.5	Stern-Volmer Quenching Studies.....	112
4.5.1	Time-Resolved Emission of [Ir] with [Ph ₂ I]BF ₄	116

4.5.2 Time-Resolved Emission of [Ir] with [Ar ₂ I]BF ₄	118
4.5.3 Time-Resolved Emission of [Ir] with Other Reaction Components.....	121
4.5.4 Transient Absorption	124
4.6 Conclusions	129
4.7 Experimental Procedures and Characterization of Data.....	131
4.8 References	139

LIST OF SCHEMES

Scheme 1.1. Example of Functional Group Interconversion.....	1
Scheme 1.2. C–H Activation and Functionalization by Transition Metal-Catalysis.....	3
Scheme 1.3. Intramolecular C–H Functionalization.....	4
Scheme 1.4. Transition Metal-Catalyzed Ligand-Directed C–H Functionalization.....	5
Scheme 1.5. Ligand-Direction Pd ^{II/IV} -Catalyzed C–H Functionalization Reaction	7
Scheme 1.6. Sequence for Nucleophilic Fluorination	8
Scheme 1.7. Arylation from Diazonium Salts via Photocatalysis	9
Scheme 2.1. General Reaction for Halex Process.....	12
Scheme 2.2. Balz-Schiemann Reaction	12
Scheme 2.3. Palladium Catalyzed Fluorination of Aryl Triflates by CsF	13
Scheme 2.4. Copper Mediated Fluorination of Aryltrifluoroborates by KF.....	13
Scheme 2.5. Pyridine Directed Catalytic C–H Fluorination with F ⁺ Reagent.....	15
Scheme 2.6. Triflamide Directed Catalytic C–H Fluorination with F ⁺ Reagent	15
Scheme 2.7. Pd-Catalyzed C-H Fluorination with F ⁺ Reagents	15
Scheme 2.8. Proposed Sequence for Nucleophilic Fluorination.....	17
Scheme 2.9. Alkene Aminofluorination with Oxidant and Fluoride Source	17
Scheme 2.10. Control Reactions for the Fluorination of 8-Methylquinoline	20
Scheme 2.11. Acetoxyated product present as additional side product	24
Scheme 2.12. Fluorination of 8-Methylquinoline with CsF as Fluoride Source	25
Scheme 2.13. Two Possible routes to 24 from 25 , AgF, and ArI(OPiv) ₂	27
Scheme 2.14. Testing <i>p</i> -MeC ₆ H ₄ IF ₂ as a Fluorinated Reagent in the Fluorination of 8-Methylquinoline.....	30
Scheme 2.15. Recent Transition Metal Catalyzed Nucleophilic C–H Fluorination Methods.....	31
Scheme 2.16. Recent Methods of Copper Catalyzed/Mediated Nucleophilic Fluorination of ArX.....	32

Scheme 3.1. Pd- and Ni-Catalyzed Cross-Coupling Reactions to form Aryl-Aryl Bonds	50
Scheme 3.2. Metal-Catalyzed Direct C–H Arylation to form Aryl-Aryl Bonds	50
Scheme 3.3. Intramolecular C–H Arylation to Form Dibenzofurans	52
Scheme 3.4. Phenol Directed Intermolecular C–H Arylation of 2-Phenylphenol	52
Scheme 3.5. Palladium-Catalyzed C–H Arylation with Diaryliodonium Salts	53
Scheme 3.6. Rate Determining Step of Pd-Catalyzed C-H Arylation with Ar_2I^+	53
Scheme 3.7. Pd-Catalyzed C–H Arylation by Decarboxylation of Dibenzoylperoxide...	54
Scheme 3.8. $\text{Ru}(\text{bpy})_3\text{Cl}_2$ -Photocatalyzed Pschorr Reaction	55
Scheme 3.9. Proposed Scheme for Arylation from Diazonium Salts via Photocatalysis.	55
Scheme 3.10. Reactions to Probe the Role of Silver in the Photocatalyzed Phenylation Reaction	59
Scheme 3.11. Synthesis of Aryl Diazonium Salts from Aniline Derivatives	70
Scheme 3.12. Background Reaction with Electron-Deficient Aryldiazonium Salts	72
Scheme 3.13. Experiment to Probe for Radical Chain Mechanism.....	75
Scheme 4.1. Pd-Catalyzed C–H Arylation with Diaryliodonium Salts via Photocatalysis	102
Scheme 4.2. Experiment to Probe for Radical Chain Mechanism.....	108
Scheme 4.3. Intramolecular Kinetic Isotope Effect Study of 43	110
Scheme 4.4. Rates Kinetic Isotope Effect Study of 42	111
Scheme 4.5. Proposed Mechanistic Step Studied using Transient Absorption Spectroscopy	124

LIST OF FIGURES

Figure 1.1. Homolytic and Heterolytic Bond Strengths for C–H Bonds.....	2
Figure 1.2. Lipitor Contains Many Unique Hydrogen Bonds	3
Figure 1.3. C–H Activation Mechanisms of Pd ^{II} versus Ir ^I	6
Figure 1.4. Ligand Directed High-Valent Pd-Catalyzed C–H Functionalization Examples (Bold Bonds Formed via Pd ^{II/IV} -Catalyzed C–H Functionalization)	7
Figure 1.5. Proposed Catalytic Cycle for the Pd-/Ir-Catalyzed C–H Arylation Reaction..	9
Figure 2.1. Examples of Fluorine in Pharmaceuticals	11
Figure 2.2. Prices for Commercial Fluorine Sources (based on largest quantity available from Sigma Aldrich in >95% purity).....	16
Figure 2.3. Oxidants Screen for the Fluorination of 8-Methylquinoline	19
Figure 2.4. Substrates Screened That Provided <5% Yield of Fluorinated Product by GC	23
Figure 2.5. Reaction of Iodotoluene Dipivalate with AgF observation by ¹⁹ F NMR.....	28
Figure 2.6. ¹³ C NMR and Proposed Components of Prestirred Reaction Mixture.....	29
Figure 3.1. Examples of the Biaryl Motif in Bioactive Molecules.....	49
Figure 3.2. Common Mechanisms for Pd-Catalyzed C–H Arylation Reactions.....	51
Figure 3.3. Proposed Mechanism for the Photocatalyzed Pschorr Reaction through an Oxidative Quenching Cycle.....	55
Figure 3.4. Aryl Diazonium Salts that were Ineffective Arylating Coupling Partners.....	70
Figure 3.5. Possible Pd ^{II/IV} Mechanism for the Pd/Ru-Catalyzed C–H Arylation Reaction	73
Figure 3.6. Alternative Pd ^{II/IV} Mechanism for the Pd/Ru-Catalyzed C–H Arylation Reaction	74
Figure 3.7. Alternative Pd ^{I/III} Mechanism for the Pd/Ru-Catalyzed C–H Arylation Reaction	74
Figure 4.1. General Reductive and Oxidative Quenching Cycles for Photocatalyst.....	99

Figure 4.2. Proposed Catalytic Cycle for the Pd-/Ir-Catalyzed C–H Arylation Reaction	101
Figure 4.3. Hammett Plot of Competition Study with $[\text{Ph}_2\text{I}]\text{BF}_4$ and $[\text{Ar}_2\text{I}]\text{BF}_4$	109
Figure 4.4. Rate Plot for Substrate 42	111
Figure 4.5. Rate Plot for Substrate 44	112
Figure 4.6. Absorption and Emission Spectra of $[\text{Ir}(\text{ppy})_2(\text{dtbbpy})]\text{PF}_6$	113
Figure 4.7. Oxidative and Reductive Quenching Cycles for $[\text{Ir}^{\text{III}}(\text{ppy})_2(\text{dtbbpy})]^{+a}$	114
Figure 4.8. Jablonski Diagram for Transition Metal Complexes.....	115
Figure 4.9. Possible Decay Routes for $[\text{Ir}(\text{ppy})_2(\text{dtbbpy})]^{+*}$	115
Figure 4.10. Basic Layout for Time-Resolved Emission Spectroscopy	116
Figure 4.11. Example of Kinetic Trace as Collected by Time-Resolved Emission	116
Figure 4.12. Time-Resolved Emission Traces of $[\text{Ir}(\text{ppy})_2(\text{dtbbpy})]\text{PF}_6$ with and without $[\text{Ph}_2\text{I}]\text{BF}_4$ in MeOH	117
Figure 4.13. Stern-Volmer Plot for the Quenching of the Excited State of $[\text{Ir}(\text{ppy})_2(\text{dtbbpy})]\text{PF}_6$ with $[\text{Ph}_2\text{I}]\text{BF}_4$	118
Figure 4.14. Stern-Volmer Plot for the Quenching of the Excited State of $[\text{Ir}(\text{ppy})_2(\text{dtbbpy})]\text{PF}_6$ with $[(p\text{-MeOC}_6\text{H}_4)_2\text{I}]\text{BF}_4$	119
Figure 4.15. Stern-Volmer Plot for the Quenching of the Excited State of $[\text{Ir}(\text{ppy})_2(\text{dtbbpy})]\text{PF}_6$ with $[(p\text{-ClC}_6\text{H}_4)_2\text{I}]\text{BF}_4$	119
Figure 4.16. Stern-Volmer Plot for the Quenching of the Excited State of $[\text{Ir}(\text{ppy})_2(\text{dtbbpy})]\text{PF}_6$ with $[(p\text{-CF}_3\text{C}_6\text{H}_4)_2\text{I}]\text{BF}_4$	120
Figure 4.17. Hammett Plot of k_q of Diaryliodonium Salts	121
Figure 4.18. Pd-Dimer 45 as a Substitute for C–H Activated Intermediate 1	122
Figure 4.19. Time-Resolved Emission Traces of $[\text{Ir}(\text{ppy})_2(\text{dtbbpy})]\text{PF}_6$ with and without $\text{Pd}(\text{OAc})_2$ in MeOH.....	123
Figure 4.20. Time-Resolved Emission Traces of $[\text{Ir}(\text{ppy})_2(\text{dtbbpy})]\text{PF}_6$ with and without Pd-Dimer 45 in MeOH.....	123
Figure 4.21. General Setup for Transient Absorption Spectroscopy	124
Figure 4.22. Spectroelectrochemistry of $[\text{Ir}(\text{ppy})_2(\text{dtbbpy})]\text{PF}_6$	125
Figure 4.23. Transient Absorption of $[\text{Ir}(\text{ppy})_2(\text{dtbbpy})]\text{PF}_6$ probing at 385 nm	126

Figure 4.24. Transient Absorption of [Ir(ppy) ₂ (dtbbpy)]PF ₆ with [Ph ₂ I]BF ₄ probing at 385 nm	127
Figure 4.25. Transient Absorption of [Ir(ppy) ₂ (dtbbpy)]PF ₆ probing at 460 nm	128
Figure 4.26. Transient Absorption of [Ir(ppy) ₂ (dtbbpy)]PF ₆ with [Ph ₂ I]BF ₄ probing at 460 nm	128
Figure 4.27. Proposed Catalytic Cycle for the Pd-/Ir-Catalyzed C–H Arylation Reaction	130
Figure 4.28. Alternative Pd ^{II/IV} Mechanism for the Pd/Ir-Catalyzed C–H Arylation Reaction	131
Figure 4.29. Alternative Pd ^{I/III} Mechanism for the Pd/Ir-Catalyzed C–H Arylation Reaction	131

LIST OF TABLES

Table 2.1. Optimization of C–H Fluorination with $\text{PhI}(\text{O}_2\text{CR})_2/\text{AgF}$	18
Table 2.2. Substrate Scope for the C–H Fluorination of 8-Methylquinoline Derivatives	21
Table 2.3. C–H Oxygenation Side Products for the Fluorination of 8-Methylquinoline Derivatives	22
Table 2.4. Fluoride Salt Screen to Replace AgF.....	25
Table 2.5 Rapid Fluorination at Multiple Temperatures for PET Imaging	26
Table 3.1. Optimization of the Phenylation Reaction Between 2 and $[\text{PhN}_2]\text{BF}_4$	57
Table 3.2. Silver Salts as Additives for the Phenylation Reaction Between 5 and $[\text{PhN}_2]\text{BF}_4$	58
Table 3.3. Control reactions for the Phenylation Reaction Between 2 and $[\text{PhN}_2]\text{BF}_4$	59
Table 3.4. Substrate Scope of the Pd/Ru-Catalyzed C–H Arylation of 2-Arylpyridine Derivatives	61
Table 3.5. Control Reactions for the Substrate Scope of the C–H Arylation of 2-Arylpyridine Derivatives	63
Table 3.6. Scope of Directing Group for the Pd/Ru-Catalyzed C–H Arylation	65
Table 3.7. Controls Reactions for the Scope of Directing Group for the C–H Arylation	67
Table 3.8. Scope of Aryldiazonium Salts for the Pd/Ru Catalyzed C–H Arylation.....	69
Table 3.9. Control Reactions for the Scope of Aryldiazonium Salts for the C–H Arylation	71
Table 4.1. Comparison of Pd/Ir-Catalyzed C–H Phenylation with Ph_2I^+ vs Pd/Ru-Catalyzed C–H Phenylation with PhN_2^+	103
Table 4.2. Substrate Scope for the Pd-/Ir-Catalyzed C-H Phenylation Reaction with Ph_2I^+	104
Table 4.3. Scope of Ar_2I^+ Salts for the Pd-/Ir-Catalyzed C–H Arylation of 4	106
Table 4.4. Addition of Radical Scavengers on the Pd-/Ir-Catalyzed C–H Arylation of 20	107

LIST OF ABBREVIATIONS

acac	acetylacetonate
Ar	aryl
^t Bu	<i>tert</i> -butyl
BDE	bond dissociation energies
bpy	bipyridine
dtbbpy	di- <i>tert</i> -butylbipyridine
DMA	dimethylacetamide
ΔG_{et}^0	change in energy of electron transfer
GC	gas chromatography
k_q	rate constant for quenching
L	ligand
Me	methyl
MLCT	metal to ligand charge transfer
NMR	nuclear magnetic resonance
Nu	nucleophile
[O]	oxidant
OAc	acetate or CH ₃ COO
OPiv	pivalate
OTf	trifluoromethanesulfonate or CF ₃ SO ₃
PC	photocatalyst
Ph	phenyl
ppm	parts per million
ppy	phenylpyridine
Q	quencher
rt	room temperature (~25 °C)

TA	transient absorption
TBAPF ₆	tetrabutylammonium hexafluorophosphate
TEMPO	(2,2,6,6-tetramethylpiperidin-1-yl)oxy
TFA	trifluoroacetate
TRE	time-resolved emission

ABSTRACT

C–H bonds are abundant in organic molecules and have great potential to be utilized as starting materials for the functionalization of many pharmaceuticals and natural products. With the use of Pd-catalysts these typically inert bonds can be activated and transformed into diverse functional groups and more complex products. Substrates with coordinating ligands can direct activation/functionalization to a specific C–H bond and help to overcome issues of site-selectivity. However, many functionalization reactions require high temperatures and forcing reaction conditions. Herein we report Pd-catalyzed C–H functionalization reactions with milder conditions as well as a mechanistic study to improve reaction conditions and increase understanding. Chapter 1 introduces these ideas with subsequent chapters devoted to the study of specific methodologies.

Chapter 2 details the palladium-catalyzed C–H fluorination of 8-methylquinoline derivatives with nucleophilic fluoride. This transformation involves the use of AgF as the fluoride source in combination with a hypervalent iodine oxidant. The scope and mechanism of the reaction are discussed. In an effort to explore conditions relevant for PET imaging, short reaction times were investigated for this transformation.

Chapter 3 describes the development of a room-temperature ligand-directed C–H arylation reaction using aryldiazonium salts. This was achieved by the successful merger of palladium-catalyzed C–H functionalization and visible-light photoredox catalysis. The unusually mild conditions utilized in this transformation (room temperature, CH₃OH solvent) are proposed to be due to the kinetically reactive aryl radical oxidants formed under the reaction conditions. This method is general for a variety of directing groups and tolerates many common functional groups.

Chapter 4 explores the mechanism of a room temperature palladium-/iridium-catalyzed C–H arylation reaction using diaryliodonium salts as the aryl source. This use

of visible-light photoredox catalysis in combination with palladium catalyzed C–H functionalization is interesting mechanistically, and could potentially lead to other functionalization reactivity through similar methods. Stern-Volmer quenching studies along with kinetic studies are discussed in detail.

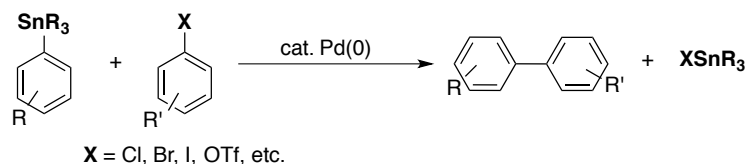
CHAPTER 1

Introduction

1.1 C–H Functionalization

In synthetic organic chemistry, chemical transformations generally involve the conversion of one functional group into another. This method of functional group interconversion is exemplified by transition metal-catalyzed cross-coupling reactions that merge two prefunctionalized starting materials. For example, biaryls can be synthesized via the palladium-catalyzed Stille coupling of an aryl tin reagent and an aryl halide (Scheme 1.1).

Scheme 1.1. Example of Functional Group Interconversion



These cross-coupling reactions are widely used because they are effective and versatile. However, there are several drawbacks to such methods. First, both coupling components need to be prefunctionalized and often, these functional groups cannot be preserved through a multi-step synthesis. Second, as shown in Scheme 1.1, a stoichiometric quantity of waste is produced as a byproduct. Therefore, functional group interconversion strategies are often not practical for the functionalization of complex molecules, especially at a late stage.

Alternatively, a more attractive strategy would be the direct conversion of C–H bonds into the desired C–X bonds. This approach would avoid the need for at least one

of the prefunctionalized starting materials. However, generally, this strategy is not possible using traditional organic transformations because unactivated C–H bonds are inert to cleavage under most conditions. Either by homolytic cleavage, as shown by the bond dissociation energies in Figure 1.1 (part a), or heterolytic cleavage, shown by the p*K*_a values in Figure 1.1(part b), typical C–H bonds cannot be broken due to their relatively high energy. These bond dissociation energies range from ~90–115 kcal/mol. For heterolytic cleavage, unactivated C–H bonds have very high p*K*_a values (≥40) and cannot be deprotonated by mild bases (Figure 1.1).

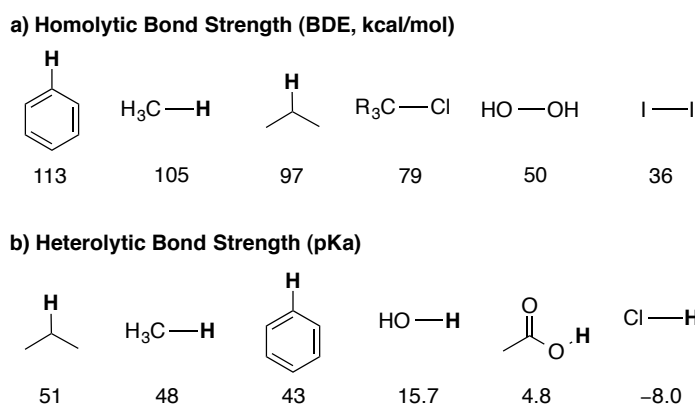
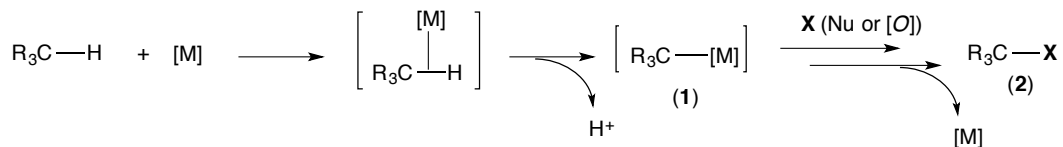


Figure 1.1. Homolytic and Heterolytic Bond Strengths for C–H Bonds¹

However, there are methods to overcome these challenges. A number of transition metals, such as Pt, Pd, Ni, Ir, Rh, and Ru have been shown to activate, or break, C–H bonds. The result is a carbon–metal species (**1**) (Scheme 1.2).² Intermediate organometallic complexes like **1** are typically unstable and readily undergo further mechanistic steps. With the addition of a nucleophile or oxidant, and release of the metal catalyst, the desired product **2** can be formed in which a C–H bond has been replaced by a new functional group. The ubiquity of C–H bonds in organic molecules and the use of the reactivity of transition metals makes such metal catalyzed C–H functionalization methods extremely useful tools for accessing many synthetic targets.

Scheme 1.2. C–H Activation and Functionalization by Transition Metal-Catalysis



1.2 Site-Selectivity for C–H Functionalization Reactions

The abundance of C–H bonds in organic molecules make them excellent starting material group to functionalize. There are many options for sites of reactivity. However, this characteristic is also a disadvantage in C–H functionalization reactions. To make useful products, functionalization needs to occur selectively at a single C–H bond. To illustrate this idea, the pharmaceutical atorvastatin, which is sold as Lipitor, is shown in Figure 1.2. Lipitor contains thirty-one total C–H bonds and seventeen chemically distinct C–H bonds. These include aromatic and heteroaromatic sp^2 C–H bonds as well as primary, secondary, and tertiary sp^3 C–H bonds. These characteristics begin to distinguish the C–H bonds one from another, however there are still multiple C–H bonds in each category and thus, multiple sites for functionalization.

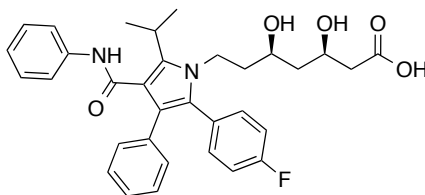
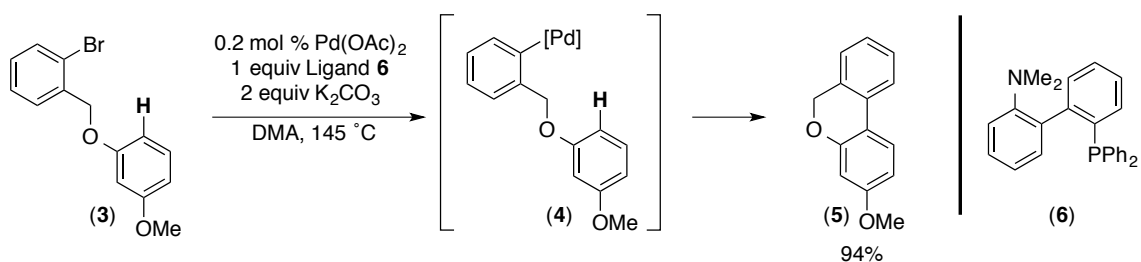


Figure 1.2. Lipitor Contains Many Unique Hydrogen Bonds

There are a number of approaches to address this challenge of site-selectivity. One method uses an intramolecular tactic, where a C–H bond is tethered proximal to a site at which a metal can coordinate. An example of this is shown in a report by Fagnou, in which substrate **3** contains a C–H bond of interest that is tethered to a C–Br bond (Scheme 1.3).³ By oxidative addition at Pd^0 , the Pd is inserted in the C–Br bond to form intermediate **4**. The selectivity is determined from this intermediate (**4**), in which the Pd

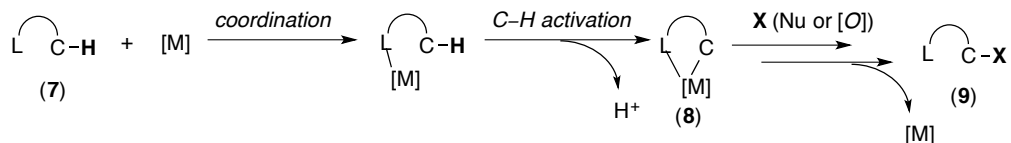
center can access a single C–H based on the molecule’s geometry. Although this compound contains thirteen C–H bonds, eight of which are different aromatic sp^2 C–H bonds, only one site is functionalized. The cyclized product **5** is formed in high yield and excellent selectivity. While exceptional selectivity is achieved by this intramolecular approach, substrates are limited to this type of tethered design, and only cyclic products are formed.

Scheme 1.3. Intramolecular C–H Functionalization



An alternative method for achieving high site selectivity is to use substrates that contain coordinating ligands, such as the generalized compound **7** (Scheme 1.4). These ligands should be able to reversibly bind to a metal center and direct towards a C–H bond at a proximal site. Thus C–H activation will only be possible at one location on a molecule, as shown by metallacycle **8**. Then with the addition of a nucleophile or oxidant, and release of the metal catalyst, the desired product **9** is formed with the installed functional group. Overall this is an intermolecular approach, as the metal and directing ligand separate and undergo no net change. Although substrates require a group that can coordination to a metal under this ligand-directed approach, these transformations are not limited to cyclizations. Palladium has been utilized as an effective and versatile metal to catalyze many ligand-directed C–H functionalization reactions.

Scheme 1.4. Transition Metal-Catalyzed Ligand-Directed C–H Functionalization



1.3 Palladium Catalysis for C–H Functionalization Reactions

There are multiple advantages of using palladium as a transition metal catalyst in C–H functionalization reactions over other alternatives.⁴ These include: (1) the ability of Pd^{II} to undergo C–H activation, (2) the square planar nature of the Pd^{II} intermediate after C–H activation, and (3) the ability of Pd to reach a +4 oxidation state under oxidizing conditions.

Palladium can participate in C–H activation at Pd^{II} and accesses an electrophilic type mechanism from which there is no oxidation change at the metal (**10**, Figure 1.3 part a). Other metal complexes that undergo C–H activation proceed by oxidative addition, and must be in low oxidation states such as Ir^I, Rh^I, and Ru⁰. Figure 1.3 part b, which displays the C–H activation at Ir^I, shows the resulting complex (**11**) is in the +3 oxidation state. Since this is already a relatively high oxidation state, further manipulations, such as oxidation, are unlikely. Pd^{II}, however, is compatible with many oxidants. Additionally Pd^{II} complexes are often stable to air unlike many of the low valent species mentioned previously, which are sensitive to oxygen. This allows reactions to be run on the benchtop instead of requiring Schlenk and glovebox techniques. Lastly, unlike Pd⁰, Pd^{II} does not undergo oxidative addition with C–X bonds (where X is halogen). This allows for a wider function group tolerance as these halogen groups can be present in compounds for C–H functionalization by Pd^{II}.

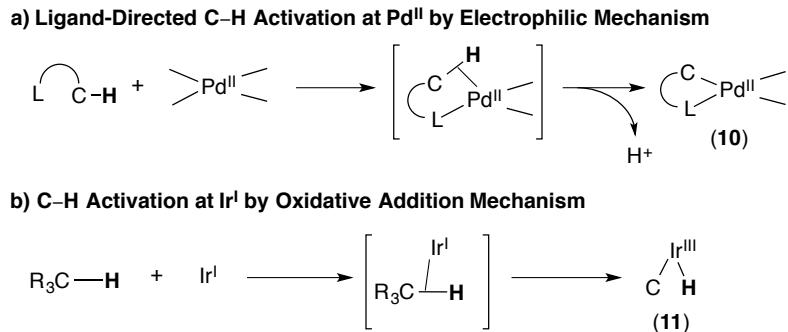
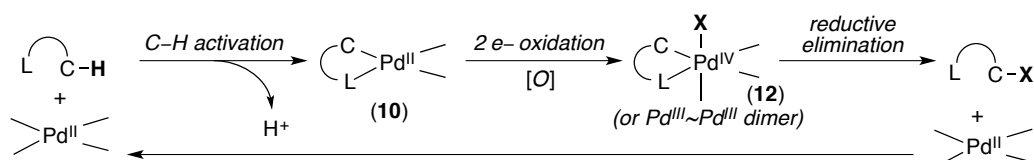


Figure 1.3. C–H Activation Mechanisms of Pd^{II} versus Ir^I

Square planar palladacycles such as **10**, which are a result of C–H activation at Pd^{II}, have open coordination sites. Thus further reactivity is possible at the metal center, especially oxidation reactions. Other metals that also go through electrophilic C–H activation pathways, such as Rh^{III} and Ir^{III}, are often octahedral complexes, which are coordinatively saturated. Therefore, the square planar geometry at Pd^{II}, post C–H activation, is important for functionalization, and makes palladium an attractive metal for these transformations.

Lastly, once a square planar Pd^{II} complex is formed, Pd can access higher oxidation states such as Pd^{III} and Pd^{IV} with the addition of an oxidant. Due to the electron-donating nature of carbon ligands, intermediates such as **10** are prone to oxidation compared to simple Pd^{II} salts. From a C–H activated Pd^{II} complex, a two-electron oxidant can form a Pd^{IV} species (**12**) while delivering a functional group (X) to the metal (Scheme 1.5). These Pd^{IV} compounds are sufficiently unstable to undergo rapid reductive elimination. A new product can be formed and the Pd^{II} starting catalyst regenerated. Reductive elimination from Pd^{IV} species enables a variety of bond constructions, such as C–O, C–N, C–F, C–Cl, C–Br, and C–I, which are challenging from Pd^{II} reductive elimination. Of particular interest is C–Br and C–I bond formations, as reductive elimination from Pd^{II} would result in reinsertion to the Pd by oxidative addition. Therefore new bond constructions and functionalization reactions are possible by Pd^{II/IV} mechanistic pathways. All of these points stated herein make palladium an excellent metal for ligand-directed C–H functionalization reactions.

Scheme 1.5. Ligand-Direction Pd^{II/IV}-Catalyzed C–H Functionalization Reaction



1.4 Challenges and Objective

Taking advantage of palladium's reactivity, there has been significant progress over the past decade in the field of ligand-directed C–H functionalization reactions by high oxidation state Pd. Numerous methods for new bond constructions have been developed, but there continues to be area for improvement. Figure 1.4 displays a wide variety of bond constructions with various directing groups and functionalities installed.^{4f,5} The following is only a handful of examples from a few researchers in the field.

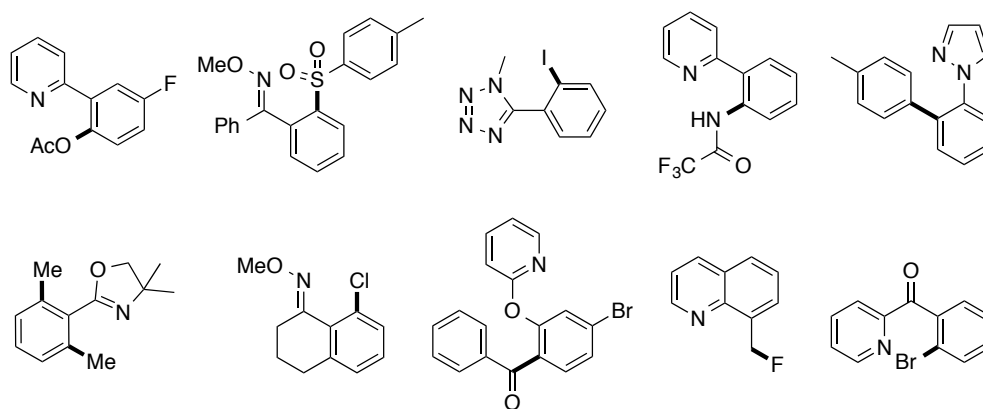


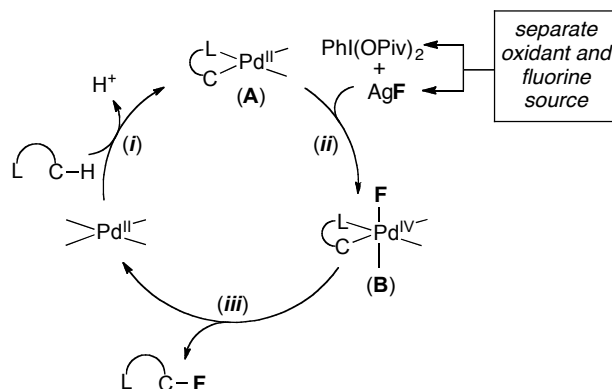
Figure 1.4. Ligand Directed High-Valent Pd-Catalyzed C–H Functionalization Examples (Bold Bonds Formed via Pd^{II/IV}-Catalyzed C–H Functionalization)

Although there have been substantial developments in the functionalization of C–H bonds by Pd catalysts, there are a number of challenges yet to be solved. One important challenge is the need for processes with milder and less forcing conditions. Often C–H functionalization reactions are slow and require high temperatures and/or strong acids or bases to become high yielding transformations. Additionally, toxic and

difficult to use reagents are common for some functionalization reactions, as strong reagents are required to drive reactivity. Therefore, for my dissertation work I chose to develop new transformations with milder conditions, in order to obtain desired compounds by easier and more efficient routes.

Chapter 2 describes a new method to Pd-catalyzed C–H fluorination by use of a nucleophilic fluorinating reagent, AgF (Scheme 1.6). Fluorination methods traditionally require harsh reagents such as F₂, which is toxic and difficult to use. More recently, electrophilic fluorinating reagents (Figure 2.2) have been utilized, which have a number of drawbacks including high cost and the generation of large quantities of organic waste. Our transformation utilizes AgF, which is a relatively inexpensive and easy to use reagent. Also of note, we were able to use a low reaction temperature of 60 °C and perform these reactions on the benchtop.

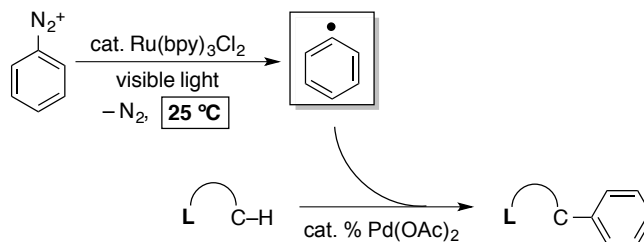
Scheme 1.6. Sequence for Nucleophilic Fluorination



Chapter 3 describes a Pd-/Ru-catalyzed C–H arylation method, which uses aryl diazonium salts as the aryl source and proceeds at room temperature (Scheme 1.7). The diazonium salts are proposed to form aryl radicals through a Ru-photocatalyzed mechanism through which the aryl radical can react with a palladacycle and undergo Pd-catalyzed functionalization. Arylation reactions typically require high reaction temperatures (≥ 100 °C) and can require acidic solvents as well. The use of photocatalysis allows for mild conditions; the reaction proceeds at 25 °C in the presence of standard household lamps. Additionally, this reaction is the first example of a merger

between Pd-catalyzed C–H functionalization and photoredox catalysis. Employing this methodology for other transformations could lead to milder conditions as well as new reactivity.

Scheme 1.7. Arylation from Diazonium Salts via Photocatalysis



Chapter 4 outlines a mechanistic study of the Pd/Ir-catalyzed C–H arylation method, by use of diaryliodonium salts (Figure 1.5). This transformation is similar to the method outlined in chapter 3, and was an ideal transformation to study, especially as it is closely related to a previously reported thermal C–H arylation method in which diaryliodonium salts were used.⁶ Through this chapter, preliminary mechanistic findings are discussed. Importantly, mechanistic investigations are important for improving reaction conditions as well as developing new transformations.

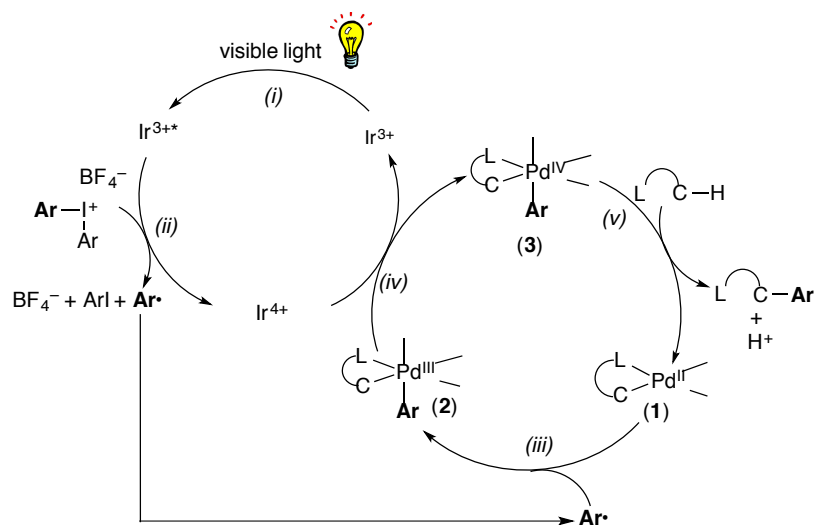


Figure 1.5. Proposed Catalytic Cycle for the Pd-/Ir-Catalyzed C–H Arylation Reaction

1.5 References

- ¹ (a) Mishra, M. K.; Yagci, Y. *Handbook of Radical Vinyl Polymerization*. Marcel Dekker: New York, 1998; p 32. (b) Blanksby, S. J.; Ellison, G. B. *Acc. Chem. Res.* **2003**, *36*, 255. (c) Evans pKa Table. Downloaded from <http://www2.lsddiv.harvard.edu/labs/evans/> on June 11, 2010. (d) Anslyn, E. V.; Dougherty, D. A. *Modern Physical Organic Chemistry*. University Science Books: Sausalito, CA, 2006.
- ² For a comprehensive review see: Hartwig, J. F. University Science Books: Sausalito, CA, 2010.
- ³ Campeau, L.-C.; Parisien, M.; Leblanc, M.; Fagnou, K. *J. Am. Chem. Soc.* **2004**, *126*, 9186.
- ⁴ (a) Alberico, D.; Scott, M. E.; Lautens, M. *Chem. Rev.* **2007**, *107*, 174. (b) Chen, X.; Engle, K. M.; Wang, D.-H.; Yu, J.-Q. *Angew. Chem. Int. Ed.* **2009**, *48*, 5094. (c) McGlacken, G. P.; Bateman, L. M. *Chem. Soc. Rev.* **2009**, *38*, 2447. (d) Muñoz, K. *Angew. Chem. Int. Ed.* **2009**, *48*, 9412. (e) Canty, A. J. *Dalton. Trans.* **2009**, *47*, 10409. (f) Lyons, T. W.; Sanford, M. S. *Chem. Rev.* **2010**, *110*, 1147. (g) Xu, L.-M.; Li, B.-J.; Yang, Z.; Shi, Z.-J. *Chem. Soc. Rev.* **2010**, *39*, 712. (h) Hickman, A. J.; Sanford, M. S. *Nature* **2012**, *484*, 177.
- ⁵ Neufeldt, S. R.; Sanford, M. S. *Acc. Chem. Res.* **2012**, *45*, 936.
- ⁶ Kalyani, D.; Deprez, N. R.; Desai, L. V.; Sanford, M. S. *J. Am. Chem. Soc.* **2005**, *127*, 7330.

CHAPTER 2

Palladium-Catalyzed C–H Fluorination using Nucleophilic Fluorideⁱ

2.1 Background and Significance

The substitution of hydrogen with fluorine can have a dramatic impact on the lipophilicity, metabolism, and overall biological activity of organic molecules.¹ As a result, carbon-fluorine bonds feature prominently in pharmaceuticals, agrochemicals, and PET imaging reagents. About 20% of pharmaceuticals and 30–40% of agrochemicals on the market contain at least one C–F bond (Figure 2.1).² Fluorine is also found in many polymers, creating effective insulating materials.³ Due to the prevalence of fluorine in several numerous industries, investigation into the fluorination of small molecules and polymers has been an area of particular interest among chemistry researchers.

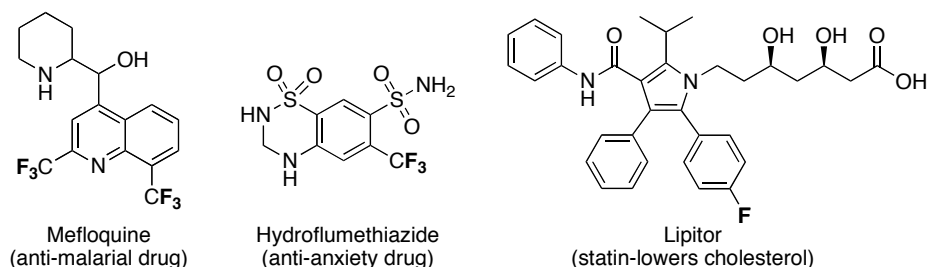


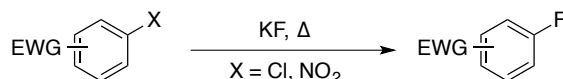
Figure 2.1. Examples of Fluorine in Pharmaceuticals

However, despite the prevalence and great utility of this functional group, synthetic methods for forming C–F bonds under mild conditions remain limited.⁴ In particular, it remains challenging to achieve C–F coupling reactions using nucleophilic sources of fluoride. These transformations often require harsh conditions because of the

ⁱ Reproduced in part with permission from McMurtrey, K. B.; Racowski, J. M.; Sanford, M. S. *Org. Lett.* **2012**, *14*, 4094. Copyright 2012 American Chemical Society.

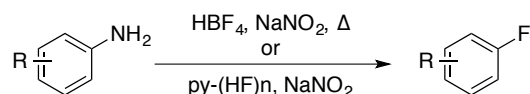
inherent properties of fluoride. Fluoride can form strong hydrogen bonds making the fluoride only weakly nucleophilic in the presence of water or other hydrogen-bond donors. Conversely, if hydrogen-bond donors are removed, fluoride can serve as a good base, causing unwanted side reactions. Despite these challenges, fluoride can still participate in nucleophilic substitution reactions under certain conditions. One common way to form C–F bonds is by the Halex process, which involves the reaction of aryl halides with MF (Scheme 2.1).⁵ However, these reactions require high reaction temperatures (typically ≥ 130 °C) as well as substrates containing electron-withdrawing groups.

Scheme 2.1. General Reaction for Halex Process



Another common fluorination method is the Balz-Schiemann reaction, which involves the reaction of aniline derivatives with fluoroboric acid and a nitrite salt to form arylfluorides (Scheme 2.2).⁶ Many aryl fluorides can be prepared in this manner; however the reaction conditions for this transformation are harsh. For example, high reaction temperatures (typically ≥ 90 °C) are required as well as a strong acid (fluoroboric acid) and potential explosive intermediate aryl diazonium salts are involved as intermediates.

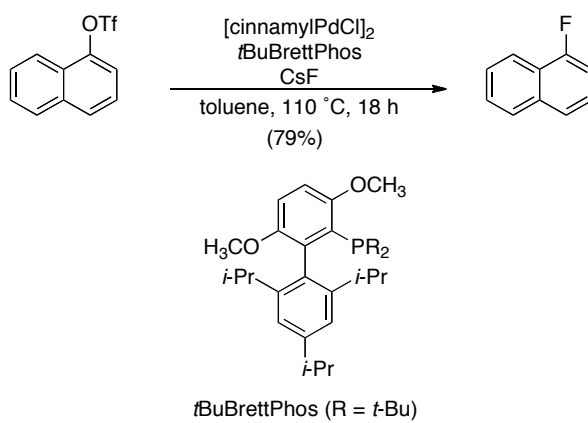
Scheme 2.2. Balz-Schiemann Reaction



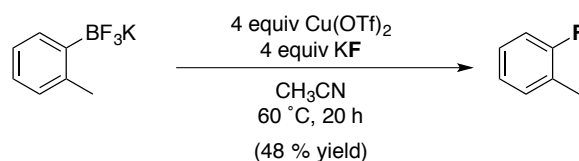
Transition-metal-catalyzed C–F coupling reactions are particularly rare and constitute powerful synthetic tools to complement more conventional methods. Of particular significance, Buchwald has demonstrated catalytic fluorination of aryl compounds from aryl triflates (OTf) using CsF as the fluorine source (Scheme 2.3).⁷ This transformation uses a simple fluoride salt and involves relatively mild conditions

and affords high yields for a large substrate scope. A recent report by our group shows another example of nucleophilic fluorination, in this case mediated by Cu(II). Here, copper (II) triflate and KF are utilized to fluorinate aryltrifluoroborates at low temperature (60 °C) and in good yields (Scheme 2.4).⁸ However, both of these examples suffer from requiring a pre-functionalized starting material, which can be a significant disadvantage for synthetic purposes.

Scheme 2.3. Palladium Catalyzed Fluorination of Aryl Triflates by CsF



Scheme 2.4. Copper Mediated Fluorination of Aryltrifluoroborates by KF

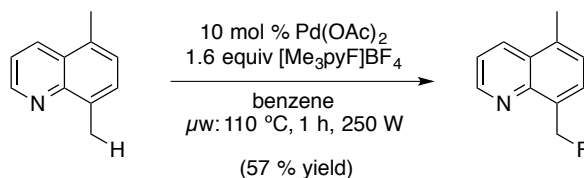


Late stage introduction of fluorine into biologically active molecules is of particular value for SAR studies. These studies require a large library of fluorinated compounds for testing. Traditionally, a C–F bond is installed in early synthetic precursors and carried forward through several steps to provide the fluorinated drug. Therefore, selective incorporation of fluorine into a molecule at the end of a synthesis would constitute a significant advance by saving time and money for SAR studies. However, there are major challenges in late-stage synthesis such as functional group tolerance and selectivity in the structurally complex molecules of interest.

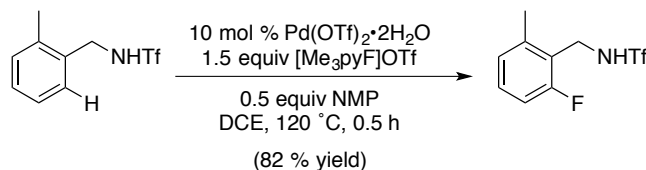
Additionally, introduction of fluorine at the end of the synthesis is essential for the construction of ^{18}F radiotracers for Positron Emission Tomography (PET) Imaging.⁴ This technique is used to trace biochemical processes in the body by imaging gamma decay of radionuclides. It can be used to diagnose or treat a variety of diseases. Of the possible radionuclides, fluorine-18 is most commonly incorporated into biologically active molecules and used as a tracer because of its relatively long half-life of ~ 110 min. While this half-life is long compared to other radionuclides, there is still a need for short reaction times and quick purification. Furthermore, incorporation of fluorine in the first stages of a synthesis would be impractical because of the time constraints imposed by the immanent ^{18}F decay. Therefore, late stage fluorination is critical for these syntheses and current methods to do so are scarce.

Selective C–H fluorination is an attractive approach towards these goals, as it would make late stage fluorination more feasible. The need for pre-functionalized starting materials as well as the hassle, because of functional group incompatibility, would be negated. Our group and others have previously reported the Pd-catalyzed conversion of C–H bonds to C–F bonds using electrophilic fluorinating reagents (abbreviated F^+ reagents or Oxidant-F).^{9,10} In 2006, an example from our group showed that 8-methylquinoline in the presence of 10 mol % $\text{Pd}(\text{OAc})_2$ and *N*-fluoro-2,4,6-trimethyl pyridinium tetrafluoroborate ($[\text{Me}_3\text{pyF}]\text{BF}_4$) in benzene under microwave conditions afforded the fluorinated product in 57% yield (Scheme 2.5).⁹ This was an important advance as it was the first method to achieve selective fluorination in a catalytic system using non-toxic, operationally simple conditions and reagents. In 2009, Yu demonstrated a closely related *ortho*-fluorinated of triflamide-protected benzylamines by a similar F^+ reagent with 10 mol % $\text{Pd}(\text{OTf})_2 \cdot 2\text{H}_2\text{O}$ as the catalyst (Scheme 2.6).^{10a} They claim that NMP is critical to obtain high yields in these transformations although its exact role is unknown. Subsequently, several other related examples have appeared in the literature.

Scheme 2.5. Pyridine Directed Catalytic C–H Fluorination with F⁺ Reagent

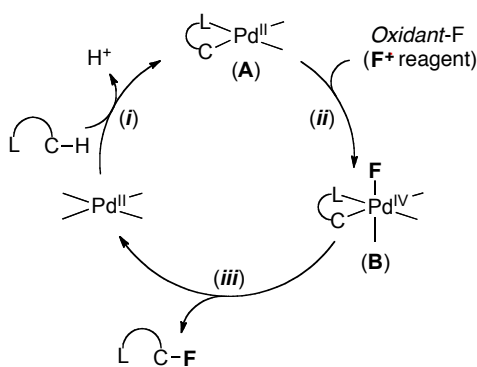


Scheme 2.6. Triflamide Directed Catalytic C–H Fluorination with F⁺ Reagent



These fluorination reactions using F⁺ are believed to proceed via a catalytic cycle such as that shown in Scheme 2.7, where C–F bond-forming reductive elimination from Pd^{IV}(R)(F) (**B**)^{11,12} serves as a key step. Thus, the role of the F⁺ reagent is twofold: (1) it oxidizes the Pd^{II} to Pd^{IV} (step *ii*), and (2) it serves as the source of fluorine that ends up in the final product (step *iii*).

Scheme 2.7. Pd-Catalyzed C–H Fluorination with F⁺ Reagents



While this first-generation approach to C–H fluorination was successful, these reactions suffer from the distinct disadvantage that they require electrophilic fluorinating reagents. Even though a number of F⁺ sources are commercially available, they are often much more expensive than fluoride reagents. For example, the Sigma-Aldrich prices for

N-fluoropyridinium salts (NFPs) and Selectfluor (both F⁺ reagents) are several orders of magnitude more expensive than CsF and KF (Figure 2.2). In addition, commonly used F⁺ reagents such as NFPs and Selectfluor generate large quantities of organic waste and exhibit modest tolerance to nucleophilic functional groups. Finally, electrophilic fluorinating reagents are much less desirable than fluoride for PET imaging applications. This is because ¹⁸F⁻ has significantly higher specific activity than ¹⁸F⁺ precursors.⁴ Also, electrophilic fluorinating reagents are synthesized from F₂ gas, which many PET facilities lack the equipment to handle.

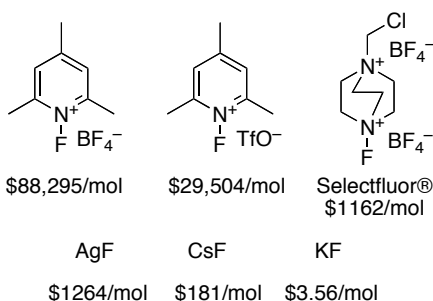
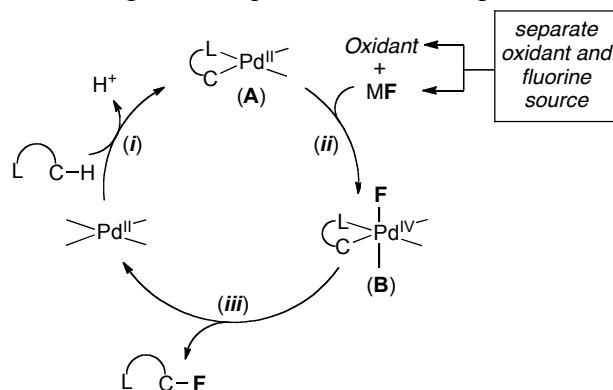


Figure 2.2. Prices for Commercial Fluorine Sources (based on largest quantity available from Sigma Aldrich in >95% purity).

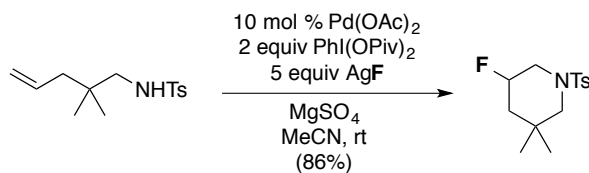
We hypothesized that Pd-catalyzed C–H fluorination with nucleophilic fluoride could be accomplished by separating the two roles played by the F⁺ reagent in these transformations.¹³ As shown in Scheme 2.8, an external oxidant could be used to convert Pd^{II} to Pd^{IV} (step *ii*) while a fluoride source could provide a ligand to Pd^{IV} that would ultimately participate in C–F bond-forming reductive elimination (step *iii*).

Scheme 2.8. Proposed Sequence for Nucleophilic Fluorination



A recent report on Pd-catalyzed alkene aminofluorination provided preliminary support for the viability of this approach. As shown in Scheme 2.9, Liu and co-workers demonstrated this transformation using $\text{PhI}(\text{OPiv})_2$ as an oxidant in conjunction with AgF as a nucleophilic fluoride source.¹⁴ We sought to use a similar strategy to achieve the Pd-catalyzed ligand-directed C-H fluorination of 8-methylquinoline derivatives using the combination of hypervalent iodine reagents and fluoride salts.¹⁵ This work was conducted in collaboration with Dr. Joy Racowski who assisted in oxidant screens as well as detection of an oxidant formed *in situ* (Figure 2.5).

Scheme 2.9. Alkene Aminofluorination with Oxidant and Fluoride Source

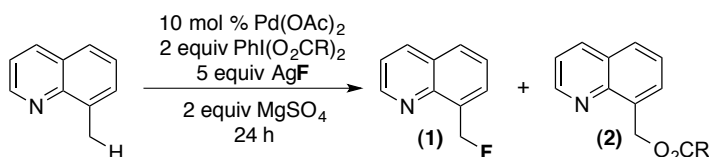


2.2 Reaction Optimization

Our initial studies focused on the C-H fluorination of 8-methylquinoline. We chose 8-methylquinoline for our study because (1) it is an excellent substrate for Pd-catalyzed fluorination with F^+ reagents,⁹ and (2) it is an inexpensive commercially available material, which was convenient for reaction optimization. The use of conditions analogous to Liu's (10 mol % of $\text{Pd}(\text{OAc})_2$ along with $\text{PhI}(\text{OAc})_2$ and AgF in

MeCN at 25 °C for 24 h) resulted in a modest yield of the desired fluorinated product **1** (14%), along with the corresponding C–H oxygenation product **2** (17%) and recovered starting material (61%) (Table 2.1, entry 1). Increasing the temperature to 60 °C resulted in nearly complete conversion of 8-methylquinoline; however, the yield of the desired fluorinated product remained low (14%) (Table 2.1, entry 2). Changing the oxidant from PhI(OAc)₂ to PhI(OPiv)₂ and the solvent from MeCN to CH₂Cl₂ resulted in quantitative conversion of 8-methylquinoline and provided a 58% yield of **1** (entry 4).

Table 2.1. Optimization of C–H Fluorination with PhI(O₂CR)₂/AgF



entry	solvent	R	temperature	conversion (%)	yield (%) ^a	
					1	2
1	MeCN	Me	25 °C	39	14	17
2	MeCN	Me	60 °C	87	14	64
3	MeCN	^t Bu	60 °C	32	8	14
4	CH ₂ Cl ₂	^t Bu	60 °C	100	58	25
5 ^b	CH ₂ Cl ₂	^t Bu	60 °C	100	62	18

^a Yields determined by GC based on an average of at least two runs. ^b AgF and PhI(OPiv)₂ were prestirred at 60 °C for 1 h in CH₂Cl₂ prior to addition of the rest of the reagents.

Significant additional experimentation led to the discovery that the yield of **1** could be enhanced by modification of the reaction conditions. Specifically, prestirring the PhI(OPiv)₂ and AgF in CH₂Cl₂ for 1 h at 60 °C before adding the Pd catalyst, substrate, and MgSO₄ resulted in a modest boost in the yield of **1** as well as an improved ratio of **1**/ **2** (Table 2.1, entry 5). We hypothesized prestirring the oxidant and AgF together would increase product yield because the formation of PhIF₂ was observed by ¹⁹F NMR (Figure 2.5).

The major side product in this transformation (**2**) derives from C–H oxygenation of the 8-methylquinoline.¹⁶ While products **1** and **2** are easily separable by column chromatography on silica gel, it would clearly be desirable to obtain higher yields of **1** in

these transformations. We initially hypothesized that the electronic/steric properties of R in the hypervalent iodine reagent could be tuned to enhance the yield of **1**. In order to investigate this theory, we screened 19 different iodine(III) oxidants as shown in Figure 2.3. In addition to the previously mentioned $\text{PhI}(\text{OAc})_2$ and $\text{PhI}(\text{OPiv})_2$, oxidants with the formula $\text{PhI}(\text{O}_2\text{CC}_6\text{H}_4\text{R}')_2$ with varying electronic properties from methoxy to nitro at R' were examined. Surprisingly, there was no clear trend seen in the data with regards to electronic effects. Additionally, several mesityl iodide carboxylates, though sterically different, performed similar to their phenyl iodide carboxylate analogs. Perfluorinated carboxylates as well as Koser's reagent and iodosobenzene all afforded <5% of **1**. Ultimately, $\text{PhI}(\text{OPiv})_2$ provided the best results (Figure 2.3).

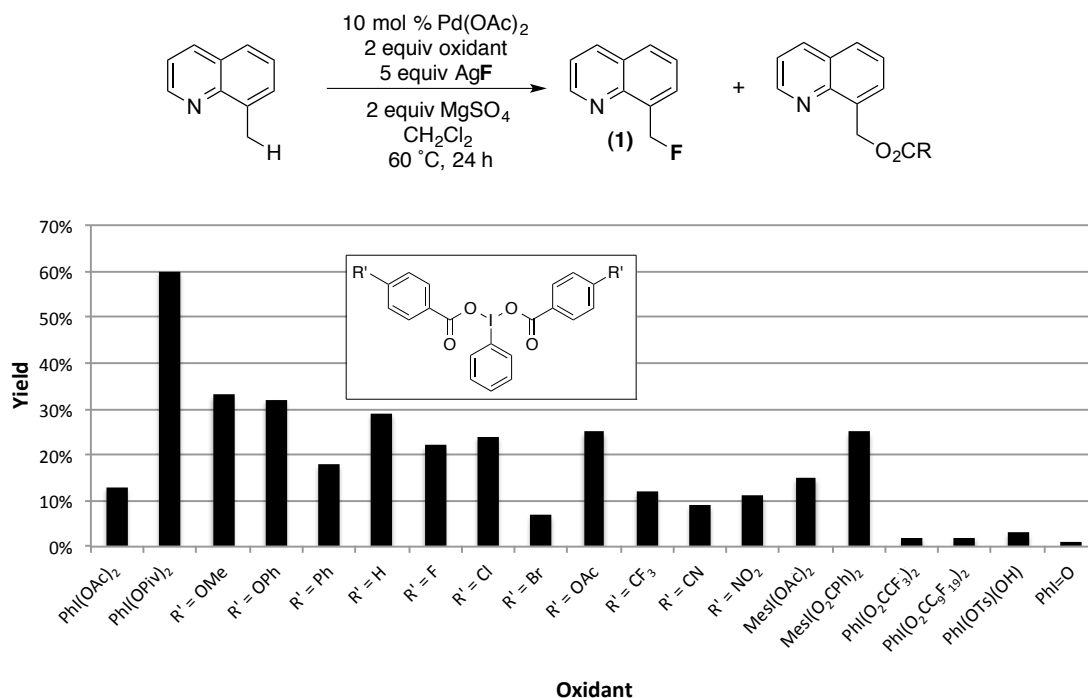
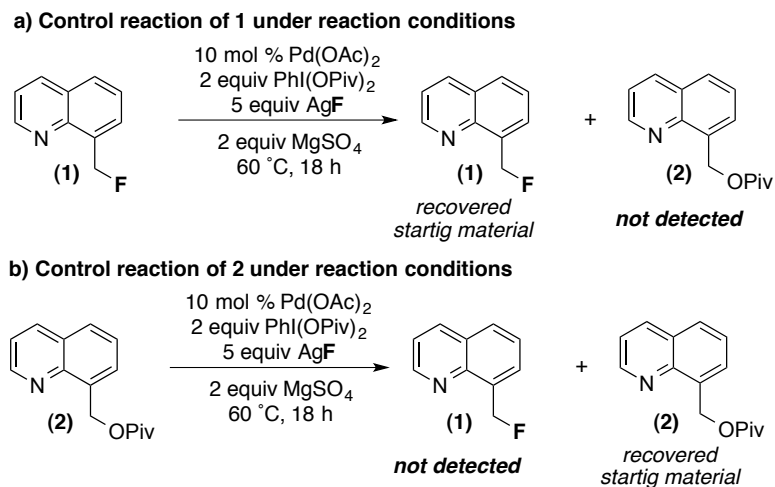


Figure 2.3. Oxidants Screen for the Fluorination of 8-Methylquinoline

A number of control experiments were conducted to verify the origin of various products. The reactions in Scheme 2.10 show that **1** and **2** do not interconvert under the reaction conditions, indicating that they are not formed from one another in this transformation. This data suggests that each product **1** and **2** is coming from the starting material, 8-methylquinoline, independently.

Scheme 2.10. Control Reactions for the Fluorination of 8-Methylquinoline



All of the fluorination reactions described herein were set up on the benchtop using commercially available reagents without further drying or purification. This is not only useful and practical for synthetic chemists but also an advantage over many nucleophilic fluorination methods, which require harsh and/or rigorously anhydrous reaction conditions.⁴

2.3 Substrate Scope

The scope of Pd-catalyzed nucleophilic C–H fluorination was evaluated with a variety of 8-methylquinoline derivatives. As shown in Table 2.2, diverse substituents at positions X and Y were tolerated under the optimized reaction conditions. Most notably, a variety of halogens were compatible (entries 5-8), providing sites for further elaboration of the products. In general, the best results were obtained when X and Y were electron-withdrawing groups (entries 2-8). Conversely, the introduction of electron-donating group resulted in a steep erosion in yields. Significantly lower yields of the fluorinated product were observed when X = phenyl or methyl (entries 9, 10). Furthermore, the substrate with X = methoxy afforded <1% of **12** (entry 11).

Table 2.2. Substrate Scope for the C–H Fluorination of 8-Methylquinoline Derivatives

entry	product	GC yield (%)	isolated yield (%)	entry	product	GC yield (%)	isolated yield (%)
1		67	49	7		49	42
2 ^a		62	41	8 ^a		67	55
3		67	70	9 ^{b,c}		43	39
4 ^a		59	59	10 ^c		41	39
5		44	30	11 ^a		<1	nd
6		53	44				

^a The reaction was run for 24 h. ^b The Reaction was run for 28 h. ^c PhF was used as a solvent in place of CH₂Cl₂.

All reactions in Table 2.2 had the C–H oxygenation product (analogue of **2**) as the major side product. Table 2.3 displays the yields of each C–O coupled product from the same reactions as shown above. In general, when X was an electron-donating group (entries 9-11), relatively high yields of the oxygenation products were formed in contrast to C–F bond formation (Table 2.2).

Table 2.3. C–H Oxygenation Side Products for the Fluorination of 8-Methylquinoline Derivatives

entry	product	GC yield (%)	isolated yield (%)	entry	product	GC yield (%)	isolated yield (%)
1	 (2)	15	11	7	 (18)	28	26
2 ^a	 (13)	7	10	8 ^a	 (19)	16	15
3	 (14)	12	9	g ^{b,c}	 (20)	35	36
4 ^a	 (15)	10	11	10 ^c	 (21)	40	38
5	 (16)	25	24	11 ^a	 (22)	55	nd
6	 (17)	19	13				

^a The reaction was run for 24 h. ^b The Reaction was run for 28 h. ^c PhF was used as a solvent in place of CH₂Cl₂.

Under these conditions, the scope of nucleophilic C–H fluorination was limited to 8-methylquinoline derivatives. This could indicate that a five-membered palladacycle are critical for this transformation. Also importantly, the C–H bond that becomes functionalized is benzylic making it more easily activated. Additionally, the sp³ character

of the substrate could be important for many reasons, especially if the mechanism involves an S_N2 type reductive elimination. To the best of our knowledge, these aspects are unique to 8-methylquinoline and its derivatives. Additional substrates with a variety of directing groups were screened for the fluorination reaction, but they yielded less than 5% of the corresponding fluorinated products as detected by GC. In each case, either C–H oxygenation product or exclusively starting material was observed. These substrates are shown in Figure 2.4.

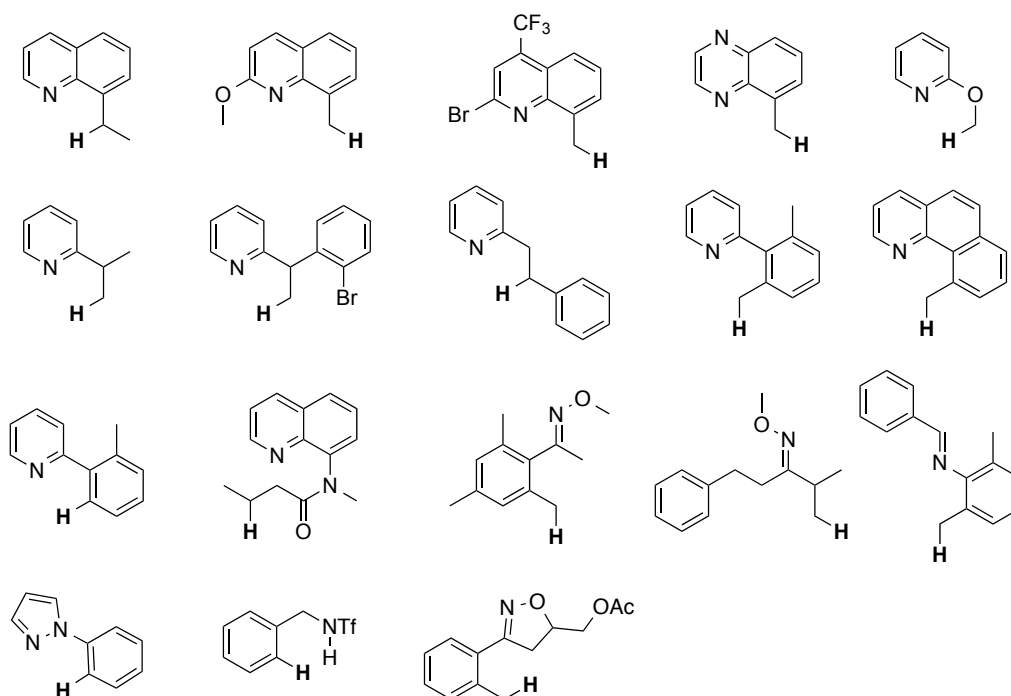
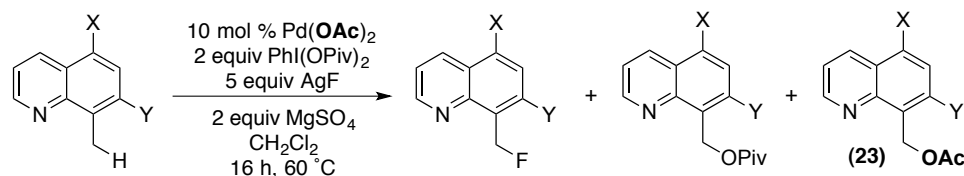


Figure 2.4. Substrates Screened That Provided <5% Yield of Fluorinated Product by GC

As evident by the sum of the yields of the fluorinated and oxygenated products from Table 2.2 and Table 2.3, the mass balance for many reactions is not completely accounted for in these two products. The starting material is consumed in all cases. The most substantial side product not shown is another C–H oxygenated product, the acetoxylation of the various 8-methylquinoline derivatives, product **23** (Scheme 2.11). This acetate group originates from the palladium catalyst and thus could be formed in up to 20% yield. $Pd(OAc)_2$ proved to be the best catalyst for the transformation, so

eliminating the side product by using a different catalyst was not a fruitful approach. Other catalysts explored included Pd(OPiv)₂, Pd(acac)₂, Pd(TFA)₂, and PdCl₂.

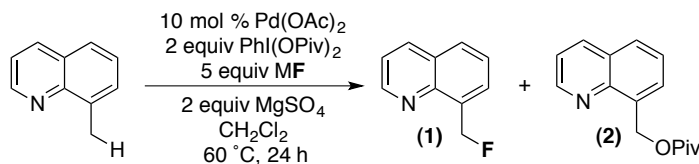
Scheme 2.11. Acetoxyated product present as additional side product



2.4 Fluorination Using CsF

Although AgF produced good results, it would be attractive to replace AgF with an alternative fluoride source. This could be practical from a price standpoint as well as useful in the context of PET imaging applications (see section 2.5). In PET imaging the most readily available ¹⁸F⁻ starting materials are Cs¹⁸F, Rb¹⁸F, NBu₄¹⁸F, and K¹⁸F-Kryptofix.¹⁷ Unfortunately, as shown in Table 2.4, entries 1-4, the substitution of AgF with CsF, RbF, KF, or NBu₄F under our optimized reaction conditions led to <1% yield of the fluorinated product. These results suggest that the presence of Ag(I) is important for the success of the desired fluorination reaction. As such, we examined the use of an exogenous Ag(I) salt in conjunction with CsF (entry 5). Gratifyingly, under these conditions the Pd-catalyzed C–H fluorination proceeded to afford **1** in 45% (Scheme 2.12). When CsF was replaced with other fluoride salts, such as NaF, KF, or TBAF, low yields of **1** were obtained.

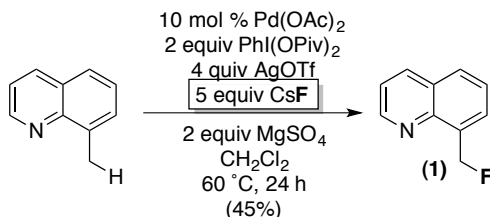
Table 2.4. Fluoride Salt Screen to Replace AgF



entry	M	additive	conversion (%)	yield (%) ^a	
				1	2
1	Cs	-	9	<1	6
2	Rb	-	15	<1	14
3	K	-	19	<1	15
4	NBu ₄	-	25	<1	11
5	Cs	AgOTf	100	45	29

^a Yields determined by GC based on an average of at least two runs. MF and PhI(OPiv)₂ were prestirred at 60 °C for 1 h in CH₂Cl₂ prior to addition of the rest of the reagents.

Scheme 2.12. Fluorination of 8-Methylquinoline with CsF as Fluoride Source



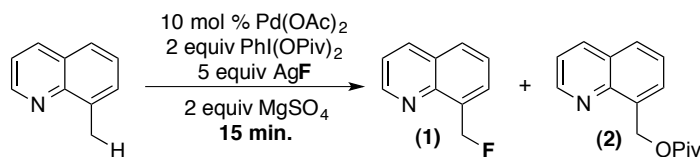
2.5 Rapid Fluorination for Positron Emission Tomography (PET)

We were also interested in addressing a specific challenge for the application of this chemistry to PET Imaging, which is the need for short reaction times. The reactions developed herein are highly desirable for PET as they use nucleophilic (rather than electrophilic) fluoride. Higher specific activity of the ¹⁸F would thus be possible with ¹⁸F over ¹⁸F⁺ reagents.¹⁸ However, short reaction times are still necessary.

The optimal conditions in Table 2.1 require 24 h to achieve maximum yield. Such long reaction times are undesirable for PET imaging applications because of the time constraints due to the half-life of ¹⁸F. Thus, we also examined a variety of approaches to accelerate this transformation. Gratifyingly, when the temperature was

increased to 80 °C, a 41% yield of product **1** could be obtained after just 15 min under the PhI(OPiv)₂/AgF conditions (Table 2.5). Increasing the temperature to 100 °C led to more of product **2** than the desired fluorinated product (entry 5).

Table 2.5 Rapid Fluorination at Multiple Temperatures for PET Imaging



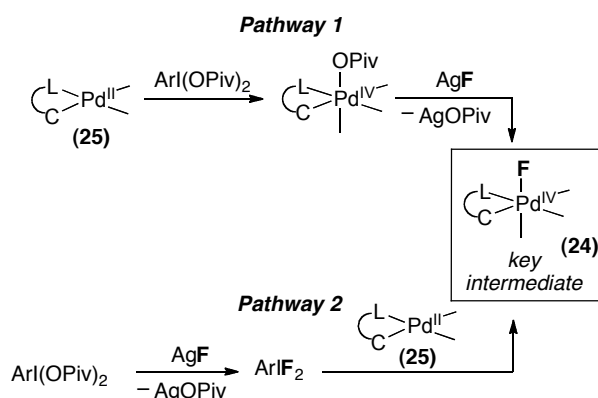
entry	temperature (°C)	conversion (%)	yield (%) ^a	
			1	2
1	60	55	29	8
2	70	69	32	26
3	80	81	41	32
4	90	94	42	43
5	100	96	39	45

^a Yields determined by GC based on an average of at least two runs.

2.6 Mechanistic Insights

We hypothesize that high valent Pd-alkyl fluorides of general structure **24** are key intermediates in this process. There are at least two possible pathways for accessing such species under the current reaction conditions. A first route would involve the oxidation of cyclometalated Pd^{II} complex **25** by PhI(OPiv)₂ followed by ligand substitution of pivalate for fluoride at the resultant Pd^{IV} intermediate (Scheme 2.13, pathway 1). A second pathway would proceed via initial substitution of pivalate for fluoride at the iodine(III) center followed by oxidation of **25** with PhIF₂ (Scheme 2.13, pathway 2). Notably, a recent report by DiMugno demonstrated that the treatment of PhI(OAc)₂ with rigorously dry TBAF affords PhIF₂ in high yield.¹⁹ This precedent suggests the potential plausibility of pathway 2.

Scheme 2.13. Two Possible routes to **24** from **25**, AgF, and ArI(OPiv)₂



To gain preliminary insights into the mechanism, we monitored the reaction by ¹⁹F NMR spectroscopy using iodotoluene dipivalate (*p*-MeC₆H₄I(OPiv)₂, **26**) as the oxidant. (Under our standard reaction conditions **26** performs nearly identically to PhI(OPiv)₂, providing **1** and **2** in 63% and 19% yield, respectively, in the Pd-catalyzed C–H fluorination of 8-methylquinoline.) Analysis of the crude reaction mixture after prestirring 1 equiv of **26** with 2.5 equiv of AgF for 30 min at 60 °C in CH₂Cl₂ showed a new resonance at -176 ppm (Figure 2.5). This signal corresponds to the literature value¹⁹ as well as to that obtained for an authentic sample of *p*-MeC₆H₄IF₂ (**27**), providing strong evidence that this iodine(III) reagent is formed under the reaction conditions.

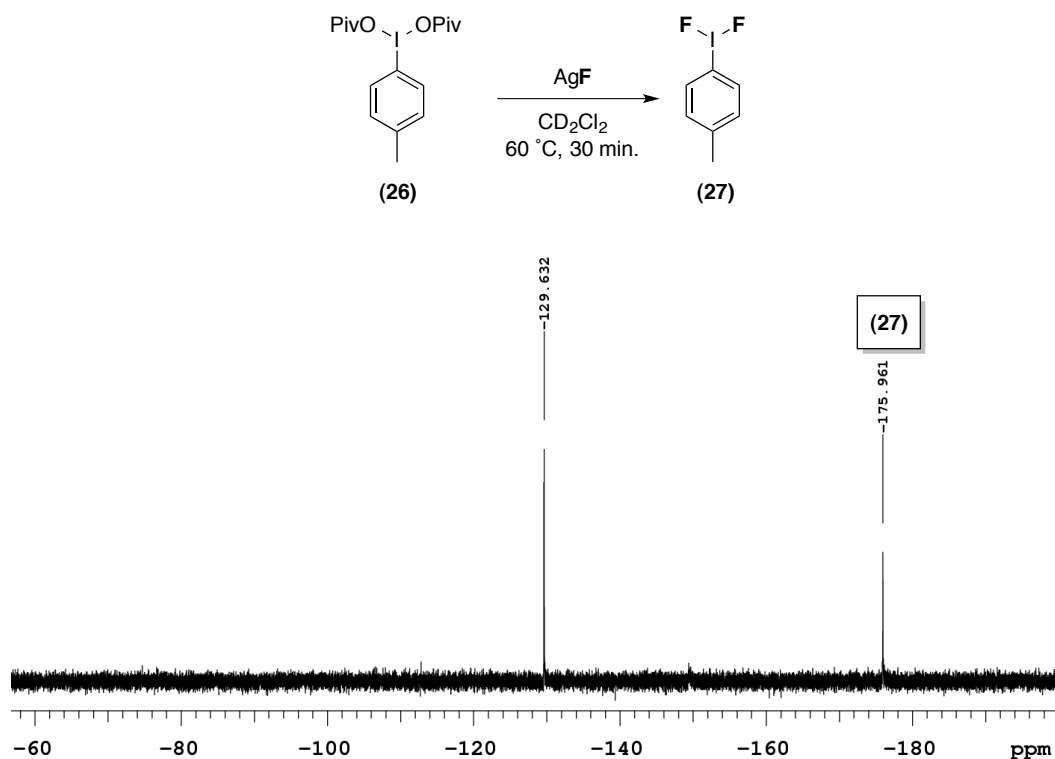


Figure 2.5. Reaction of Iodotoluene Dipivalate with AgF observation by ^{19}F NMR

A second resonance at -129.6 ppm is also visible in the ^{19}F NMR spectrum of the prestirred reaction mixture (Figure 2.5). The identity of this species has not been definitively established. However, the ^{13}C and ^1H NMR spectra of the prestirred reaction mixture increased our understanding about the contents of the reaction. The number of peaks in the ^{13}C NMR spectrum suggested there are three compounds present. One region of interest between 122 and 125 ppm, contained a singlet, doublet, and triplet (Figure 2.6). We believed the carbon under investigation to be the one directly attached to the iodine. We were able to match the singlet to an authentic sample of $\text{PhI}(\text{OPiv})_2$ (**28**), and the triplet to literature reports of PhIF_2 (**29**) in which they report fluorine splitting.²⁰ The doublet had a similar coupling constant to the triplet. Also there were two signals in the ^1H NMR spectrum with a chemical shift characteristic of *tert*-butyl protons. One matched $\text{PhI}(\text{OPiv})_2$ and the other we believed could correlate to the doublet in the ^{13}C NMR spectrum and the ^{19}F NMR peak at -129.6 ppm. These data led us to hypothesize the formation of **30** (Figure 2.6).

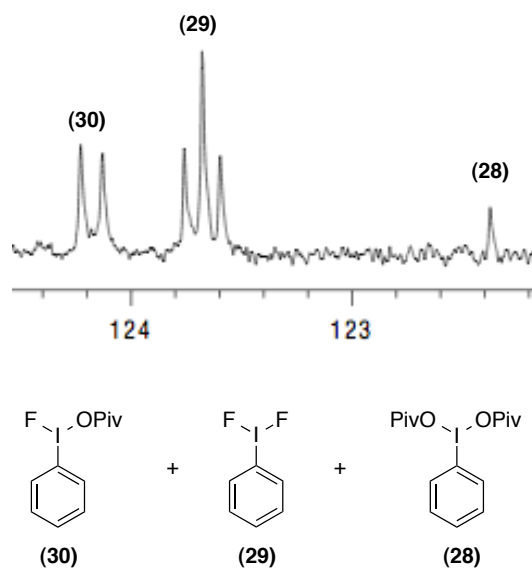
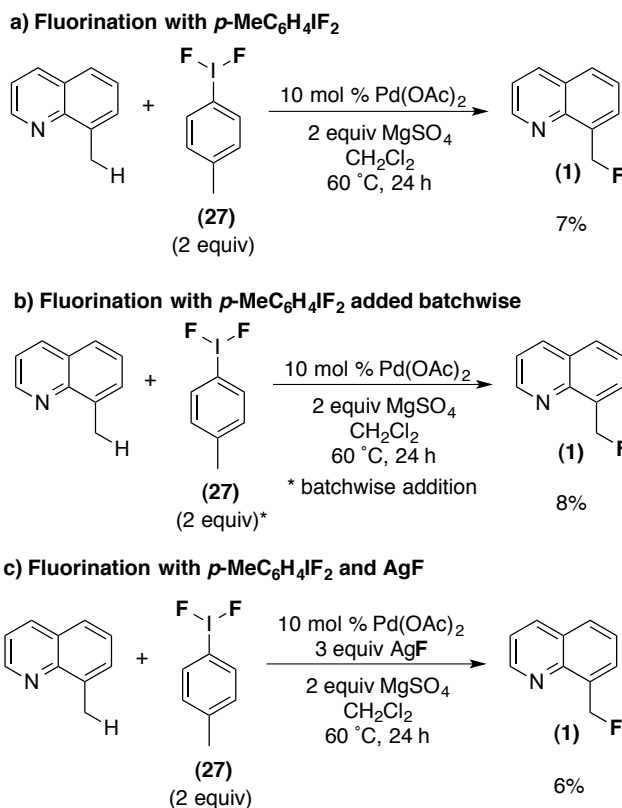


Figure 2.6. ^{13}C NMR and Proposed Components of Prestirred Reaction Mixture

We next independently synthesized a pure sample of **27**²¹ to establish whether it is effective at promoting C–H fluorination in the absence of **26**/AgF. Intriguingly, the use of 2 equiv of **27** in place of **26**/AgF under otherwise analogous conditions afforded only a 7% yield of **1** along with 42% recovered starting material (Scheme 2.14, part a). We hypothesized that this might be because this reagent is formed relatively slowly under the reaction conditions (whereas it was added all at once in the preceding experiment). Thus, we next examined the batchwise addition of **27** (three batches over 1 h in CH_2Cl_2). However, this experiment provided very similar results (Scheme 2.14, part b). We then hypothesized that AgF was playing a critical role in the reaction in combination with **27**, as there is excess AgF of 3 equiv in our standard reaction conditions. However, the combination of 2 equiv of **27** and 3 equiv of AgF did not enhance the yield, instead providing 6% of **1** and 27% starting material (Scheme 2.14, part c). *Collectively, these results suggest that, while ArIF_2 is present under these reaction conditions, it is not the primary active fluorinating reagent in this transformation.* More detailed investigations will be required to establish a comprehensive mechanistic understanding of this transformation. Further investigation of the compound showing the ^{19}F NMR resonance at -129.6 ppm, which has been hypothesized as $\text{PhI}(\text{OPiv})\text{F}$, should be conducted to determine if it is serving as the active fluorinating reagent in this transformation.

Scheme 2.14. Testing $p\text{-MeC}_6\text{H}_4\text{IF}_2$ as a Fluorinated Reagent in the Fluorination of 8-Methylquinoline



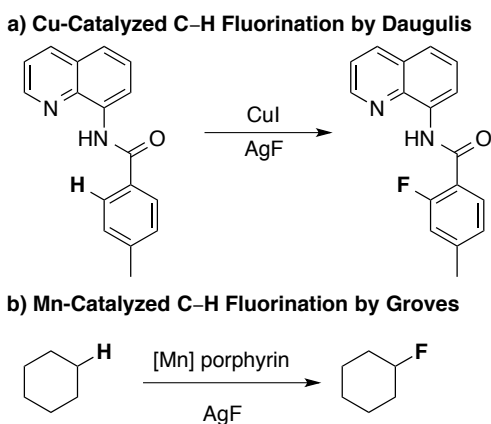
2.7 Conclusions

In summary, we have demonstrated a transformation that is, to our knowledge, the first example of palladium-catalyzed C–H fluorination using nucleophilic fluoride. The fluoride source can be either AgF or CsF (the latter in combination with AgOTf). The reactions typically proceed in modest to good yield over 24 h, and the use of a higher reaction temperature leads to the formation of significant quantities of fluorinated product in just 15 min. Ongoing work to probe the mechanism and expand the scope of this transformation to diverse C–H substrates would be not only beneficial for this system but instructive for the development of additional fluorination processes.

Since the publication of this work there have been a number of recent developments of metal-catalyzed and metal-mediated nucleophilic fluorination methods.

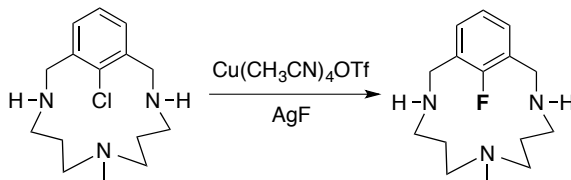
Scheme 2.15 shows examples by Daugulis and Groves of C–H fluorination.^{22,23} Both examples use AgF as their source of fluorine. Additionally, there are a number of nucleophilic fluorinating methods of aryl–X, as shown in Scheme 2.16, which are all catalyzed or mediated by copper.^{24,8,25} These methods can all undergo the desired fluorination transformation utilizing AgF, however, Sanford’s method can also use KF. These significant transformations reflect the rapid growth of fluorination in just a couple years. Additionally, the high number of methods using AgF is intriguing. Silver fluoride in many cases could be acting as a redox-active species, instead of simply a fluoride salt. However, mechanistic studies would be needed to further determine the role of AgF.

Scheme 2.15. Recent Transition Metal Catalyzed Nucleophilic C–H Fluorination Methods

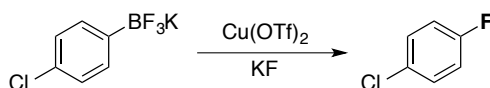


Scheme 2.16. Recent Methods of Copper Catalyzed/Mediated Nucleophilic Fluorination of ArX

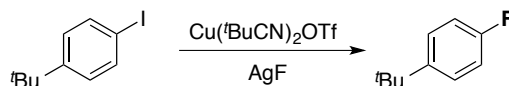
a) Cu-Catalyzed Fluorination of ArCl by Ribas



b) Cu-Mediated Fluorination of ArBF_3K by Sanford



c) Cu-Mediated Fluorination of ArX by Hartwig



2.8 Experimental Procedures and Characterization of Data

General Procedures

NMR spectra were obtained on a Varian vnmrs 700 (699.76 MHz for ^1H ; 175.95 MHz for ^{13}C), Varian vnmrs 500 (500.03 MHz for ^1H ; 125.72 MHz for ^{13}C ; 470.56 MHz for ^{19}F) or Varian Inova 400 (399.96 MHz for ^1H ; 100.71 MHz for ^{13}C ; 375.94 MHz for ^{19}F) spectrometer. ^1H NMR chemical shifts are reported in parts per million (ppm), with the residual solvent peak used as an internal reference. Multiplicities are reported as follows: singlet (s), doublet (d), doublet of doublets (dd), doublet of doublets of doublets (ddd), doublet of triplets (dt), triplet (t), and multiplet (m). IR spectra were obtained on a Perkin-Elmer Spectrum BX FT-IR spectrometer.

Materials and Methods

The substrates 8-methyl-5-nitroquinoline,²⁶ 5-fluoro-8-methylquinoline,²⁶ 5-bromo-8-methylquinoline,²⁶ 5-methoxy-8-methylquinoline,²⁶ 5-iodo-8-methylquinoline,²⁷ 8-methylquinoline-5-carbonitrile,²⁷ methyl 8-methylquinoline-5-carboxylate,²⁸ and 5,8-dimethylquinoline²⁹ were prepared according to literature procedures. The substrate 8-

methyl-5-phenylquinoline was prepared by Pd-catalyzed Suzuki coupling between phenylboronic acid and 5-bromo-8-methylquinoline.³⁰ The substrate 7-bromo-8-methylquinoline was prepared by the reaction of 3-bromo-2-methylaniline with glycerine.²⁹ 8-Methylquinoline was obtained from Oakwood Products and used as received. $\text{PhI}(\text{OPiv})_2$ was prepared by the reaction of $\text{PhI}(\text{OAc})_2$ with trimethylacetic acid according to a literature procedure.³¹ Iodosobenzene was prepared by the reaction of $\text{PhI}(\text{OAc})_2$ with sodium hydroxide.³² $\text{PhI}(\text{OTf})(\text{OH})$ and CsF were obtained from Matrix Scientific. $\text{PhI}(\text{O}_2\text{CCF}_3)_2$, $\text{PhI}(\text{OAc})_2$, $\text{MesI}(\text{OAc})_2$ were obtained from Acros, Sigma-Aldrich, and TCI America, respectively. All other oxidants were synthesized from $\text{PhI}(\text{OAc})_2$ with the corresponding acid.³¹ $\text{Pd}(\text{OAc})_2$, AgF , AgOTf , and MgSO_4 were obtained from Pressure Chemical, Oakwood Products, SynQuest Labs, and Fisher Scientific, respectively. All were used as received unless otherwise noted. Dichloromethane and other solvents were obtained from Fisher Scientific and used as received. Flash chromatography was performed on Dynamic Adsorbents silica gel 60A (0.032–0.063 mm particle size, 230–400 mesh) or Biotage® silica gel (0.050 mm particle size) and thin layer chromatography was performed on EMD Chemicals Inc. plates pre-coated with silica gel 60 F₂₅₄.

Experimental Details

Synthesis of Products in Table 2.1 (entries 1-4): Non-prestirred conditions

On the benchtop, $\text{PhI}(\text{O}_2\text{CR})_2$ (0.38 mmol, 2.0 equiv), MgSO_4 (45.9 mg, 0.38 mmol, 2.0 equiv), $\text{Pd}(\text{OAc})_2$ (4.3 mg, 0.02 mmol, 0.10 equiv), and AgF (121 mg, 0.96 mmol, 5.0 equiv) were weighed into a 4 mL vial. 8-Methylquinoline (27.4 mg, 0.19 mmol, 1.0 equiv) and solvent (1.9 mL) were added, and the vial was sealed with a Teflon-lined cap (with Teflon tape covering the threads of the vial). This mixture was heated at 60 °C for 24 h. GC yields were obtained by analysis of the crude reaction mixture using hexadecane as a standard.

Synthesis of Products in Table 2.1(entry 5) and Table 2.4(entries 1-4): Prestirred conditions

On the benchtop, $\text{PhI}(\text{OPiv})_2$ (154 mg, 0.38 mmol, 2.0 equiv) and MF (0.96 mmol, 5.0 equiv) were weighed into a 4 mL vial, and DCM (1.9 mL) was added. The vial was sealed with a Teflon-lined cap (with Teflon tape covering the threads of the vial), and this mixture was heated at 60 °C for 1 h. The vial was removed from the heat and allowed to cool to rt (~5 min). Then $\text{Pd}(\text{OAc})_2$ (4.3 mg, 0.02 mmol, 0.10 equiv), MgSO_4 (45.9 mg, 0.38 mmol, 2.0 equiv), and 8-methylquinoline (27.4 mg, 0.19 mmol, 1.0 equiv) were added. The vial was sealed with a Teflon-lined cap and heated at 60 °C for an additional 24 h. GC yields were obtained by analysis of the crude reaction mixture using hexadecane as a standard.

Synthesis of Products in Table 2.5: Rapid Fluorination

On the benchtop, $\text{PhI}(\text{OPiv})_2$ (154 mg, 0.38 mmol, 2.0 equiv), MgSO_4 (45.9 mg, 0.38 mmol, 2.0 equiv), $\text{Pd}(\text{OAc})_2$ (4.3 mg, 0.02 mmol, 0.10 equiv), and AgF (121 mg, 0.96 mmol, 5.0 equiv) were weighed into a 4 mL vial. 8-Methylquinoline (27.4 mg, 0.19 mmol, 1.0 equiv) and DCM (1.9 mL) were added and the vial was sealed with a Teflon-lined cap (with Teflon tape covering the threads of the vial). This mixture was heated for 15 min at the appropriate temperature and the cooled to rt. GC yields were obtained by analysis of the crude reaction mixture using hexadecane as a standard.

Synthesis of Products in Table 2.4(entry 5) and Scheme 2.12: CsF Fluorination

On the benchtop, $\text{PhI}(\text{OPiv})_2$ (154 mg, 0.38 mmol, 2.0 equiv), CsF (145 mg, 0.96 mmol, 5.0 equiv), and AgOTf (196 mg, 0.76 mmol, 4.0 equiv) were weighed into a 4 mL vial, and DCM (1.9 mL) was added. The vial was sealed with a Teflon-lined cap (with Teflon tape covering the threads of the vial), and this mixture was heated at 60 °C for 1 h. The vial was removed from the heat and allowed to cool to rt (~5 min). Then $\text{Pd}(\text{OAc})_2$ (4.3 mg, 0.02 mmol, 0.10 equiv), MgSO_4 (45.9 mg, 0.38 mmol, 2.0 equiv), and 8-methylquinoline (27.4 mg, 0.19 mmol, 1.0 equiv) were added. The vial was sealed with a Teflon-lined cap and heated at 60 °C for an additional 24 h. GC yields were obtained by analysis of the crude reaction mixture using hexadecane as a standard.

Observation of p -MeC₆H₄IF₂ by ¹⁹F NMR Spectroscopy

On the benchtop, p -MeC₆H₄I(OPiv)₂ (21.0 mg, 0.05 mmol, 1.0 equiv) and AgF (15.9 mg, 0.13 mmol, 2.5 equiv) were weighed into a 4 mL vial, and CD₂Cl₂ (0.5 mL) was added. The vial was sealed with a Teflon-lined cap (with Teflon tape covering the threads of the vial), and this mixture was heated at 60 °C for 30 min. The reaction mixture was cooled to rt and was then transferred to an NMR tube for analysis. The ¹⁹F NMR spectrum of this crude mixture is shown in section 2.6.

Testing p -MeC₆H₄IF₂ as fluorination reagent

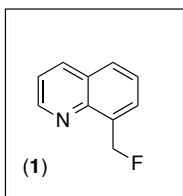
p -MeC₆H₄IF₂ (49.2 mg, 0.19 mmol, 2.0 equiv, stored in glovebox, but reaction was set up on the benchtop), MgSO₄ (23.1 mg, 0.19 mmol, 2.0 equiv), and Pd(OAc)₂ (2.2 mg, 0.01 mmol, 0.10 equiv) were weighed into a 4 mL vial. Dry DCM (0.96 mL) was added and the vial was sealed with a Teflon-lined cap (with Teflon tape covering the threads of the vial) and removed from the glovebox. 8-Methylquinoline (13.8 mg, 0.10 mmol, 1.0 equiv) was added through the septum vial cap, and the mixture was heated at 60 °C for 24 h. GC yields were obtained by analysis of the crude reaction mixture using hexadecane as a standard. Notably, nearly identical results were obtained when this reaction was set up in the glovebox.

Synthesis and Characterization of Products in Table 2.2 and Table 2.3

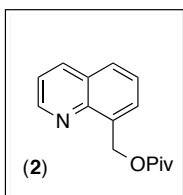
General Procedure. On the benchtop, PhI(OPiv)₂ (650 mg, 1.60 mmol, 2.0 equiv) and AgF (508 mg, 4.00 mmol, 5.0 equiv) were weighed into a 20 mL vial, and solvent (8.0 mL) was added. The vial was sealed with a Teflon-lined cap (with Teflon tape covering the threads of the vial), and this mixture was heated at 60 °C for 1 h. The vial was removed from the heat and allowed to cool to rt (~10 min). Then Pd(OAc)₂ (18 mg, 0.08 mmol, 0.10 equiv), MgSO₄ (193 mg, 1.60 mmol, 2.0 equiv), and substrate (0.80 mmol, 1.0 equiv) were added. The vial was sealed with a Teflon-lined cap and heated at 60 °C for an additional 16-28 h. GC yields were obtained by analysis of the crude reaction mixture using hexadecane as a standard. The reaction mixture was then filtered through a plug of Celite, the plug was washed with CH₂Cl₂ (100 mL), and the filtrate was

concentrated under vacuum. The resulting crude product was purified by chromatography on silica gel.

8-Methylquinoline. 8-Methylquinoline was obtained from Oakwood Products and used as received.

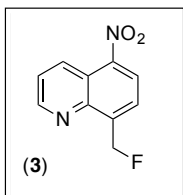


8-Methylquinoline (115 mg, 0.80 mmol, 1.0 equiv) was used as the substrate. The solvent was dichloromethane (8.0 mL), and the reaction was heated for 16 h. GC analysis of the crude reaction mixture showed 67% yield of **1** and 16% yield of **2**. The crude brown oil was purified by chromatography on silica gel with a gradient of 0%-8% EtOAc in CH₂Cl₂. Product **1** was obtained as a viscous yellow oil (63.0 mg, 49% isolated yield, R_f = 0.49 in 96% CH₂Cl₂/4% EtOAc). ¹H NMR (500 MHz, CDCl₃): δ 8.93 (dd, *J* = 4.2, 1.7 Hz, 1H), 8.18 (dd, *J* = 8.2, 1.8 Hz, 1H), 7.83-7.81 (multiple peaks, 2H), 7.58 (t, *J* = 7.7 Hz, 1H), 7.44 (dd, *J* = 8.3, 4.2 Hz, 1H), 6.15 (d, *J*_{HF} = 48 Hz, 2H). ¹³C{¹H} NMR (175 MHz, CDCl₃): δ 150.1, 145.7 (d, *J*_{CF} = 3.3 Hz), 136.4, 134.9 (d, *J*_{CF} = 16 Hz), 128.4 (d, *J*_{CF} = 2.1 Hz), 128.2, 127.6 (d, *J*_{CF} = 10 Hz), 126.5, 121.6, 82.0 (d, *J*_{CF} = 165 Hz). ¹⁹F NMR (470 MHz, CDCl₃): δ -219.2 (t, *J*_{FH} = 48 Hz). IR (thin film, CH₂Cl₂): 2924, 1596, 1581, 1500, 1353 cm⁻¹. HRMS [M+H]⁺ Calcd for C₁₀H₈NF: 161.0641; Found: 161.0638.

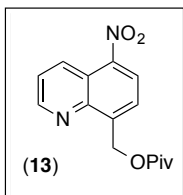


Product **2** was also obtained from this transformation as a viscous clear oil (21.6 mg, 11% isolated yield, R_f = 0.29 in 96% CH₂Cl₂/4% EtOAc). ¹H NMR (700 MHz, CDCl₃): δ 8.94 (dd, *J* = 4.2, 1.7 Hz, 1H), 8.17 (dd, *J* = 8.3, 1.7 Hz, 1H), 7.78 (d, *J* = 8.1 Hz, 1H), 7.74 (d, *J* = 6.8 Hz, 1H), 7.54 (app. t, *J* = 7.7 Hz, 1H), 7.43 (dd, *J* = 8.3, 4.2 Hz, 1H), 5.87 (s, 2H), 1.28 (s, 9H). ¹³C{¹H} NMR (175 MHz, CDCl₃): δ 178.6, 149.9, 146.1, 136.4, 135.1, 128.3, 127.8, 127.6, 126.4, 121.5, 62.9, 39.2, 27.5. IR (thin film, CH₂Cl₂): 2972, 1726, 1500, 1282, 1149 cm⁻¹. HRMS [M+H]⁺ Calcd for C₁₅H₁₇NO₂: 244.1332; Found: 244.1332.

8-Methyl-5-nitroquinoline. 8-Methyl-5-nitroquinoline was prepared according to a literature procedure.²⁶ NMR data matched that reported in the literature. ¹H and ¹³C NMR spectra for this substrate are provided below.



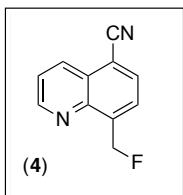
8-Methyl-5-nitroquinoline (151 mg, 0.80 mmol, 1.0 equiv) was used as the substrate. The solvent was dichloromethane (8.0 mL), and the reaction was heated for 24 h. GC analysis of the crude reaction mixture showed 61% yield of **3** and 6% yield of **13**. The orange solid was purified by chromatography on silica gel with a gradient of 0%-2% EtOAc in CH₂Cl₂. Product **3** was obtained as a light yellow solid (67.9 mg, 41% isolated yield, R_f = 0.55 in 99% CH₂Cl₂/1% EtOAc, mp = 143.9-148.6 °C). ¹H NMR (500 MHz, CDCl₃): δ 9.06 (dd, *J* = 8.8, 1.7 Hz, 1H), 8.99 (dd, *J* = 4.2, 1.7 Hz, 1H), 8.44 (d, *J* = 8.1 Hz, 1H), 7.93 (d, *J* = 8.1 Hz, 1H), 7.69 (dd, *J* = 8.8, 4.2 Hz, 1H), 6.22 (d, *J*_{HF} = 47 Hz, 2H). ¹³C{¹H} NMR (175 MHz, CDCl₃): δ 150.8, 145.2, 144.8 (d, *J*_{CF} = 3.5 Hz), 143.3 (d, *J*_{CF} = 18 Hz), 132.5, 124.8, 124.4, 123.9 (d, *J*_{CF} = 13 Hz), 120.9, 81.8 (d, *J*_{CF} = 170 Hz). ¹⁹F NMR (376 MHz, CDCl₃): δ -228.1 (t, *J*_{FH} = 47 Hz). IR (thin film, CH₂Cl₂): 3112, 1518, 1335 cm⁻¹. HRMS [M+H]⁺ Calcd for C₁₀H₇N₂O₂F: 206.0491; Found: 206.0491.



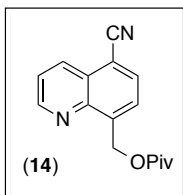
Product **13** was also obtained from this transformation as a yellow solid (22.2 mg, 10% isolated yield, R_f = 0.40 in 99% CH₂Cl₂/1% EtOAc, mp = 103.4-105.9 °C). ¹H NMR (500 MHz, CDCl₃): δ 9.04-9.01 (multiple peaks, 2H), 8.38 (d, *J* = 8.1 Hz, 1H), 7.79 (d, *J* = 8.1 Hz, 1H), 7.67 (dd, *J* = 8.7, 4.3 Hz, 1H), 5.91 (s, 2H), 1.32 (s, 9H). ¹³C{¹H} NMR (125 MHz, CDCl₃): δ 178.2, 150.8, 145.6, 145.0, 143.3, 132.4, 124.6, 124.6, 124.3, 121.1, 62.8, 39.3, 27.5. IR (thin film, CH₂Cl₂): 2975, 1730, 1522, 1335, 1145 cm⁻¹. HRMS [M+H]⁺ Calcd for C₁₅H₁₆N₂O₄: 289.1183; Found: 289.1191.

8-Methylquinoline-5-carbonitrile. 8-Methylquinoline-5-carbonitrile was prepared according to a literature procedure.²⁷ ¹H NMR (500 MHz, CDCl₃): δ 9.05 (dd, *J* = 4.2, 1.7 Hz, 1H), 8.52 (dd, *J* = 8.6, 1.7 Hz, 1H), 7.88 (d, *J* = 7.3 Hz, 1H), 7.63-7.60 (multiple peaks, 2H), 2.88 (s, 3H). ¹³C{¹H} NMR (125 MHz, CDCl₃): δ 150.9, 146.8, 144.6, 133.8,

133.0, 129.1, 127.9, 123.2, 117.3, 108.3, 18.9. Mp = 108.5-111.3 °C. IR (thin film, CH₂Cl₂): 2928, 2222, 1501 cm⁻¹. HRMS [M+H]⁺ Calcd for C₁₁H₈N₂: 169.0760; Found: 169.0761.



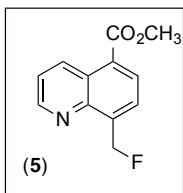
8-Methylquinoline-5-carbonitrile (135 mg, 0.80 mmol, 1.0 equiv) was used as the substrate. The solvent was dichloromethane (8.0 mL), and the reaction was heated for 16 h. GC analysis of the crude reaction mixture showed 67% yield of **4** and 12% yield of **14**. The crude mixture was purified by chromatography on silica gel with a gradient of 0%-4% EtOAc in CH₂Cl₂. Product **4** was obtained as a tan solid (105 mg, 70% isolated yield, R_f = 0.61 in 98% CH₂Cl₂/2% EtOAc, mp = 149.8-151.0 °C). ¹H NMR (700 MHz, CDCl₃): δ 9.01 (dd, *J* = 4, 1.5 Hz, 1H), 8.57 (dd, *J* = 8.4, 1.5 Hz, 1H), 8.03 (d, *J* = 7.4 Hz, 1H), 7.90 (d, *J* = 7.4 Hz, 1H), 7.66 (dd, *J* = 8.4, 4 Hz, 1H), 6.21 (d, *J*_{HF} = 47 Hz, 2H). ¹³C{¹H} NMR (100 MHz, CDCl₃): δ 151.3, 144.3 (d, *J*_{CF} = 4.0 Hz), 141.7 (d, *J*_{CF} = 18 Hz), 133.8, 133.1, 127.5, 125.1 (d, *J*_{CF} = 12 Hz), 123.7, 116.8, 110.1, 81.5 (d, *J*_{CF} = 169 Hz). ¹⁹F NMR (376 MHz, CDCl₃): δ -227.5 (m, *J*_{FH} = 47 Hz). IR (thin film, CH₂Cl₂): 2227, 1500, 1440, 1353 cm⁻¹. HRMS [M+H]⁺ Calcd for C₁₁H₇N₂F: 186.0593; Found: 186.0592.



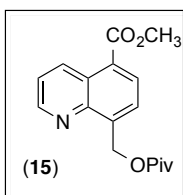
Product **14** was also obtained from this transformation as a white solid (19.5 mg, 9% isolated yield, R_f = 0.41 in 98% CH₂Cl₂/2% EtOAc, mp = 94.4-97.9 °C). ¹H NMR (700 MHz, CDCl₃): δ 9.04 (m, 1H), 8.54 (dd, *J* = 8.4, 1.5 Hz, 1H), 7.98 (d, *J* = 7.5 Hz, 1H), 7.76 (dd, *J* = 7.5, 0.7 Hz, 1H), 7.64 (dd, *J* = 8.4, 4.2 Hz, 1H), 5.89 (s, 2H), 1.31 (s, 9H). ¹³C{¹H} NMR (175 MHz, CDCl₃): δ 178.3, 151.3, 145.2, 141.8, 133.7, 133.0, 127.7, 125.8, 123.6, 116.9, 109.8, 62.4, 39.2, 27.5. IR (thin film, CH₂Cl₂): 2975, 2227, 1731, 1501, 1158 cm⁻¹. HRMS [M+H]⁺ Calcd for C₁₆H₁₆N₂O₂: 269.1285; Found: 269.1280.

Methyl 8-methylquinoline-5-carboxylate. Methyl 8-methylquinoline-5-carboxylate was prepared according to a literature procedure.²⁸ ¹H NMR (500 MHz, CDCl₃): δ 9.38 (dd, *J* = 8.8, 1.7 Hz, 1H), 8.97 (dd, *J* = 4.2, 1.7 Hz, 1H), 8.20 (d, *J* = 7.6 Hz, 1H), 7.59 (d, *J* = 7.6 Hz, 1H), 7.52 (dd, *J* = 8.8, 4.2 Hz, 1H), 3.99 (s, 3H), 2.87 (s, 3H). ¹³C{¹H} NMR

(125 MHz, CDCl₃): δ 167.3, 149.5, 147.4, 143.8, 134.8, 131.0, 128.5, 127.2, 124.9, 122.5, 52.4, 19.2. Mp = 55.4-57.8 °C. IR (thin film, CH₂Cl₂): 2955, 1712, 1505 cm⁻¹. HRMS [M+H]⁺ Calcd for C₁₂H₁₁NO₂: 202.0863; Found: 202.0865.

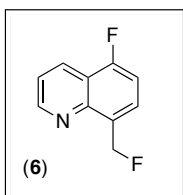


Methyl 8-methylquinoline-5-carboxylate (161 mg, 0.80 mmol, 1.0 equiv) was used as the substrate. The solvent was dichloromethane (8.0 mL), and the reaction was heated for 24 h. GC analysis of the crude reaction mixture showed 59% yield of **5** and 10% yield of **15**. The crude mixture was purified by chromatography on silica gel with a gradient of 1%-8% EtOAc in CH₂Cl₂. Product **5** was obtained as an off-white solid (104 mg, 59% isolated yield, R_f = 0.52 in 96% CH₂Cl₂/4% EtOAc, mp = 94.0-94.8 °C). ¹H NMR (500 MHz, CDCl₃): δ 9.38 (dd, *J* = 8.8, 1.5 Hz, 1H), 8.92 (dd, *J* = 4.2, 1.5 Hz, 1H), 8.33 (d, *J* = 7.6 Hz, 1H), 7.86 (d, *J* = 7.6 Hz, 1H), 7.55 (dd, *J* = 8.8, 4.2 Hz, 1H), 6.20 (d, *J*_{HF} = 47 Hz, 2H), 4.01 (s, 3H). ¹³C{¹H} NMR (175 MHz, CDCl₃): δ 167.5, 149.9, 145.1 (d, *J*_{CF} = 3.3 Hz), 140.9 (d, *J*_{CF} = 18 Hz), 134.8, 130.9, 126.8, 126.5 (d, *J*_{CF} = 1.4 Hz), 124.6 (d, *J*_{CF} = 12 Hz), 122.9, 81.5 (d, *J*_{CF} = 167 Hz), 52.6. ¹⁹F NMR (376 MHz, CDCl₃): δ -226.3 (t, *J*_{FH} = 47 Hz). IR (thin film, CH₂Cl₂): 2955, 1714, 1506 cm⁻¹. HRMS [M+H]⁺ Calcd for C₁₂H₁₀NO₂F: 220.0768; Found: 220.0772.

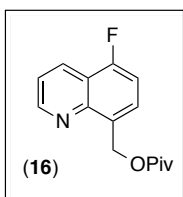


Product **15** was also obtained from this reaction as an off-white solid (25.4 mg, 11% isolated yield, R_f = 0.27 in 96% CH₂Cl₂/4% EtOAc, mp = 78.8-84.3 °C). ¹H NMR (700 MHz, CDCl₃): δ 9.36 (dd, *J* = 8.7, 1.7 Hz, 1H), 8.95 (dd, *J* = 4.0, 1.7 Hz, 1H), 8.29 (d, *J* = 7.7 Hz, 1H), 7.73 (dd, *J* = 7.7, 0.9 Hz, 1H), 7.54 (dd, *J* = 8.7, 4.0 Hz, 1H), 5.90 (s, 2H), 4.01 (s, 3H), 1.31 (s, 9H). ¹³C{¹H} NMR (175 MHz, CDCl₃): δ 178.4, 167.1, 149.9, 145.9, 141.0, 134.7, 130.7, 127.0, 126.3, 125.3, 122.8, 63.0, 52.5, 39.2, 27.6. IR (thin film, CH₂Cl₂): 2973, 1717, 1504, 1159 cm⁻¹. HRMS [M+H]⁺ Calcd for C₁₇H₁₉NO₄: 302.1387; Found: 302.1397.

5-Fluoro-8-methylquinoline. 5-Fluoro-8-methylquinoline was prepared according to a literature procedure.²⁶ NMR data matched that reported in the literature. ¹H and ¹³C NMR spectra for this substrate are provided below.

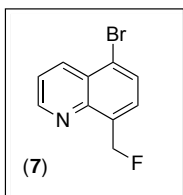


5-Fluoro-8-methylquinoline (129 mg, 0.80 mmol, 1.0 equiv) was used as the substrate. The solvent was dichloromethane (8.0 mL), and the reaction was heated for 16 h. GC analysis of the crude reaction mixture showed 44% yield of **6** and 25% yield of **16**. The crude mixture was purified by chromatography on silica gel with a gradient of 1%-8% EtOAc in CH₂Cl₂. Product **6** was obtained as a tan solid (43.3 mg, 30% isolated yield, R_f = 0.49 in 96% CH₂Cl₂/4% EtOAc, mp = 52.9-57.0 °C). ¹H NMR (700 MHz, CDCl₃): δ 9.00 (m, 1H), 8.47 (d, *J* = 8.5 Hz, 1H), 7.78 (t, *J* = 6.9 Hz, 1H), 7.53 (dd, *J* = 8.5, 4.2 Hz, 1H), 7.27 (m, 1H), 6.08 (d, *J*_{HF} = 48 Hz, 2H). ¹³C{¹H} NMR (175 MHz, CDCl₃): δ 158.2 (dd, *J*_{CF} = 256, 2.6 Hz), 151.0, 146.3 (t, *J*_{CF} = 3.4 Hz), 130.9 (dd, *J*_{CF} = 17, 4.4 Hz), 129.7 (d, *J*_{CF} = 4.8 Hz), 128.0 (t, *J*_{CF} = 9.6 Hz), 121.7 (d, *J*_{CF} = 2.6 Hz), 119.1 (d, *J*_{CF} = 16 Hz), 120.0 (d, *J*_{CF} = 20 Hz), 81.5 (d, *J*_{CF} = 165 Hz). ¹⁹F NMR (376 MHz, CDCl₃): δ -121.9, -216.0 (t, *J*_{FH} = 48 Hz). IR (thin film, CH₂Cl₂): 2917, 1597 cm⁻¹. HRMS [M+H]⁺ Calcd for C₁₀H₇NF₂: 180.0619; Found: 180.0616.

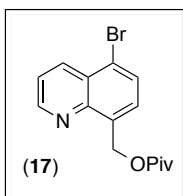


Product **16** was also obtained from this reaction as a clear oil (50.5 mg, 24% isolated yield, R_f = 0.27 in 96% CH₂Cl₂/4% EtOAc). ¹H NMR (500 MHz, CDCl₃): δ 8.97 (dd, *J* = 4.2, 2 Hz, 1H), 8.43 (dd, *J* = 8.4, 2 Hz, 1H), 7.68 (m, 1H), 7.49 (dd, *J* = 8.4, 4.2 Hz, 1H), 7.21 (m, 1H), 5.78 (s, 2H), 1.25 (s, 9H). ¹³C{¹H} NMR (175 MHz, CDCl₃): δ 178.6, 157.7 (d, *J*_{CF} = 255 Hz), 150.7, 146.7 (d, *J*_{CF} = 3.3 Hz), 131.1 (d, *J*_{CF} = 4.8 Hz), 129.6 (d, *J*_{CF} = 4.8 Hz), 127.8 (d, *J*_{CF} = 8.8 Hz), 121.5 (d, *J*_{CF} = 2.8 Hz), 119.1 (d, *J*_{CF} = 16 Hz), 109.8 (d, *J*_{CF} = 20 Hz), 62.5, 39.2, 27.5. IR (thin film, CH₂Cl₂): 2974, 1728, 1156 cm⁻¹. HRMS [M+H]⁺ Calcd for C₁₅H₁₆NO₂F: 262.1238; Found: 262.1237.

5-Bromo-8-methylquinoline. 5-Bromo-8-methylquinoline was prepared according to a literature procedure.²⁶ NMR data matched that reported in the literature. ¹H and ¹³C NMR spectra for this substrate are provided below.



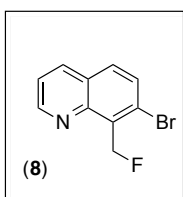
5-Bromo-8-methylquinoline (178 mg, 0.80 mmol, 1.0 equiv) was used as the substrate. The solvent was dichloromethane (8.0 mL), and the reaction was heated for 16 h. GC analysis of the crude reaction mixture showed 53% yield of **7** and 19% yield of **17**. The crude mixture was purified by chromatography on silica gel with a gradient of 0%-4% EtOAc in CH₂Cl₂. Product **7** was obtained as a white solid (83.8 mg, 44% isolated yield, R_f = 0.65 in 98% CH₂Cl₂/2% EtOAc, mp = 67.7-69.0 °C). ¹H NMR (700 MHz, CDCl₃): δ 8.93 (dd, *J* = 4.2, 1.6 Hz, 1H), 8.57 (dd, *J* = 8.6, 1.6 Hz, 1H), 7.87 (d, *J* = 7.7 Hz, 1H), 7.69 (d, *J* = 7.7 Hz, 1H), 7.55 (dd, *J* = 8.6, 4.2 Hz, 1H), 6.10 (d, *J*_{HF} = 47 Hz, 2H). ¹³C{¹H} NMR (175 MHz, CDCl₃): δ 150.5, 146.0, 136.1, 135.1 (d, *J*_{CF} = 17 Hz), 130.3, 127.6 (d, *J*_{CF} = 11 Hz), 127.5, 122.7, 122.2, 81.7 (d, *J*_{CF} = 167 Hz). ¹⁹F NMR (376 MHz, CDCl₃): δ -221.4 (t, *J*_{FH} = 47 Hz). IR (thin film, CH₂Cl₂): 1569, 1496, 1350 cm⁻¹. HRMS [M]⁺ Calcd for C₁₀H₇NFBr: 238.9746; Found: 238.9754.



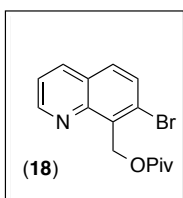
Product **17** was also obtained from this reaction as an off-white solid (33.4 mg, 13% isolated yield, R_f = 0.53 in 98% CH₂Cl₂/2% EtOAc, mp = 65.0-67.4 °C). ¹H NMR (500 MHz, CDCl₃): δ 8.94 (dd, *J* = 4.2, 1.7 Hz, 1H), 8.55 (dd, *J* = 8.6, 1.7 Hz, 1H), 7.82 (d, *J* = 7.8 Hz, 1H), 7.59 (d, *J* = 7.8 Hz, 1H), 7.54 (dd, *J* = 8.6, 4.2 Hz, 1H), 5.80 (s, 2H), 1.27 (s, 9H). ¹³C{¹H} NMR (175 MHz, CDCl₃): δ 178.5, 150.5, 146.7, 135.8, 135.3, 130.2, 127.9, 127.6, 122.6, 121.7, 62.6, 39.2, 27.5. IR (thin film, CH₂Cl₂): 2973, 1729, 1156 cm⁻¹. HRMS [M+H]⁺ Calcd for C₁₅H₁₆NO₂Br: 322.0437; Found: 322.0432.

7-Bromo-8-methylquinoline. 7-Bromo-8-methylquinoline was prepared according to the following procedure. 3-Bromo-2-methylaniline (6.3 g, 33.9 mmol, 1.0 equiv) and NaI (66.0 mg, 0.441 mmol, 0.013 equiv) were dissolved in H₂SO₄ (8.7 mL) and water (2.2 mL) in a round-bottomed flask. The reaction was heated to 145 °C, and glycerol (3.7 g)

was added via addition funnel over 1.5 h. The reaction stirred for 2 h. Once cooled, the crude mixture was extracted twice with toluene. The organic phase was washed with water and brine and dried (MgSO₄). The filtrate was concentrated under vacuum, and the residue was purified by chromatography on silica gel eluting with hexane/EtOAc (1:1). The product was obtained as a beige solid (5.3 g, 71% yield, R_f = 0.53, mp = 50.9-52.5 °C). ¹H NMR (500 MHz, CDCl₃): δ 8.94 (dd, *J* = 4.2, 1.7 Hz, 1H), 8.11 (dd, *J* = 8, 2 Hz, 1H), 7.69 (d, *J* = 8.8 Hz, 1H), 7.53 (d, *J* = 8.8 Hz, 1H), 7.42 (dd, *J* = 8, 4 Hz, 1H), 2.93 (s, 3H). ¹³C{¹H} NMR (125 MHz, CDCl₃): δ 150.1, 147.8, 137.3, 136.6, 131.0, 127.4, 126.6, 126.1, 121.2, 17.8. IR (thin film, CH₂Cl₂): 2918, 1604, 1490 cm⁻¹. HRMS [M+H]⁺ Calcd for C₁₀H₈NBr: 221.9913; Found: 221.9914.



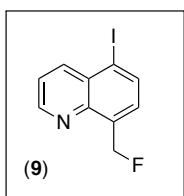
7-Bromo-8-methylquinoline (178 mg, 0.80 mmol, 1.0 equiv) was used as the substrate. The solvent was dichloromethane (8.0 mL), and the reaction was heated for 16 h. GC analysis of the crude reaction mixture showed 49% yield of **8** and 26% yield of **18**. The crude mixture was purified by chromatography on silica gel with a gradient of 0%-4% EtOAc in CH₂Cl₂. Product **8** was obtained as a white solid (80.7 mg, 42% isolated yield, R_f = 0.48 in 98% CH₂Cl₂/2% EtOAc, mp = 90.3-94.5 °C). ¹H NMR (500 MHz, CDCl₃): δ 9.01 (dd, *J* = 4, 2 Hz, 1H), 8.16 (dd, *J* = 8.3, 2 Hz, 1H), 7.78-7.73 (multiple peaks, 2H), 7.48 (dd, *J* = 8.3, 4 Hz, 1H), 6.30 (d, *J*_{HF} = 47 Hz, 2H). ¹³C{¹H} NMR (175 MHz, CDCl₃): δ 151.5, 147.8 (d, *J*_{CF} = 1.4 Hz), 136.4, 133.3 (d, *J*_{CF} = 14 Hz), 131.3 (d, *J*_{CF} = 3.3 Hz), 130.7 (d, *J*_{CF} = 4.8 Hz), 128.4 (d, *J*_{CF} = 6.2 Hz), 127.5 (d, *J*_{CF} = 1.9 Hz), 121.9, 79.5 (d, *J*_{CF} = 163 Hz). ¹⁹F NMR (470 MHz, CDCl₃): δ -209.8 (t, *J*_{FH} = 47 Hz). IR (thin film, CH₂Cl₂): 2985, 1570, 1488 cm⁻¹. HRMS [M+H]⁺ Calcd for C₁₀H₇NFBr: 239.9819; Found: 239.9821.



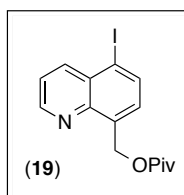
Product **18** was also obtained from this reaction as a light brown solid (68.2 mg, 26% isolated yield, R_f = 0.19 in 98% CH₂Cl₂/2% EtOAc, mp = 92.3-102.5 °C). ¹H NMR (700 MHz, CDCl₃): δ 8.96 (dd, *J* = 4.1, 1.7 Hz, 1H), 8.14 (dd, *J* = 8.2, 1.7 Hz, 1H), 7.74 (d, *J* = 8.9 Hz, 1H), 7.69 (d, *J* = 8.9 Hz, 1H), 7.45 (dd, *J* = 8.2, 4.1 Hz, 1H), 5.94 (s, 2H), 1.19 (s, 9H). ¹³C{¹H} NMR (175 MHz, CDCl₃): δ 178.6, 151.0, 147.8, 136.3, 134.2, 131.2, 129.7, 127.8, 127.4,

121.7, 61.7, 39.2, 27.5. IR (thin film, CH₂Cl₂): 2971, 1723, 1152 cm⁻¹. HRMS [M+H]⁺ Calcd for C₁₅H₁₆NO₂Br: 322.0437; Found: 322.0442.

5-Iodo-8-methylquinoline. 5-Iodo-8-methylquinoline was prepared according to a literature procedure.²⁷ ¹H NMR (500 MHz, CDCl₃): δ 8.90 (dd, *J* = 4.2, 1.7 Hz, 1H), 8.37 (dd, *J* = 8.6, 1.7 Hz, 1H), 8.00 (d, *J* = 7.6 Hz, 1H), 7.47 (dd, *J* = 8.6, 4.2 Hz, 1H), 7.30 (m, 1H), 2.78 (s, 3H). ¹³C{¹H} NMR (125 MHz, CDCl₃): δ 150.1, 148.1, 140.8, 138.7, 137.6, 130.9, 130.1, 122.7, 95.6, 18.3. Mp = 52.1-55.0 °C. IR (thin film, CH₂Cl₂): 2919, 1560, 1491 cm⁻¹. HRMS [M+H]⁺ Calcd for C₁₀H₈NI: 269.9774; Found: 269.9778.



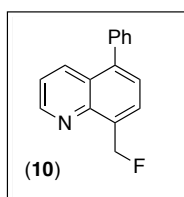
5-Iodo-8-methylquinoline (215 mg, 0.80 mmol, 1.0 equiv) was used as the substrate. The solvent was dichloromethane (8.0 mL), and the reaction was heated for 24 h. GC analysis of the crude reaction mixture showed 67% yield of **9** and 16% yield of **19**. The crude mixture was purified by chromatography on silica gel with a gradient of 1%-8% EtOAc in CH₂Cl₂. Product **9** was obtained as a light brown solid (125.5 mg, 55% isolated yield, *R*_f = 0.58 in 96% CH₂Cl₂/4% EtOAc, mp = 78.5-82.7 °C). ¹H NMR (700 MHz, CDCl₃): δ 8.88 (m, 1H), 8.40 (d, *J* = 8.6 Hz, 1H), 8.16 (d, *J* = 7.6 Hz, 1H), 7.55 (d, *J* = 7.6 Hz, 1H), 7.52 (dd, *J* = 8, 4.0 Hz, 1H), 6.10 (d, *J*_{HF} = 48 Hz, 2H). ¹³C{¹H} NMR (175 MHz, CDCl₃): δ 150.6 (d, *J*_{CF} = 21 Hz), 145.8, 140.6 (d, *J*_{CF} = 22 Hz), 137.6 (d, *J*_{CF} = 22 Hz), 136.2 (d, *J*_{CF} = 19 Hz), 129.9, 128.1 (d, *J*_{CF} = 11 Hz), 123.1 (d, *J*_{CF} = 22 Hz), 98.6, 81.7 (d, ¹*J*_{CF} = 166 Hz). ¹⁹F NMR (376 MHz, CDCl₃): δ -222.1 (t, *J*_{FH} = 48 Hz). IR (thin film, CH₂Cl₂): 1564, 1494, 1344 cm⁻¹. HRMS [M+H]⁺ Calcd for C₁₀H₇NFI: 286.9607; Found: 286.9608.



Product **19** was also obtained from this reaction as a light yellow solid (44.3 mg, 15% isolated yield, *R*_f = 0.38 in 96% CH₂Cl₂/4% EtOAc, mp = 78.5-82.7 °C). ¹H NMR (700 MHz, CDCl₃): δ 8.89 (dd, *J* = 4.1, 1.4 Hz, 1H), 8.39 (dd, *J* = 8.5, 1.4 Hz, 1H), 8.12 (d, *J* = 7.7 Hz, 1H), 7.51 (dd, *J* = 8.5, 4.1 Hz, 1H), 7.45 (dd, *J* = 7.7, 0.8 Hz, 1H), 5.81 (s, 2H), 1.27 (s, 9H). ¹³C{¹H} NMR (125 MHz, CDCl₃): δ 178.5, 150.6, 146.5, 140.6, 137.6, 136.4, 130.1,

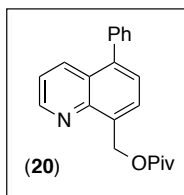
128.6, 123.1, 98.1, 62.6, 39.2, 27.5. IR (thin film, CH₂Cl₂): 2972, 1729, 1156 cm⁻¹. HRMS [M+H]⁺ Calcd for C₁₅H₁₆NO₂I: 370.0298; Found: 370.0300.

8-Methyl-5-phenylquinoline. 8-Methyl-5-phenylquinoline was prepared according to the following procedure. 5-Bromo-8-methylquinoline (1.00 g, 4.50 mmol, 1.0 equiv), phenylboronic acid (603 mg, 4.95 mmol, 1.1 equiv), Pd₂(dba)₃ (206 mg, 0.225 mmol, 0.05 equiv), and K₃PO₄ (1.91 g, 9.01 mmol, 2.0 equiv) were added to an oven-dried Schlenk flask equipped with a stirbar. Dioxane (20 mL) and P(OMe)₃ (55.8 mg, 0.450 mmol, 0.1 equiv) were added in a glovebox. The reaction was heated to 95 °C for 24 h. The reaction mixture was cooled to rt, diluted with diethyl ether, and filtered through celite. The filtrate was concentrated under vacuum and the residue was purified by chromatography on silica gel eluting with DCM/EtOAc (98:2). The product was obtained as a white solid (0.56 g, 57% yield, R_f = 0.39, mp = 56.6-58.4 °C). ¹H NMR (500 MHz, CDCl₃): δ 8.97 (dd, *J* = 4.2, 1.7 Hz, 1H), 8.24 (dd, *J* = 8.6, 1.7 Hz, 1H), 7.62 (dd, *J* = 7, 1 Hz, 1H), 7.51-7.48 (multiple peaks, 2H), 7.46-7.40 (multiple peaks, 4H), 7.36 (dd, *J* = 8.6, 4 Hz, 1H), 2.87 (s, 3H). ¹³C{¹H} NMR (125 MHz, CDCl₃): δ 149.2, 147.6, 139.8, 138.7, 136.7, 134.8, 130.3, 129.3, 128.6, 127.6, 127.1, 126.8, 121.0, 18.6. IR (thin film, CH₂Cl₂): 2920, 1592, 1504 cm⁻¹. HRMS [M+H]⁺ Calcd for C₁₆H₁₃N: 220.1121; Found: 220.1126.



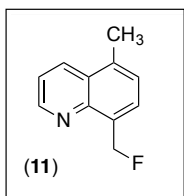
8-Methyl-5-phenylquinoline (175 mg, 0.80 mmol, 1.0 equiv) was used as the substrate. The solvent was fluorobenzene (8.0 mL), and the reaction was heated for 28 h. GC analysis of the crude reaction mixture showed 43% yield of **10** and 35% yield of **20**. The crude mixture was purified by chromatography on silica gel with a gradient of 0%-4% EtOAc in CH₂Cl₂. Product **10** was obtained as an off-white solid (74.6 mg, 39% isolated yield, R_f = 0.45 in 98% CH₂Cl₂/2% EtOAc, mp = 63.5-67.0 °C). ¹H NMR (700 MHz, CDCl₃): δ 8.94 (dd, *J* = 4.1, 1.5 Hz, 1H), 8.26 (dd, *J* = 8.6, 1.5 Hz, 1H), 7.88 (d, *J* = 7.2 Hz, 1H), 7.55 (d, *J* = 7.2 Hz, 1H), 7.52 (m, 2H), 7.48-7.45 (multiple peaks, 3H), 7.39 (dd, *J* = 8.5, 4.1 Hz, 1H), 6.20 (d, *J*_{HF} = 48 Hz, 2H). ¹³C{¹H} NMR (125 MHz, CDCl₃): δ 149.8, 145.8 (d, *J*_{CF} = 2.9 Hz), 141.1 (d, *J*_{CF} = 2.9 Hz), 139.3, 134.9, 134.2 (d, *J*_{CF} = 16 Hz), 130.2, 128.7, 128.0,

127.1 (d, $J_{CF} = 3.8$ Hz), 127.1, 126.7, 121.5, 82.1 (d, $J_{CF} = 166$ Hz). ^{19}F NMR (376 MHz, CDCl_3): δ -219.1 (t, $J_{FH} = 48$ Hz). IR (thin film, CH_2Cl_2): 3029, 1584, 1504, 1352 cm^{-1} . HRMS $[\text{M}+\text{H}]^+$ Calcd for $\text{C}_{16}\text{H}_{12}\text{NF}$: 238.1027; Found: 238.1033.



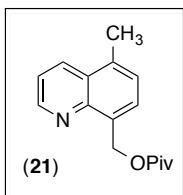
Product **20** was also obtained from this reaction as a light yellow oil (91.0 mg, 36% isolated yield, $R_f = 0.21$ in 98% $\text{CH}_2\text{Cl}_2/2\%$ EtOAc). ^1H NMR (700 MHz, CDCl_3): δ 8.94 (dd, $J = 4.1, 1.7$ Hz, 1H), 8.24 (dd, $J = 8.5, 1.7$ Hz, 1H), 7.77 (d, $J = 7.3$ Hz, 1H), 7.51-7.50 (multiple peaks, 3H), 7.47-7.45 (multiple peaks, 3H), 7.38 (dd, $J = 8.5, 4.1$ Hz, 1H), 5.91 (s, 2H), 1.30 (s, 9H). $^{13}\text{C}\{^1\text{H}\}$ NMR (125 MHz, CDCl_3): δ 178.6, 149.6, 146.2, 140.4, 139.5, 134.8, 134.4, 130.2, 128.7, 127.9, 127.1, 127.1, 126.7, 121.4, 63.0, 39.2, 27.6. IR (thin film, CH_2Cl_2): 3060, 2972, 1726, 1504, 1480, 1280 cm^{-1} . HRMS $[\text{M}+\text{H}]^+$ Calcd for $\text{C}_{21}\text{H}_{21}\text{NO}_2$: 320.1645; Found: 320.1652.

5,8-Dimethylquinoline. 5,8-Dimethylquinoline was prepared according to a literature procedure.²⁹ ^1H NMR (500 MHz, CDCl_3): δ 8.96 (dd, $J = 4.2, 1.7$ Hz, 1H), 8.31 (dd, $J = 8.6, 1.7$ Hz, 1H), 7.46-7.41 (multiple peaks, 2H), 7.27 (m, 1H), 2.79 (s, 3H), 2.65 (s, 3H). $^{13}\text{C}\{^1\text{H}\}$ NMR (125 MHz, CDCl_3): δ 148.9, 147.7, 135.1, 132.9, 132.5, 129.5, 127.8, 126.9, 120.6, 18.7, 18.4. IR (thin film, CH_2Cl_2): 2921, 1600, 1501 cm^{-1} . HRMS $[\text{M}+\text{H}]^+$ Calcd for $\text{C}_{11}\text{H}_{11}\text{N}$: 158.0964; Found: 158.0964.



5,8-Dimethylquinoline (126 mg, 0.80 mmol, 1.0 equiv) was used as the substrate. The solvent was fluorobenzene (8.0 mL), and the reaction was heated for 16 h. GC analysis of the crude reaction mixture showed 41% yield of **11** and 40% yield of **21**. The crude mixture was purified by chromatography on silica gel with a gradient of 1%-8% EtOAc in CH_2Cl_2 . Product **11** was obtained as a viscous yellow oil (54.1 mg, 39% isolated yield, $R_f = 0.44$ in 96% $\text{CH}_2\text{Cl}_2/4\%$ EtOAc). ^1H NMR (700 MHz, CDCl_3): δ 8.94 (m, 1H), 8.34 (dd, $J = 8.5, 1.5$ Hz, 1H), 7.70 (d, $J = 7.2$ Hz, 1H), 7.46 (dd, $J = 8.5, 4.1$ Hz, 1H), 7.40 (d, $J = 7.2$ Hz, 1H), 6.10 (d, $J_{HF} = 48$ Hz, 2H), 2.69 (s, 3H). $^{13}\text{C}\{^1\text{H}\}$ NMR (125 MHz, CDCl_3): δ 149.5,

145.8, 135.5 (d, $J_{CF} = 2.4$ Hz), 133.0, 132.7 (d, $J_{CF} = 16.3$ Hz), 127.9 (d, $J_{CF} = 9.6$ Hz), 127.6, 126.9, 121.1, 82.1 (d, $^1J_{CF} = 165$ Hz), 18.9. ^{19}F NMR (376 MHz, CDCl_3): δ -216.6 (t, $J_{FH} = 48$ Hz). IR (thin film, CH_2Cl_2): 2951, 1599, 1504, 1352 cm^{-1} . HRMS $[\text{M}+\text{H}]^+$ Calcd for $\text{C}_{11}\text{H}_{10}\text{NF}$: 175.0797; Found: 175.0794.



Product **21** was also obtained from this reaction as a viscous yellow oil (77.9 mg, 38% isolated yield, $R_f = 0.19$ in 96% CH_2Cl_2 /4% EtOAc). ^1H NMR (400 MHz, CDCl_3): δ 8.95 (dd, $J = 4.1, 1.5$ Hz, 1H), 8.35 (dd, $J = 8.5, 1.5$ Hz, 1H), 7.63 (d, $J = 7.2$ Hz, 1H), 7.47 (dd, $J = 8.5, 4.1$ Hz, 1H), 7.38 (d, $J = 7.2$ Hz, 1H), 5.83 (s, 2H), 2.69 (s, 3H), 1.26 (s, 9H). $^{13}\text{C}\{^1\text{H}\}$ NMR (175 MHz, acetone- d_6): δ 179.0, 151.0, 147.8, 136.4, 134.6, 134.3, 129.0, 128.8, 128.2, 122.7, 64.0, 40.2, 28.3, 19.3. IR (thin film, CH_2Cl_2): 2972, 1726, 1480, 1282, 1159 cm^{-1} . HRMS $[\text{M}+\text{H}]^+$ Calcd for $\text{C}_{16}\text{H}_{19}\text{NO}_2$: 257.1416; Found: 257.1415.

5-Methoxy-8-methylquinoline. 5-Methoxy-8-methylquinoline was prepared according to a literature procedure.²⁶ NMR data matched that reported in the literature.

On the benchtop, $\text{PhI}(\text{OPiv})_2$ (154 mg, 0.38 mmol, 2.0 equiv) and AgF (121 mg, 0.96 mmol, 5.0 equiv) were weighed into a 4 mL vial, and DCM (1.9 mL) was added. The vial was sealed with a Teflon-lined cap (with Teflon tape covering the threads of the vial), and this mixture was heated at 60 °C for 1 h. The vial was removed from the heat and allowed to cool to rt (~5 min). Then $\text{Pd}(\text{OAc})_2$ (4.3 mg, 0.02 mmol, 0.10 equiv), MgSO_4 (45.9 mg, 0.38 mmol, 2.0 equiv), and 5-methoxy-8-methylquinoline (33.1 mg, 0.19 mmol, 1.0 equiv) were added. The vial was sealed with a Teflon-lined cap and heated at 60 °C for an additional 24 h. GC analysis of the crude reaction mixture showed <1% yield of **12** and ~55% yield of **22**, using hexadecane as a standard.

2.9 References

- ¹ For recent reviews, see: (a) Jeschke, P. *Pest Manag. Sci.* **2010**, *66*, 10. (b) Purser, S.; Moore, P. R.; Swallow, S.; Gouverneur, V. *Chem. Soc. Rev.* **2008**, *37*, 320.
- ² Thayer, A. M. *C&E News.* **2006**, *84*, 15.
- ³ Tsuchiya, K.; Shibasaki, Y.; Aoyagi, M.; Ueda, M. *Macromolecules.* **2006**, *39*, 3964.
- ⁴ For recent reviews, see: (a) Hollingworth, C.; Gouverneur, V. *Chem. Commun.* **2012**, *48*, 2929. (b) Furuya, T.; Kamlet, A. S.; Ritter, T. *Nature* **2011**, *473*, 7348. (c) Furuya, T.; Kuttruff, C. A.; Ritter, T. *Curr. Opin. Drug Disc. Devel.* **2008**, *11*, 803.
- ⁵ Adams, D. J.; Clark, J. H. *Chem. Soc. Rev.* **1999**, *28*, 225.
- ⁶ Balz, G.; Schiemann, G. *Chem. Ber.* **1927**, *60*, 1186.
- ⁷ Watson, D.A., Su, M., Teverovskiy, G., Zhang, Y., Garcia-Fortanet, J., Kinzel, T. and Buchwald, S.L. *Science.* **2009**, *325*, 1661.
- ⁸ Ye, Y.; Schimler, S. D.; Hanley, P. S.; Sanford, M. S. *J. Am. Chem. Soc.* **2013**, *135*, 16292.
- ⁹ Hull, K. L.; Anani, W. Q.; Sanford, M. S. *J. Am. Chem. Soc.* **2006**, *128*, 7134.
- ¹⁰ (a) Chan, C. S. L.; Wasa, M.; Wang, X.; Yu, J. Q. *Angew. Chem. Int. Ed.* **2011**, *50*, 9081. (b) Wang, X.; Mei, T. S.; Yu, J. Q. *J. Am. Chem. Soc.* **2009**, *131*, 7520.
- ¹¹ For examples of C–F bond-formation from Pd^{IV}(R)(F) species, see: (a) Racowski, J. M.; Kampf, J. W.; Sanford, M. S. *Angew. Chem. Int. Ed.* **2012**, *51*, 3414. (b) Ball, N. D.; Kampf, J. W.; Sanford, M. S. *J. Am. Chem. Soc.* **2010**, *132*, 2878. (c) Furuya, T.; Benitez, D.; Tkatchouk, E.; Strom, A. E.; Tang, P.; Goddard, W. A.; Ritter, T. *J. Am. Chem. Soc.* **2010**, *132*, 3793.
- ¹² Hickman, A. J.; Sanford, M. S. *Nature* **2012**, *484*, 177.
- ¹³ For related “umpolung” strategies to achieve fluorination with F[−] reagents, see: (a) Gao, Z.; Lim, Y. H.; Tredwell, M.; Li, L.; Verhoog, S.; Hopkinson, M.; Kaluza, W.; Collier, T. L.; Passchier, J.; Huiban, M.; Gouverneur, V. *Angew. Chem. Int. Ed.* **2012**, *51*, 6733. (b) Lee, E.; Kamlet, A. S.; Powers, D. C.; Neumann, C. N.; Boursalian, G. B.; Furuya, T.; Choi, D. C.; Hooker, J. M.; Ritter, T. *Science* **2011**, *334*, 639.
- ¹⁴ Wu, T.; Yin, G.; Liu, G. *J. Am. Chem. Soc.* **2009**, *131*, 16354.
- ¹⁵ McMurtrey, K. B.; Racowski, J. M.; Sanford, M. S. *Org. Lett.* **2012**, *14*, 4094.
- ¹⁶ Dick, A. R.; Hull, K. L.; Sanford, M. S. *J. Am. Chem. Soc.* **2004**, *124*, 2300.

- ¹⁷ Schlyer, D. J. *Ann. Acad. Med. Singapore* **2004**, *33*, 146.
- ¹⁸ Miller, P. W.; Long, N. J.; Vilar, R.; Gee, A. D. *Angew. Chem. Int. Ed.* **2008**, *47*, 8998.
- ¹⁹ Sun, H.; Wang, B.; DiMagno, S. G. *Org. Lett.* **2008**, *10*, 4413.
- ²⁰ Ruppert, I. *J. Fluorine Chem.* **1980**, *15*, 173-178.
- ²¹ Shreeve, J. M.; Ye, C.; Twamley, B. *Org. Lett.* **2005**, *7*, 3961.
- ²² Truong, T.; Klimovica, K.; Daugulis, O. *J. Am. Chem. Soc.* **2013**, *135*, 9342.
- ²³ (a) Liu, W.; Huang, X.; Cheng, M.-J.; Nielsen, R. J.; Goddard III, W. A.; Groves, J. T. *Science* **2012**, *337*, 1322. (b) Liu, W.; Groves, J. T. *Angew. Chem. Int. Ed.* **2013**, *52*, 6024. (c) Liu, W.; Huang, X.; Groves, J. T. *Nature Protocols* **2013**, *8*, 2348. (d) Huang, X.; Liu, W.; Ren, H.; Neelamegam, R.; Hooker, J. M.; Groves, J. T. *J. Am. Chem. Soc.* **2014**, *136*, 6842.
- ²⁴ Casitas, A.; Canta, M.; Sola, M.; Costas, M.; Ribas, X. *J. Am. Chem. Soc.* **2011**, *133*, 19386.
- ²⁵ Fier, P. S.; Hartwig, J. F. *J. Am. Chem. Soc.* **2012**, *134*, 10795.
- ²⁶ Evans et al. *Tetrahedron* **2005**, *61*, 9696.
- ²⁷ Tochilkin, A. I. et al. *Chem. Heterocycl. Compd. (Russ)* **1983**, 1373.
- ²⁸ Tochilkin, A. I. et al. *Chem. Heterocycl. Compd. (Russ)* **1982**, 785.
- ²⁹ O'Murchu, C. *Synthesis* **1989**, *11*, 880.
- ³⁰ Leadbeater, N. E.; Griffiths, C. *Tetrahedron Lett.* **2000**, *41*, 2487.
- ³¹ Stang, P. J.; Boehshar, M.; Wingert, H.; Kitamura, T. *J. Am. Chem. Soc.* **1988**, *110*, 3272.
- ³² Blackmond, D. G.; Hodnett, N. S.; Lloyd-Jones, G. C. *J. Am. Chem. Soc.* **2006**, *128*, 7450.

CHAPTER 3

Room-Temperature C–H Arylation by Palladium-Catalysis and Visible-Light Photocatalysisⁱ

3.1 Background and Significance

The biaryl motif is an important structural component of numerous natural products, pharmaceutical agents, and agrochemicals.¹ Biaryl motifs are also found in polymers, dyes, and semiconductors.¹ Additionally, many ligands for asymmetric catalysis contain aryl–aryl linkages.¹ The presence of this scaffold in small molecules has been shown to aid in the binding affinity to many proteins.² Due to the importance and prevalence of this motif, the design of mild, general, and efficient methods for aryl–aryl bond construction continues to be an area of tremendous research effort.¹

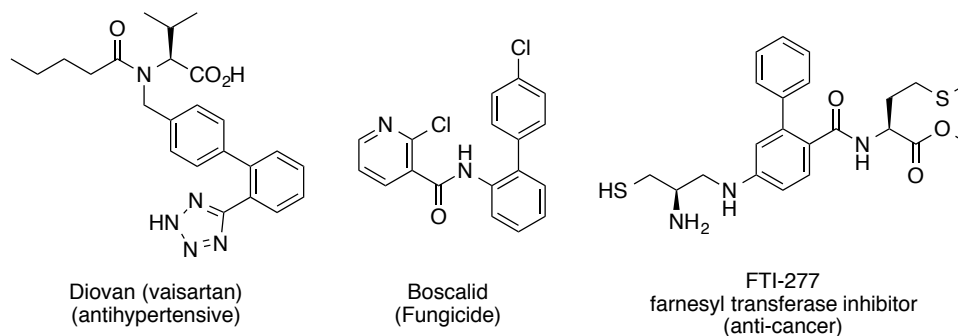
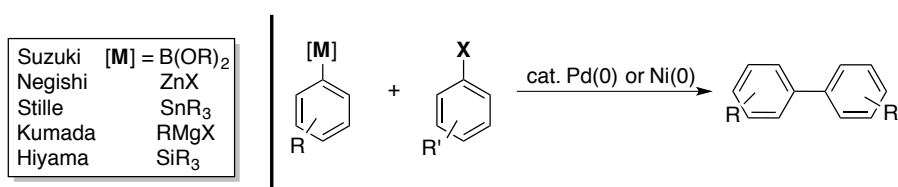


Figure 3.1. Examples of the Biaryl Motif in Bioactive Molecules

ⁱ Reproduced in part with permission from Kalyani, D; McMurtrey, K. B.; Neufeldt, S. R.; Sanford, M. S. *J. Am. Chem. Soc.* **2011**, 133, 18566. Copyright 2011 American Chemical Society.

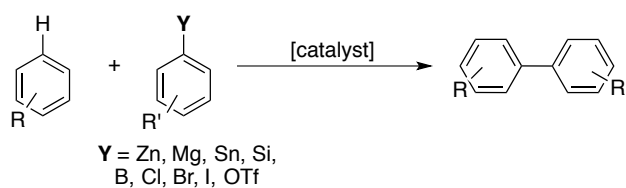
Unquestionably the best-known and most used method for aryl-aryl bond formation is the cross-coupling between an aryl organometallic reagent and an aryl halide (Scheme 3.1). The Nobel Prize in 2010 recognized the significance of this work. Despite the versatility of these cross-coupling reactions, they require functionalization of both aryl starting materials. Carrying these sites of prefunctionalization through multistep synthetic sequences can lead to functional group compatibility issues and can also limit the structural derivatives that are accessible to researchers.

Scheme 3.1. Pd- and Ni-Catalyzed Cross-Coupling Reactions to form Aryl-Aryl Bonds



An alternative approach to traditional cross-coupling would be direct C–H arylation reactions (Scheme 3.2). This would eliminate the need for the prefunctionalization of one of the aryl starting materials. Such an approach is also desirable for aryl-aryl bond formation in late-stage synthesis, as the organometallic reagent would not need to be carried through the synthesis or installed prior to the arylation reaction.

Scheme 3.2. Metal-Catalyzed Direct C–H Arylation to form Aryl-Aryl Bonds



Over the past decade, transition-metal-catalyzed C–H arylation reactions have been particularly well studied. There have been numerous advances in the substrate scope, functional group tolerance, and range of catalysts for promoting these transformations.³ Palladium salts have been commonly used as catalysts and have proven

successful for many systems.³ There are three common mechanisms that operate in these Pd-catalyzed transformations. Figure 3.2 shows generic versions of the typical mechanisms, which include a Pd^{0/II}, Pd^{II/0}, or Pd^{II/IV} catalytic cycle.

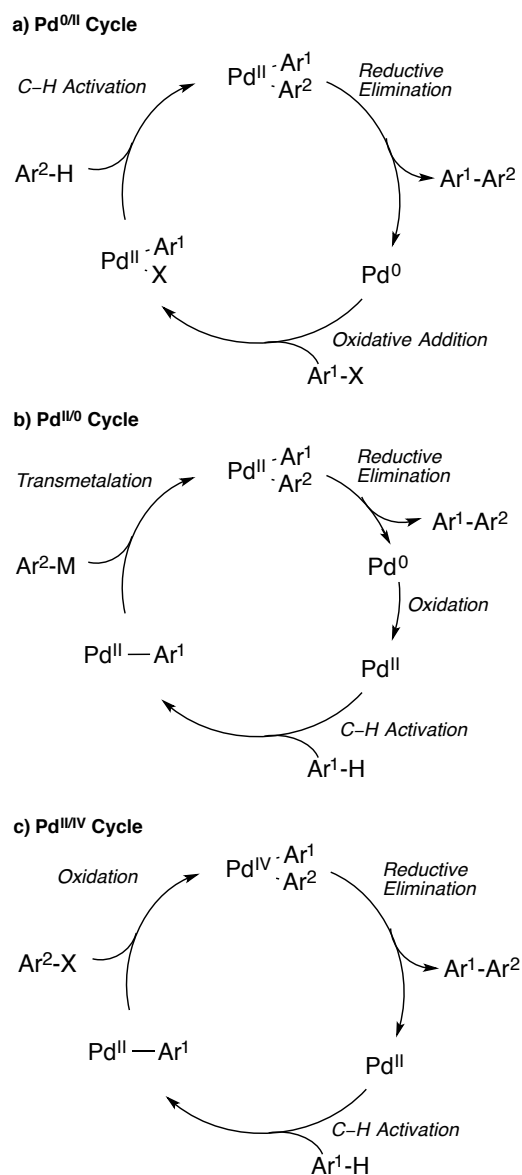
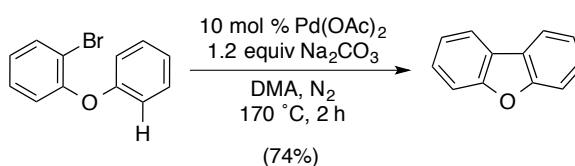


Figure 3.2. Common Mechanisms for Pd-Catalyzed C-H Arylation Reactions

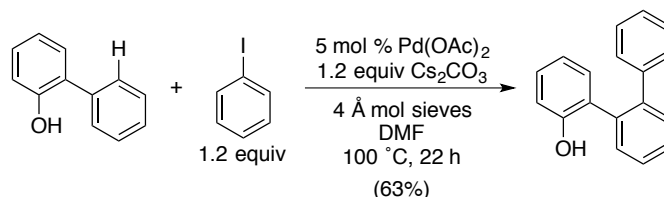
As described in Chapter 1, site selectivity is a challenge for C-H functionalization, and for C-H arylation this is also the case. One approach to overcome this issue is to have the two aryl groups bound together in the same molecule (Scheme

3.3).⁴ However, this intramolecular tactic limits the substrate scope and versatility of the reaction substantially. A more recent and widely-used method is to employ substrates containing directing groups that bind to the metal center and align a proximal C–H bond for activation (see section 1.2). One of the first examples using the directing group approach for arylation was reported by Miura and coworkers, in which they reported a Pd-catalyzed direct C–H arylation using phenol as the directing group (Scheme 3.4).⁵ In this system, the substrate 2-phenylphenol was selectively arylated at the *ortho* position.

Scheme 3.3. Intramolecular C–H Arylation to Form Dibenzofurans



Scheme 3.4. Phenol Directed Intermolecular C–H Arylation of 2-Phenylphenol

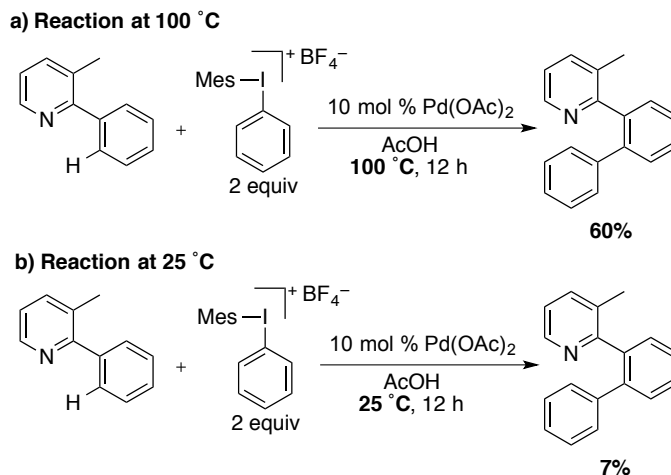


Despite progress in the study of aryl-aryl bond formation, the vast majority of C–H arylation methods still require elevated temperatures (>80 °C), as seen in examples above (Scheme 3.3 and Scheme 3.4) and numerous others.⁶ The development of general room-temperature C–H arylation reactions (particularly in nonacidic solvents) remains an important challenge for the field.^{6,7}

In 2005, our group reported a Pd-catalyzed, ligand-directed C–H arylation method that uses diaryliodonium salts as the aryl source.⁸ This method is successful at arylating substrates with a variety of directing groups such as pyridines, quinolines, pyrrolidinones, and oxazolidinones. However, this Ar₂I⁺ arylation system, like most other Pd-catalyzed C–H arylation methodologies, requires high reaction temperatures. This transformation

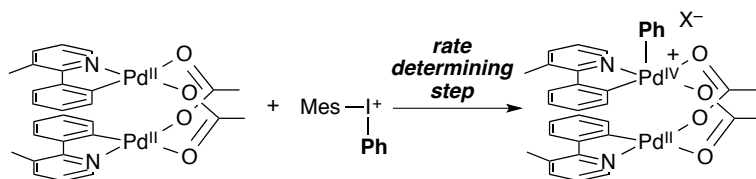
proceeds at 100 °C to obtain 60% of the desired product; however, as shown in Scheme 3.5, very little product is obtained at room temperature.

Scheme 3.5. Palladium-Catalyzed C–H Arylation with Diaryliodonium Salts



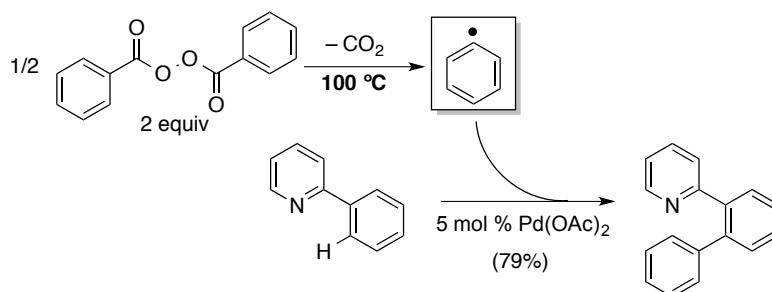
More recently our group conducted detailed studies of the mechanism of this Pd-catalyzed/ Ph_2I^+ C–H arylation method. One mechanistic conclusion, of particular interest to us, was that the rate-determining step of the catalytic cycle involves oxidation of a dimeric intermediate by $[\text{Mes-I-Ph}]\text{BF}_4$ (Scheme 3.6).⁹ This result led us to hypothesize that the rate of the reaction could be accelerated (and therefore the temperature lowered) by substituting diaryliodonium salts with more kinetically reactive arylating reagents. We reasoned that room-temperature C–H arylation might be achieved by using $\text{Ph}\cdot$ as a highly kinetically reactive alternative to the diaryliodonium oxidant in Scheme 3.6.

Scheme 3.6. Rate Determining Step of Pd-Catalyzed C-H Arylation with Ar_2I^+



A recent report by Yu demonstrated the Pd-catalyzed C–H arylation of arylpyridines and other substrates by acylperoxides (Scheme 3.7).¹⁰ We were intrigued by this example because it suggested that phenyl radicals (generated through decarboxylative decompositions of the peroxides) can react with palladacycles and participate in Pd-catalyzed C–H arylation. In this system, Ph• is generated from dibenzoylperoxide, and thus, high temperatures were required to initiate the decarboxylation (Scheme 3.7).

Scheme 3.7. Pd-Catalyzed C–H Arylation by Decarboxylation of Dibenzoylperoxide



We sought to identify reagents that could form aryl radicals at room temperature. A literature survey uncovered Deronzier's Ru(bpy)₃Cl₂-photocatalyzed Pschorr reaction (Scheme 3.8).^{11a-e} In this transformation Ru(bpy)₃Cl₂ in combination with visible light generates aryl radicals from aryldiazonium salts at 25 °C. As proposed in the same report, the mechanism is believed to proceed through an oxidative quenching cycle (Figure 3.3). First the Ru(bpy)₃²⁺ catalyst is promoted by visible light to the excited state (Ru(bpy)₃^{2+*}) (step *i*). This species reduces the aryldiazonium salt to form an aryl radical intermediate along with concomitant release of N₂ (step *ii*). Ru(bpy)₃^{2+*} is oxidized to Ru(bpy)₃³⁺ in the process. Rapid cyclization of the aryl radical intermediate forms another radical intermediate **1** (step *iii*). The Ru(bpy)₃³⁺ is then able to reduce the now cyclized intermediate so that aromaticity can be regained and the final product formed (step *iv*). Additionally, this step regenerates the starting catalyst Ru(bpy)₃²⁺.

Scheme 3.8. Ru(bpy)₃Cl₂-Photocatalyzed Pschorr Reaction

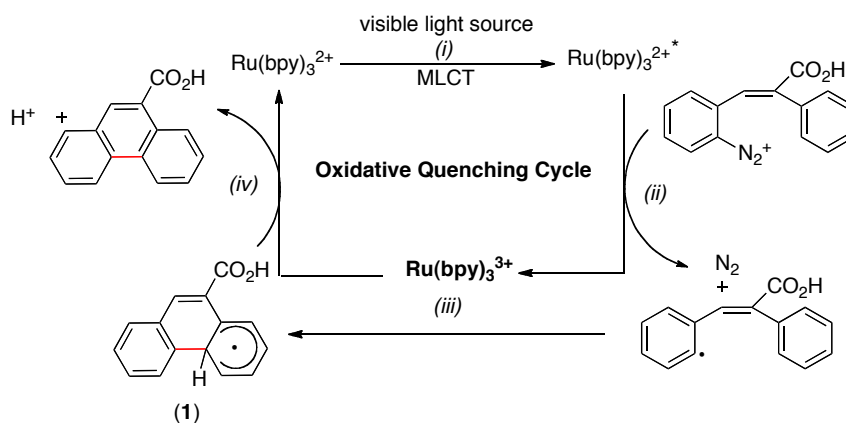
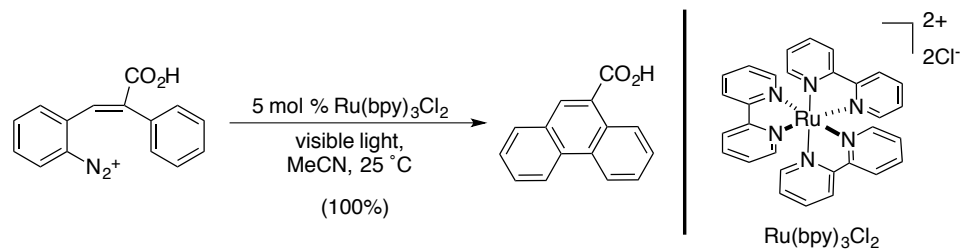
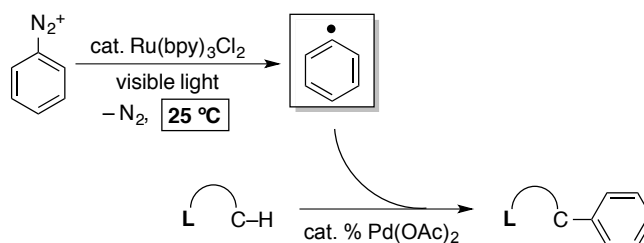


Figure 3.3. Proposed Mechanism for the Photocatalyzed Pschorr Reaction through an Oxidative Quenching Cycle

Inspired by Deronzier's transformation, we envisioned that palladacycle intermediates could be intercepted by aryl radicals via visible-light photocatalysis (Scheme 3.9). This proposed transformation could potentially be accomplished at room temperature based on the work reported by Deronzier.

Scheme 3.9. Proposed Scheme for Arylation from Diazonium Salts via Photocatalysis

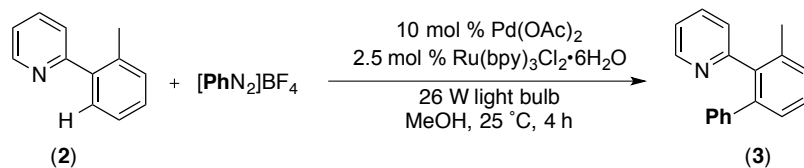


In this chapter, I describe the use of this strategy for the rational design of a new room-temperature C–H arylation reaction.¹² This achievement was made possible by merging Pd-catalyzed C–H functionalization with visible-light photoredox catalysis. This work was conducted in collaboration with Dr. Dipannita Kalyani and Dr. Sharon Neufeldt. Dr. Kalyani proposed and initiated the project as well as completed the substrate scope of 2-arylpyridines (Table 3.4) and the directing group scope (Table 3.6). Further optimizations and investigations were complete as a joint effort. Dr. Neufeldt assisted in issues of irreproducibility and discovered that regulating reaction temperature is critical to obtaining high yields.

3.2 Reaction Optimization

Initial investigations focused on the Pd-catalyzed C–H arylation of **2** (Table 3.1) with phenyldiazonium tetrafluoroborate. Substrate **2** was chosen for optimization studies because phenylpyridines are excellent substrates for a similar Pd-catalyzed arylation reaction reported by our group under thermal conditions (Scheme 3.5).⁸ Additionally, the use of a similar substrate lead us to be able to make more accurate comparisons between both systems. Ru(bpy)₃Cl₂•6H₂O was employed as the photocatalyst, and two 26 W household fluorescent compact bulbs were utilized as the source of visible light. We were pleased to find that the desired C–H arylation product **3** was formed in 31% yield at room temperature with 10 mol % Pd(OAc)₂, 2.5 mol % Ru(bpy)₃Cl₂•6H₂O, and 2 equiv of [PhN₂]BF₄ in MeOH (Table 3.1, entry 1). The yield was improved to 49% by using 4 equivalents of [PhN₂]BF₄ (entry 2), and up to 84% by adding 10 mol % Ag₂CO₃ as an additive in conjunction with the increase in equivalents of diazonium salt (entry 4).

Table 3.1. Optimization of the Phenylation Reaction Between **2** and [PhN₂]BF₄

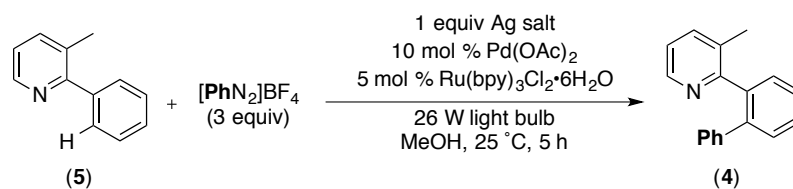


entry ^{a,b}	[PhN ₂]BF ₄ (equiv)	additive	yield (%)
1	2	none	31
2	4	none	49
3	4	0.05 equiv Ag ₂ CO ₃	60
4	4	0.10 equiv Ag ₂ CO ₃	84

^a General conditions: Pd(OAc)₂ (0.1 equiv), Ru(bpy)₃Cl₂·6H₂O (0.025 equiv), MeOH (0.1 M in substrate), rt, 4 h, two 26 W compact fluorescent light bulbs. ^b Calibrated yields determined by gas chromatographic analysis of the crude reaction mixtures.

We found that the addition various silver salts was advantageous in increasing the yield of arylated product. This was true for certain substrates but not all seemed to benefit from the addition of silver salts (see section 3.3 and 3.4). Under slightly altered conditions from above, no added silver gave product **4** in 25% yield (Table 3.2, entry 1). Other than Ag₂CO₃, one salt in particular that increased product yield was AgPF₆ (entry 2). However, adding AgPF₆ afforded a high background reaction of 38% of **4**, when [Ru] was omitted (entry 3). Adding Ag₂CO₃ instead afforded product **4** in 58% yield with a low yielding background reaction of 16% (entry 4-5).

Table 3.2. Silver Salts as Additives for the Phenylation Reaction Between **5** and $[\text{PhN}_2]\text{BF}_4$

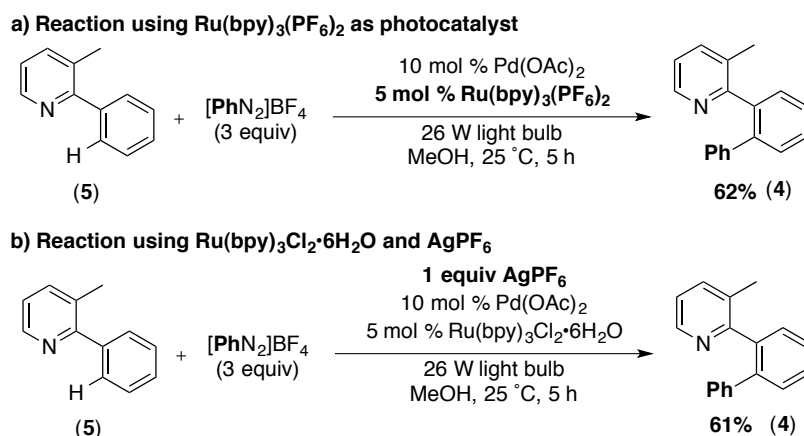


entry ^{a,b}	Ag salt	$\text{Ru(bpy)}_3\text{Cl}_2\cdot\text{6H}_2\text{O}$	yield (%)
1	none	yes	25
2	AgPF_6	yes	75
3	AgPF_6	no	38
4	Ag_2CO_3	yes	58
5	Ag_2CO_3	no	16

^a General conditions: Pd(OAc)_2 (0.1 equiv), $\text{Ru(bpy)}_3\text{Cl}_2\cdot\text{6H}_2\text{O}$ (0.025 equiv), $[\text{PhN}_2]\text{BF}_4$ (3.0 equiv), Ag salt (1.0 equiv), MeOH (0.1 M in substrate), rt, 5 h, two 26 W compact fluorescent light bulbs. ^b Calibrated yields determined by gas chromatographic analysis of the crude reaction mixtures.

With this data in mind, we hypothesized that the chlorides from $\text{Ru(bpy)}_3\text{Cl}_2\cdot\text{6H}_2\text{O}$ were being sequestered by silver salts and being replaced by the silver salts counterions. Additionally, we postulated that other counterions on Ru(bpy)_3^{2+} , such as PF_6^- , made for a better photocatalyst than chloride (see Table 3.2). Thus, we synthesized $\text{Ru(bpy)}_3(\text{PF}_6)_2$ to test it in the reaction conditions to learn if $\text{Ru(bpy)}_3(\text{PF}_6)_2$ performed similarly to $\text{Ru(bpy)}_3\text{Cl}_2\cdot\text{6H}_2\text{O}$ with AgPF_6 . To our delight, **4** was formed in similar yields by the use of $\text{Ru(bpy)}_3(\text{PF}_6)_2$ or $\text{Ru(bpy)}_3\text{Cl}_2\cdot\text{6H}_2\text{O}$ with AgPF_6 (Scheme 3.10). This suggests that silver salts are swapping counter ions on the $[\text{Ru}]$ catalyst as theorized.

Scheme 3.10. Reactions to Probe the Role of Silver in the Photocatalyzed Phenylation Reaction



Control reactions were essential to assess whether the proposed dual catalytic reaction was in operation. Importantly, [Pd], [Ru], and visible light were all essential for this transformation. In the absence of any of these components, significantly reduced yields of **3** ($\leq 8\%$) were observed (Table 3.3).

Table 3.3. Control reactions for the Phenylation Reaction Between **2** and [PhN₂]BF₄

entry ^{a,b}	Pd(OAc) ₂	Ru(bpy) ₃ Cl ₂ ·6H ₂ O	Light	yield (%)
1	No	Yes	Yes	0
2	Yes	No	Yes	8
3	Yes	Yes	No	5

^a General conditions: Pd(OAc)₂ (0.1 equiv), Ru(bpy)₃Cl₂·6H₂O (0.025 equiv), [PhN₂]BF₄ (4.0 equiv), Ag₂CO₃ (0.1 equiv), MeOH (0.1 M in substrate), rt, 4 h, two 26 W compact fluorescent light bulbs. ^b Calibrated yields determined by gas chromatographic analysis of the crude reaction mixtures.

Regulation of the reaction temperature at 25 °C was found to be critically important for obtaining reproducible yields in these reactions. Irreproducibility of yields

was seen when there was an increase in reaction temperature due to the warming from the light bulbs. To control the temperature, the reaction vials were placed in a water bath of room temperature water. The temperature was monitored and stayed fairly consistent at 25 °C over the course of the reaction. Furthermore, the need to control the reaction temperature provided key information; specifically, it indicated that slight heat from the lamps was not needed for the reaction to occur and the reaction truly proceeded at room temperature (~25 °C).

This transformation has several attractive features in comparison with most current C–H arylation methods,³ including a low operating temperature (25 °C), a nonacidic solvent (MeOH), and the generation of innocuous dinitrogen and easily removable HBF₄ as the only stoichiometric by-products. In addition, this is the first example of palladium-catalyzed C–H functionalization using visible-light photoredox catalysis.

3.3 Substrate Scope of 2-Arylpyridine Derivatives

With the optimal conditions in hand, we next explored the functional group compatibility of this transformation using a series of 2-arylpyridine derivatives. As shown in Table 3.4, C–H phenylation proceeded at room temperature in modest to good yields with a variety of electronically diverse pyridine substrates. Electron-donating and electron-withdrawing substituents were well tolerated on both the pyridine (entries 1–6) and the aryl ring undergoing functionalization (entries 7 and 8). Additionally, chloride and bromide substituents on the pyridine ring were compatible with the reaction conditions (entries 3 and 4), suggesting against Pd⁰ being an intermediate in this transformation. Minor optimization was performed on each substrate to ensure high conversion and yield. Such changes from the standard conditions include the addition of Ag₂CO₃, an increase in the loading of Pd(OAc)₂ or [PhN₂]BF₄, an increase in the reaction time, and/or an increase in the reaction concentration.

Table 3.4. Substrate Scope of the Pd/Ru-Catalyzed C–H Arylation of 2-Arylpyridine Derivatives

entry ^a	substrate	product	GC yield ^b (%)	isolated yield (%)
1 ^c			84	76
2 ^{d,e}			73	66
3 ^{c,e,f,g}			74	62
4 ^{c,d,e,f,g}			62	63
5 ^{e,h}			62	59
6 ^{d,e,f,i}			51	47
7 ^{e,g}			77	69
8 ^{d,e,f,h}			76	60

^a General procedure: Substrate (1.0 equiv), Pd(OAc)₂ (0.1 equiv), Ru(bpy)₃Cl₂·6H₂O (0.025 equiv), [PhN₂]BF₄ (4.0 equiv), MeOH (0.1 M in substrate), rt, 4 h, 26 W compact fluorescent light bulb. ^b Calibrated yields determined by gas chromatographic analysis of the crude reaction mixtures.

^c Ag₂CO₃ (0.1 equiv) was used as an additive. ^d 0.15 equiv of Pd(OAc)₂. ^e MeOH (0.05 M in substrate). ^f 5.0 equiv of [PhN₂]BF₄. ^g Reaction was run for 10 h. ^h Reaction was run for 8 h. ⁱ Reaction was run for 9.5 h.

Yields obtained by gas chromatographic analysis of the crude reaction mixtures matched well with the isolated yield in most cases, indicating that these compounds could be isolated efficiently by column chromatography. The isolations were relatively straightforward because of the lack of substantial by-products from these arylation reactions.

Importantly, control reactions for these substrates, under the same conditions as outlined above, were performed to ensure the catalysts were operating in this system. In all cases, Pd(OAc)₂, Ru(bpy)₃Cl₂•6H₂O, and visible light were required to achieve >9% yield (see Table 3.5).

Table 3.5. Control Reactions for the Substrate Scope of the C–H Arylation of 2-Arylpyridine Derivatives

entry ^{a,b}	product	yield without light (%)	yield without Ru cat (%)	yield without Pd cat (%)
1 ^c	 Ph (3)	5	8	0
2 ^{d,e}	 Ph (7)	0	3	0
3 ^{c,e,f,g}	 Ph (9)	0	<1	0
4 ^{c,d,e,f,g}	 Ph (11)	0	4	0
5 ^{e,g}	 Ph (13)	0	4	2
6 ^{d,e,f,g}	 Ph (15)	0	8	0
7 ^{e,g}	 Ph (17)	<1	9	0
8 ^{d,e,h}	 Ph (19)	1	7	0

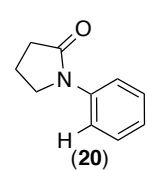
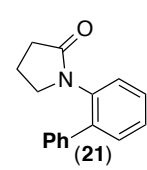
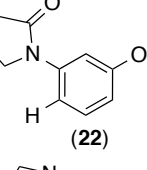
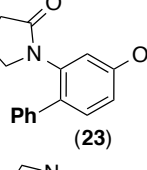
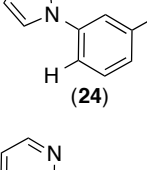
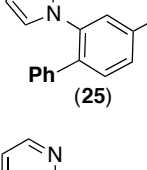
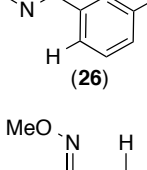
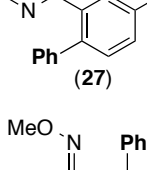
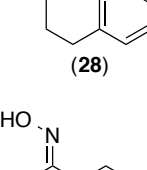
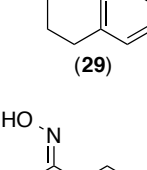
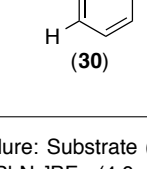
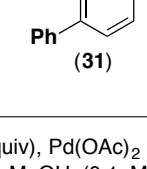
^a General procedure: Substrate (1.0 equiv), Pd(OAc)₂ (0.1 equiv), Ru(bpy)₃Cl₂·6H₂O (0.025 equiv), [PhN₂]BF₄ (4.0 equiv), MeOH (0.1 M in substrate), rt, 4 h, 26 W compact fluorescent light bulb. ^b Calibrated yields determined by gas chromatographic analysis of the crude reaction mixtures. ^c Ag₂CO₃ (0.1 equiv) was used as an additive. ^d 0.15 equiv of Pd(OAc)₂. ^e MeOH (0.05 M in substrate). ^f 5.0 equiv of [PhN₂]BF₄. ^g Reaction was run for 10 h. ^h Reaction was run for 8 h. ⁱ Reaction was run for 9.5 h.

3.4 Directing Group Scope

This room-temperature C–H arylation system was also effective for substrates containing different directing groups, including amides, pyrazoles, pyrimidines, and oxime ethers (Table 3.6, entries 1–5). In addition, the mild reaction conditions enabled the first example of Pd-catalyzed C–H functionalization directed by a free oxime (entry 6). This functional group typically undergoes rapid hydrolysis in the acidic solvents and at the elevated temperatures required for most related reactions.¹³ The oxime serves as a versatile handle for elaboration of the products, as it can be readily transformed into a ketone, alcohol, amine, or amide.^{13b} Minor optimization was again performed on each substrate and some required slight adjustment from the standard reaction conditions. These changes were similar to before, however an increase in Ru(bpy)₃Cl₂•6H₂O to 5 mol % was needed in one case (entry 2) to afford a higher yield.

Table 3.6. Scope of Directing Group for the Pd/Ru-Catalyzed C–H Arylation

$$\text{L} \text{---} \text{C} \text{---} \text{H} + [\text{PhN}_2]\text{BF}_4 \xrightarrow[\text{MeOH, 25 }^\circ\text{C}]{\substack{10 \text{ mol } \% \text{ Pd(OAc)}_2 \\ 2.5 \text{ mol } \% \text{ Ru(bpy)}_3\text{Cl}_2 \cdot 6\text{H}_2\text{O} \\ 26 \text{ W light bulb}}} \text{L} \text{---} \text{C} \text{---} \text{Ph}$$

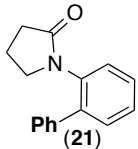
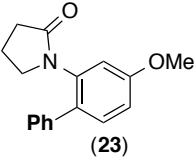
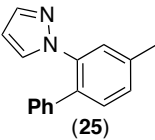
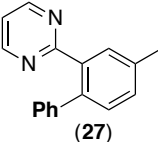
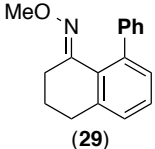
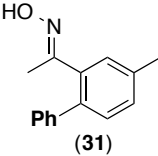
entry ^a	substrate	product	GC yield ^b (%)	isolated yield (%)
1			85	72
2 ^c			92	79
3 ^{d,e}			53	53
4 ^e			47	44
5 ^f			58	49
6 ^{g,h,i}			66	50

^aGeneral procedure: Substrate (1.0 equiv), Pd(OAc)₂ (0.1 equiv), Ru(bpy)₃Cl₂·6H₂O (0.025 equiv), [PhN₂]BF₄ (4.0 equiv), MeOH (0.1 M in substrate), rt, 4 h, 26 W compact fluorescent light bulb. ^bCalibrated yields determined by gas chromatographic analysis of the crude reaction mixtures. ^c0.05 equiv of Ru(bpy)₃Cl₂·6H₂O. ^dAg₂CO₃ (1.0 equiv) was used as an additive. ^eReaction was run for 5 h. ^f3.5 equiv of [PhN₂]BF₄. ^g0.20 equiv of Pd(OAc)₂. ^hReaction was run for 5.5 h. ⁱMeOH (0.2 M in substrate).

Control reactions were performed for the examples in Table 3.6. Again, Pd(OAc)₂, Ru(bpy)₃Cl₂•6H₂O, and visible light were all critical for achieving good yields of the products (Table 3.7).

Table 3.7. Controls Reactions for the Scope of Directing Group for the C–H Arylation

$$\text{L} \text{---} \text{C-H} + [\text{PhN}_2]\text{BF}_4 \xrightarrow[\text{MeOH, 25 }^\circ\text{C}]{\substack{10 \text{ mol } \% \text{ Pd(OAc)}_2 \\ 2.5 \text{ mol } \% \text{ Ru(bpy)}_3\text{Cl}_2 \cdot 6\text{H}_2\text{O} \\ 26 \text{ W light bulb}}} \text{L} \text{---} \text{C-Ph}$$

entry ^{ab}	product	yield without light (%)	yield without Ru cat (%)	yield without Pd cat (%)
1	 (21)	7	30	4
2 ^c	 (23)	1	5	<1
3 ^{d,e}	 (25)	3	13	3
4 ^e	 (27)	3	17	2
5 ^f	 (29)	9	9	2
6 ^{g,h,i}	 (31)	9	9	0

^a General procedure: Substrate (1.0 equiv), Pd(OAc)₂ (0.1 equiv), Ru(bpy)₃Cl₂·6H₂O (0.025 equiv), [PhN₂]BF₄ (4.0 equiv), MeOH (0.1 M in substrate), rt, 4 h, 26 W compact fluorescent light bulb. ^b Calibrated yields determined by gas chromatographic analysis of the crude reaction mixtures. ^c 0.05 equiv of Ru(bpy)₃Cl₂·6H₂O. ^d Ag₂CO₃ (1.0 equiv) was used as an additive. ^e Reaction was run for 5 h. ^f 3.5 equiv of [PhN₂]BF₄. ^g 0.20 equiv of Pd(OAc)₂. ^h Reaction was run for 5.5 h. ⁱ MeOH (0.2 M in substrate).

3.5 Scope of Aryldiazonium Salts

We next examined the use of diverse aryldiazonium salts in the coupling reaction with 1-phenyl-pyrrolidin-2-one (**20**). As depicted in Table 3.8, C–H arylation proceeded in good to excellent yield with electron-deficient, electron-rich, and relatively sterically hindered arylating reagents. A number of diazonium salts were not effective arylating coupling partners and only afforded products in low yields (<25% yield) (Figure 3.4). These salts contained aryl groups that were either sterically bulky or considerably electron-rich. Additionally, some of the salts were brightly colored, which suggests they could be absorbing light and decomposing under the reaction conditions. These reasons, among others, could explain the low yields of desired product formed from these diazonium salts.

Table 3.8. Scope of Aryldiazonium Salts for the Pd/Ru Catalyzed C–H Arylation

entry ^a	[ArN ₂]BF ₄	product	GC yield ^b (%)	isolated yield (%)
1 ^c			76	76
2 ^d			92	87
3			86	76
4			99	78
5 ^e			81	79
6 ^{e,f,g}			55	57

^a General procedure: Substrate **X** (1.0 equiv), Pd(OAc)₂ (0.1 equiv), Ru(bpy)₃Cl₂·6H₂O (0.025 equiv), [ArN₂]BF₄ (4.0 equiv), MeOH (0.1 M in substrate), rt, 4 h, 26 W compact fluorescent light bulb. ^b Calibrated yields determined by gas chromatographic analysis of the crude reaction mixtures. ^c Reaction was run for 6 h. ^d 3.4 equiv of [ArN₂]BF₄. ^e 0.05 equiv of Ru(bpy)₃Cl₂·6H₂O. ^f Reaction was run for 10 h. ^g MeOH (0.2 M in substrate).

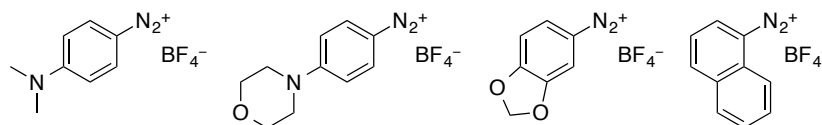
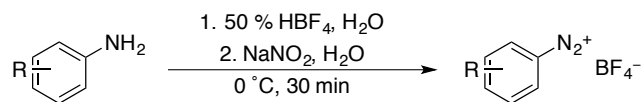


Figure 3.4. Aryl Diazonium Salts that were Ineffective Arylating Coupling Partners

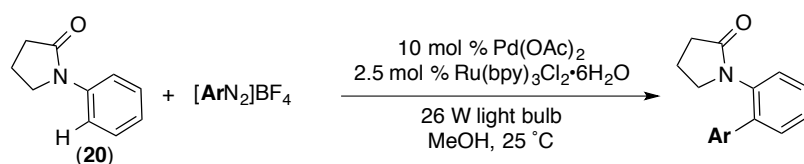
The diazonium salts were readily synthesized in a simple one step procedure from aniline derivatives (Scheme 3.11).¹⁴ These salts were easily recrystallized from acetone and diethyl ether. Precaution with the diazonium salts was taken, including the use of blast shields and minimal exposure, because of their explosive nature. However, the tetrafluoroborate salts are among the safest forms of these materials.¹⁵ The salts were stored in a freezer under inert atmosphere.

Scheme 3.11. Synthesis of Aryl Diazonium Salts from Aniline Derivatives



Control reactions were performed omitting $\text{Pd}(\text{OAc})_2$, $\text{Ru}(\text{bpy})_3\text{Cl}_2 \cdot 6\text{H}_2\text{O}$, or visible light (Table 3.9). Interestingly, the electron-deficient derivatives (**34**, **36**, and **38**) showed modest to high photoreactivities with **20** in the absence of $\text{Ru}(\text{bpy})_3\text{Cl}_2 \cdot 6\text{H}_2\text{O}$. (For more discussion on this topic see section 3.6.)

Table 3.9. Control Reactions for the Scope of Aryldiazonium Salts for the C–H Arylation



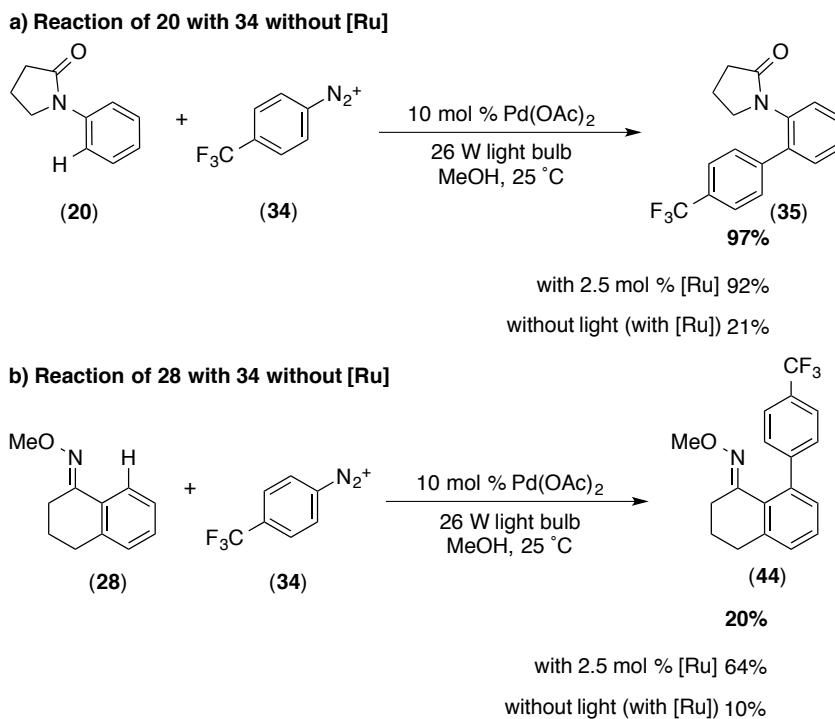
entry ^{ab}	$[\text{ArN}_2]\text{BF}_4$	yield without light (%)	yield without Ru cat (%)	yield without Pd cat (%)
1 ^c		10	25	7
2		21	97 ^d	8
3		14	62	7
4		20	97	6
5 ^e		3	56	2
6 ^{e,f,g}		3	5	2

^a General procedure: Substrate **X** (1.0 equiv), $\text{Pd}(\text{OAc})_2$ (0.1 equiv), $\text{Ru}(\text{bpy})_3\text{Cl}_2 \cdot 6\text{H}_2\text{O}$ (0.025 equiv), $[\text{ArN}_2]\text{BF}_4$ (4.0 equiv), MeOH (0.1 M in substrate), rt, 4 h, 26 W compact fluorescent light bulb. ^b Calibrated yields determined by gas chromatographic analysis of the crude reaction mixtures. ^c Reaction was run for 6 h. ^d 3.4 equiv of $[\text{ArN}_2]\text{BF}_4$. ^e 0.05 equiv of $\text{Ru}(\text{bpy})_3\text{Cl}_2 \cdot 6\text{H}_2\text{O}$. ^f Reaction was run for 10 h. ^g MeOH (0.2 M in substrate).

3.6 Background Reaction

When certain aryldiazonium salts were reacted with **20**, high yields of the desired product were observed in the absence of Ru(bpy)₃Cl₂•6H₂O (see section 3.5). This high background reaction was predominantly observed with electron-deficient aryldiazonium salts. In one of the most pronounced cases, **20** underwent Pd-catalyzed photoreaction with [4-CF₃C₆H₄N₂]⁺BF₄⁻ (**34**) to afford **35** in 97% calibrated GC yield without [Ru] (Scheme 3.12a). This yield was comparable to that obtained using 2.5 mol % Ru(bpy)₃Cl₂•6H₂O under otherwise analogous conditions (92% by GC). Interestingly, this uncatalyzed photoreaction was highly substrate-dependent; for example, relatively little reaction was observed between **34** and oxime ether **28** in the absence of [Ru] (Scheme 3.12b).

Scheme 3.12. Background Reaction with Electron-Deficient Aryldiazonium Salts



The origin of this photoreactivity in the absence of [Ru] has not been definitively established. We tentatively hypothesize that certain palladacyclic intermediates may participate in photoinduced electron transfer to electron-deficient aryldiazonium salts to initiate this transformation. This theory would explain the difference in reactivity with

various substrates and is in accordance with the electron-deficient aryldiazonium salts being more willing to be reduced by one electron by a palladacycle intermediate.

3.7 Proposed Mechanism

Although the mechanistic details of this Pd/Ru photocatalyzed C–H arylation remain to be elucidated, a possible catalytic cycle is shown in Figure 3.5. First there is photoexcitation of the Ru catalyst to generate $\text{Ru}(\text{bpy})_3^{2+*}$ (step *i*), followed by reduction of the aryldiazonium salt to Ar^\bullet and concomitant oxidation of the Ru center to $\text{Ru}(\text{bpy})_3^{3+}$ (step *ii*).¹¹ The reaction of Ar^\bullet with palladacycle **45**, which was generated by C–H activation of the substrate, could then occur to afford the Pd^{III} intermediate **46** (step *iii*). Next the one-electron oxidation of **46** by $\text{Ru}(\text{bpy})_3^{3+}$ would regenerate the photocatalyst and form Pd^{IV} intermediate **47** (step *iv*). The final step would be C–C bond-forming reductive elimination to release the arylated product and regenerate the Pd^{II} catalyst (step *v*). This mechanism however is only one possibility and given the current data other routes cannot be discarded.

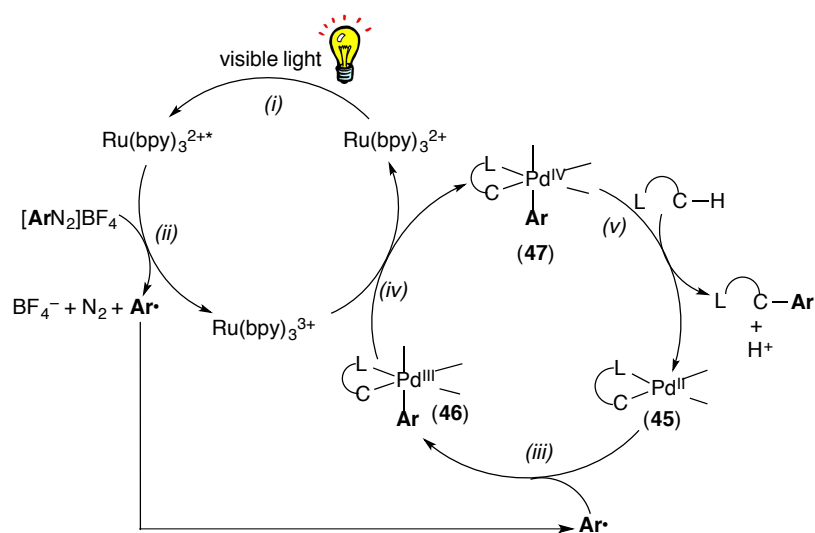


Figure 3.5. Possible $\text{Pd}^{\text{II/IV}}$ Mechanism for the Pd/Ru-Catalyzed C–H Arylation Reaction

Cautious to accept the first proposal, other mechanisms have been considered for this transformation. One possible mechanism would reverse steps *iii* and *iv*, proposing

the one-electron oxidation of **45** by $\text{Ru}(\text{bpy})_3^{3+}$, regenerating the photocatalyst, and forming Pd^{III} intermediate **48**, followed by reaction of Ar^\bullet with palladacycle **48** to form a Pd^{IV} species (**49**) (Figure 3.6). Another mechanism outlines a scheme similar to that described in Figure 3.5, however it proceeds through a $\text{Pd}^{\text{I/III}}$ pathway (Figure 3.7).

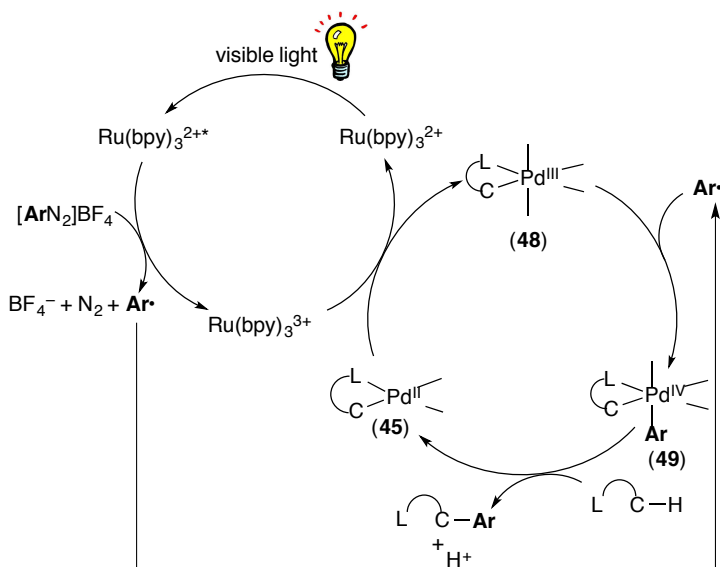


Figure 3.6. Alternative $\text{Pd}^{\text{II/IV}}$ Mechanism for the Pd/Ru-Catalyzed C–H Arylation Reaction

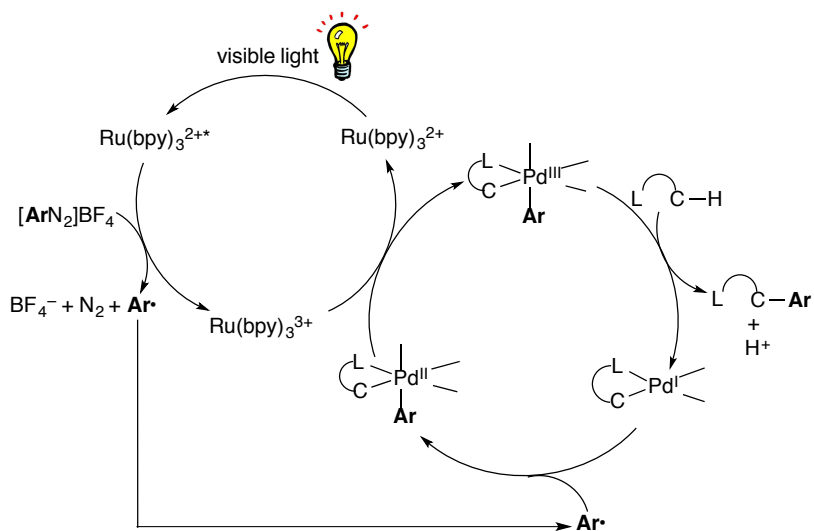
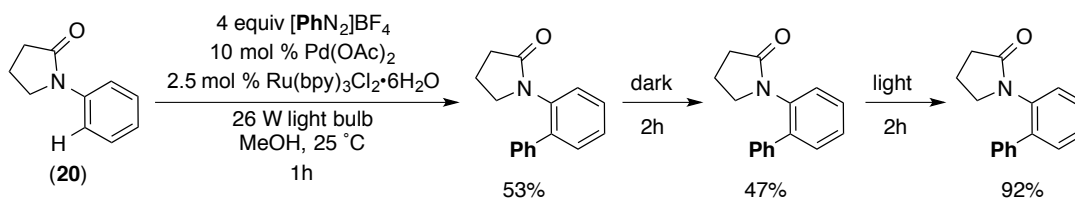


Figure 3.7. Alternative $\text{Pd}^{\text{I/III}}$ Mechanism for the Pd/Ru-Catalyzed C–H Arylation Reaction

To test for the possibility of a radical chain mechanism, an experiment was conducted that has been used in other photocatalytic transformations.¹⁶ The experiment was constructed of periods of time alternating between light and dark for an otherwise analogous reaction set up. As shown in Scheme 3.13, **20** was submitted to the standard reaction conditions and yielded 53% of product after 1 hour. Upon subjecting the reaction to the dark for 2 hours, the yield of product (within error) did not change. However, resubmitting the reaction to the light for 2 hours led to near full conversion and 92% yield. These experiments suggest that if a radical chain pathway is operating the chains terminate rapidly in the absence of light. Thus we hypothesize that the proposed photocatalyzed mechanism could be the major pathway in this C–H arylation reaction.

Scheme 3.13. Experiment to Probe for Radical Chain Mechanism



3.8 Conclusions

In summary, this chapter has described a mild approach for palladium-catalyzed, ligand-directed arylation of aromatic C–H bonds. These reactions proceed at room temperature and are compatible with a range of functional groups, directing ligands, and aryldiazonium salts. This system introduces the idea of merging visible-light photoredox catalysis (which can be used to generate diverse reactive intermediates) with palladium-catalyzed C–H functionalization. We anticipate that this new concept will find application in the development of many new synthetically useful transformations.¹⁷ Although the mechanism of this exact system has not been studied in detail, the mechanism of a similar system has been studied and is further outlined in Chapter 4.

3.9 Experimental Procedures and Characterization of Data

General Procedures

NMR spectra were obtained on a Varian vnmrs 700 (699.76 MHz for ^1H ; 175.95 MHz for ^{13}C), Varian vnmrs 500 (500.10 MHz for ^1H ; 125.75 MHz for ^{13}C , 470.56 MHz for ^{19}F), Varian Inova 500 (499.90 MHz for ^1H ; 125.70 MHz for ^{13}C), Varian MR400 (400.52 MHz for ^1H ; 100.71 for ^{13}C , 376.87 MHz for ^{19}F), or a Varian Inova 400 (399.96 MHz for ^1H ; 100.57 MHz for ^{13}C ; 376.34 MHz for ^{19}F) spectrometer. ^1H NMR chemical shifts are reported in parts per million (ppm) relative to TMS, with the residual solvent peak used as an internal reference. Multiplicities are reported as follows: singlet (s), doublet (d), doublet of doublets (dd), doublet of doublets of doublets (ddd), doublet of triplets (dt), triplet (t), quartet (q), quintet (quin), multiplet (m), and broad resonance (br). IR spectra were obtained on a Perkin-Elmer Spectrum BX FT-IR spectrometer. Melting points were determined with a Mel-Temp 3.0, a Laboratory Devices Inc, USA instrument, and are uncorrected. HRMS data were obtained on a Micromass AutoSpec Ultima Magnetic Sector mass spectrometer. Gas chromatography was carried out on a Shimadzu 17A using a Restek Rtx®-5 (Crossbond 5% diphenyl – 95% dimethyl polysiloxane; 15 m, 0.25 mm ID, 0.25 μm df) column.

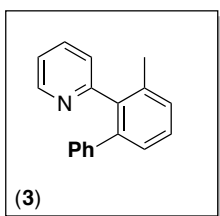
Materials and Methods

Substrates **2**,¹⁸ **6**,¹⁸ **10**,¹⁹ **12**,¹⁸ **22**,²⁰ **24**,²¹ **26**,²² and **30**²³ were prepared according to literature procedures. Substrate **8** was prepared by Pd-catalyzed Suzuki coupling between 2-tolylboronic acid and 2-bromo-5-chloropyridine.¹⁹ Substrate **14** was prepared by Suzuki coupling between 2-tolylboronic acid and 2-bromo-4-nitropyridine.¹⁸ Substrate **16** was prepared by palladium-catalyzed Suzuki coupling between 2-methoxyboronic acid and 2-bromopyridine. Substrate **18** was prepared by palladium-catalyzed Suzuki coupling between 4-trifluoromethylboronic acid and 3-methyl-2-bromopyridine. Oxime ether substrate **28** was prepared by the reaction of the corresponding ketone with $\text{MeONH}_2\cdot\text{HCl}$ /pyridine.^{13a} Aryl diazonium tetrafluoroborate salts were prepared according to a literature procedure.²⁴ 1-Phenyl-2-pyrrolidinone **20** was obtained from Aldrich and used as received. $\text{Pd}(\text{OAc})_2$, $\text{Ru}(\text{bpy})_3\text{Cl}_2\cdot 6\text{H}_2\text{O}$, and Ag_2CO_3 were obtained from Pressure Chemical, Aldrich or Strem, and Acros, respectively, and used as received.

MeOH was dried over sodium and distilled under N₂ prior to use. Although the use of wet, non-degassed MeOH as a reaction solvent provided satisfactory yields in some trials, dry oxygen-free MeOH was found to be important to achieving reliably reproducible results. Other solvents were obtained from Fisher Chemical and used without further purification. Flash chromatography was performed on EM Science silica gel 60 (0.040–0.063 mm particle size, 230–400 mesh) and thin layer chromatography was performed on Merck TLC plates pre-coated with silica gel 60 F₂₅₄. Regulation of ambient temperature was found to be critical to achieving reproducibility in many of the reactions that were examined; this was accomplished by submerging the reaction vials into a 25 °C water bath contained in a transparent colorless glass vessel (large beaker or crystallizing dish).

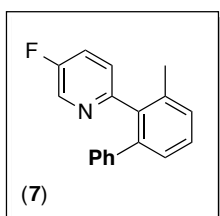
Experimental Details

Synthesis of Products in Table 3.4



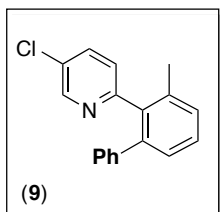
Ru(bpy)₃Cl₂•6H₂O (8.27 mg, 0.01 mmol, 0.025 equiv), Ag₂CO₃ (12.2 mg, 0.04 mmol, 0.10 equiv), and Pd(OAc)₂ (9.90 mg, 0.04 mmol, 0.10 equiv) were weighed into a 20 mL vial. The vial was taken into a glove box, and [PhN₂]BF₄ (339 mg, 1.77 mmol, 4.0 equiv) and MeOH (2.2 mL) were added. Substrate **2** (75.0 mg, 0.44 mmol, 1.0 equiv) was added to the reaction vial as a solution in MeOH (2.2 mL). The vial was sealed with a Teflon lined cap, removed from the glove box and placed on a stir plate with two 26 W compact fluorescent light bulbs (one on either side of the vial about 5 cm away). The reaction mixture was allowed to stir at room temperature for 4 h. The reaction was then quenched with brine (2 mL), 10% aqueous Na₂SO₃ (2 mL) and EtOAc (10 mL). The calibrated GC yield of the crude product was determined to be 84% (using hexadecane as the standard). The reaction mixture was then diluted with additional Et₂O (50 mL) and H₂O (25 mL) and extracted with 10% aqueous Na₂SO₃ (2 x 35 mL). The combined aqueous layers

were extracted with Et₂O (1 x 100 mL). Finally, the combined organic layers were washed with brine (1 x 50 mL), dried over MgSO₄, filtered, concentrated, and chromatographed on a 21 cm x 3 cm silica gel column (*R_f* = 0.10 in 90% hexanes/10% diethyl ether). Product **3** was obtained as a clear viscous oil (83.0 mg, 76% yield). ¹H NMR (700 MHz, CDCl₃): δ 8.64-8.63 (m, 1H), 7.44 (td, *J* = 7.4, 2.1 Hz, 1H), 7.37 (t, *J* = 7.4 Hz, 1H), 7.30 (dd, *J* = 7.7, 0.7 Hz, 1H), 7.28 (d, *J* = 7.7 Hz, 1H), 7.15-7.08 (multiple peaks, 6H), 6.89 (d, *J* = 7.7 Hz, 1H), 2.20 (s, 3H). ¹³C{¹H} NMR (700 MHz, CDCl₃): δ 159.53, 148.76, 141.61, 141.19, 139.26, 136.64, 135.64, 129.59, 129.35, 127.98, 127.54, 127.52, 126.16, 125.57, 121.22, 20.42. HRMS [M+H]⁺ Calcd for C₁₈H₁₆N: 246.1277; Found: 246.1282.



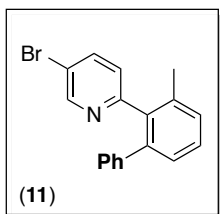
Ru(bpy)₃Cl₂•6H₂O (7.50 mg, 0.01 mmol, 0.025 equiv), and Pd(OAc)₂ (13.5 mg, 0.06 mmol, 0.15 equiv) were weighed into a 20 mL vial. The vial was taken into a glove box, and [PhN₂]BF₄ (306 mg, 1.60 mmol, 4.0 equiv) and MeOH (4.0 mL) were added. Substrate **6** (75.0 mg, 0.40 mmol, 1.0 equiv) was added to the reaction vial as a solution in MeOH (4.0 mL). The vial was sealed with a Teflon lined cap, removed from the glove box and placed on a stir plate with two 26 W compact fluorescent light bulbs (one on either side of the vial about 5 cm away). The reaction mixture was allowed to stir at room temperature for 4 h. The reaction was then quenched with brine (2 mL), 10% aqueous Na₂SO₃ (2 mL), and EtOAc (10 mL). The calibrated GC yield of the crude product was determined to be 73% (using hexadecane as the standard). The reaction mixture was then diluted with additional Et₂O (50 mL) and H₂O (25 mL) and extracted with 10% aqueous Na₂SO₃ (2 x 35 mL). The combined aqueous layers were extracted with Et₂O (1 x 100 mL). Finally, the combined organic layers were washed with brine (1 x 50 mL), dried over MgSO₄, filtered, concentrated, and chromatographed on a 22 cm x 3 cm silica gel column (*R_f* = 0.08 in 97.5% hexanes/2.5% diethyl ether). Product **7** was obtained as a clear viscous oil (69.1 mg, 65% yield). ¹H NMR (700 MHz, CD₂Cl₂): δ 8.47 (d, *J* = 2.8

Hz, 1H), 7.38 (t, $J = 7.0$ Hz, 1H), 7.30 (d, $J = 7.7$ Hz, 1H), 7.27 (d, $J = 7.0$ Hz, 1H), 7.21-7.12 (multiple peaks, 4H), 7.06-7.04 (multiple peaks, 2H), 6.89 (dd, $J = 8.4, 4.9$ Hz 1H), 2.15 (s, 3H). $^{13}\text{C}\{^1\text{H}\}$ NMR (125 MHz, CD_2Cl_2): δ 158.59 (d, $^1J_{\text{C-F}} = 253$ Hz), 156.29 (d, $^3J_{\text{C-F}} = 4.4$ Hz), 142.14, 141.97, 139.16 (d, $^4J_{\text{C-F}} = 1.0$ Hz), 137.47 (d, $^2J_{\text{C-F}} = 23$ Hz), 130.19, 129.87, 128.68, 128.25, 128.14, 127.07, 127.03, 126.89, 122.95 (d, $^2J_{\text{C-F}} = 18$ Hz), 20.77. ^{19}F NMR (470 MHz, CD_2Cl_2): δ -130.89 to -130.91 (m). HRMS $[\text{M}+\text{H}]^+$ Calcd for $\text{C}_{18}\text{H}_{15}\text{FN}$: 264.1183; Found: 264.1186.

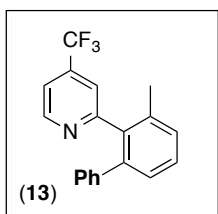


$\text{Ru}(\text{bpy})_3\text{Cl}_2 \cdot 6\text{H}_2\text{O}$ (6.80 mg, 0.01 mmol, 0.025 equiv), Ag_2CO_3 (10.1 mg, 0.04 mmol, 0.10 equiv), and $\text{Pd}(\text{OAc})_2$ (8.25 mg, 0.04 mmol, 0.10 equiv) were weighed into a 20 mL vial. The vial was taken into a glove box, and $[\text{PhN}_2]\text{BF}_4$ (352 mg, 1.84 mmol, 5.0 equiv) and MeOH (3.7 mL) were added. Substrate **8** (75.0 mg, 0.37 mmol, 1.0 equiv) was added to the reaction vial as a solution in MeOH (3.7 mL). The vial was sealed with a Teflon lined cap, removed from the glove box and placed on a stir plate with two 26 W compact fluorescent light bulbs (one on either side of the vial about 5 cm away). The reaction mixture was allowed to stir at room temperature for 10 h. The reaction was quenched with brine (2 mL), 10% aqueous Na_2SO_3 (2 mL), and EtOAc (10 mL). The calibrated GC yield of the crude product was determined to be 64% (using hexadecane as the standard). The reaction mixture was then diluted with additional Et_2O (50 mL) and H_2O (25 mL) and extracted with 10% aqueous Na_2SO_3 (2 x 35 mL). The combined aqueous layers were extracted with Et_2O (1 x 100 mL). Finally, the combined organic layers were washed with brine (1 x 50 mL), dried over MgSO_4 , filtered, concentrated, and chromatographed on a 22 cm x 3 cm silica gel column ($R_f = 0.13$ in 97.5% hexanes/2.5% diethyl ether). Product **9** was obtained as a white solid (63.3 mg, 61% yield). Mp = 61.9-63.4 $^\circ\text{C}$. ^1H NMR (700 MHz, CDCl_3): δ 8.58 (d, $J = 2.1$ Hz, 1H), 7.42-7.40 (m, 1H), 7.36 (t, $J = 7.7$ Hz, 1H), 7.29 (d, $J = 7.7$ Hz, 1H), 7.26 (d, $J = 7.7$ Hz, 1H), 7.17-7.14 (multiple peaks, 3H), 7.05-7.04 (multiple peaks, 2H), 6.81 (d, $J = 8.4$ Hz 1H), 2.19 (s, 3H).

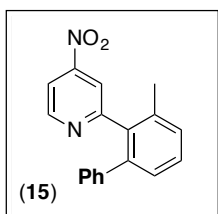
$^{13}\text{C}\{^1\text{H}\}$ NMR (176 MHz, CDCl_3): δ 157.73, 147.73, 141.36, 141.29, 138.07, 136.71, 135.50, 129.78, 129.59, 129.52, 128.32, 127.77, 127.69, 126.42, 126.41, 20.48. HRMS $[\text{M}+\text{H}]^+$ Calcd for $\text{C}_{18}\text{H}_{15}\text{ClN}$: 280.0888; Found: 280.0891.



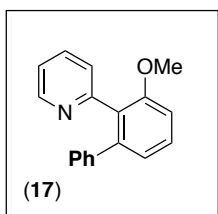
$\text{Ru}(\text{bpy})_3\text{Cl}_2\cdot 6\text{H}_2\text{O}$ (5.64 mg, 0.007 mmol, 0.025 equiv), Ag_2CO_3 (8.3 mg, 0.03 mmol, 0.10 equiv), and $\text{Pd}(\text{OAc})_2$ (10.2 mg, 0.04 mmol, 0.15 equiv) were weighed into a 20 mL vial. The vial was taken into a glove box, and $[\text{PhN}_2]\text{BF}_4$ (289 mg, 1.51 mmol, 5.0 equiv) and MeOH (3.0 mL) were added. Substrate **10** (75.0 mg, 0.30 mmol, 1.0 equiv) was added to the reaction vial as a solution in MeOH (3.0 mL). The vial was sealed with a Teflon lined cap, removed from the glove box, and placed on a stir plate with two 26 W compact fluorescent light bulbs (one on either side of the vial about 5 cm away). The reaction mixture was allowed to stir at room temperature for 10 h. The reaction was quenched with brine (2 mL), 10% aqueous Na_2SO_3 (2 mL), and EtOAc (10 mL). The calibrated GC yield of the crude product was determined to be 62% (using undecane as the standard). The reaction mixture was then diluted with additional Et_2O (50 mL) and H_2O (25 mL) and extracted with 10% aqueous Na_2SO_3 (2 x 35 mL). The combined aqueous layers were extracted with Et_2O (1 x 100 mL). Finally, the combined organic layers were washed with brine (1 x 50 mL), dried over MgSO_4 , filtered, concentrated, and chromatographed on a 20 cm x 3 cm silica gel column ($R_f = 0.14$ in 97.5% hexanes/2.5% diethyl ether). Product **11** was obtained as a white solid (62.1 mg, 63% yield). Mp = 87.6-91.4 $^\circ\text{C}$. ^1H NMR (700 MHz, CDCl_3): δ 8.69 (d, $J = 2.1$ Hz, 1H), 7.57 (dd, $J = 8.4, 2.8$ Hz, 1H), 7.37 (t, $J = 7.7$ Hz, 1H), 7.29 (d, $J = 7.7$ Hz, 1H), 7.27 (d, $J = 7.7$ Hz, 1H), 7.17-7.15 (multiple peaks, 3H), 7.07-7.05 (multiple peaks, 2H), 6.77 (d, $J = 8.4$ Hz, 1H), 2.18 (s, 3H). $^{13}\text{C}\{^1\text{H}\}$ NMR (176 MHz, CDCl_3): δ 158.10, 149.92, 141.34, 141.22, 138.35, 138.05, 136.65, 129.59, 129.53, 128.34, 127.79, 127.71, 126.94, 126.45, 118.52, 20.49. HRMS $[\text{M}+\text{H}]^+$ Calcd for $\text{C}_{18}\text{H}_{15}\text{BrN}$: 324.0382; Found: 324.0386.



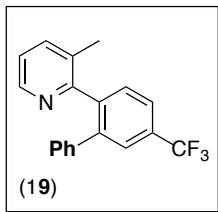
Ru(bpy)₃Cl₂•6H₂O (5.90 mg, 0.007 mmol, 0.025 equiv) and Pd(OAc)₂ (7.1 mg, 0.03 mmol, 0.1 equiv) were weighed into a 20 mL vial. The vial was taken into a glove box, and [PhN₂]BF₄ (242 mg, 1.26 mmol, 4.0 equiv) and MeOH (3.1 mL) were added. Substrate **12** (75.0 mg, 0.32 mmol, 1.0 equiv) was added to the reaction vial as a solution in MeOH (3.2 mL). The vial was sealed with a Teflon lined cap, removed from the glove box, and placed on a stir plate with two 26 W compact fluorescent light bulbs (one on either side of the vial about 5 cm away). The reaction mixture was allowed to stir at room temperature for 8 h. The reaction was then quenched with brine (2 mL), 10% aqueous Na₂SO₃ (2 mL), and EtOAc (10 mL). The calibrated GC yield of the crude product was determined to be 62% (using hexadecane as the standard). The reaction mixture was then diluted with additional Et₂O (50 mL) and H₂O (25 mL), and extracted with 10% aqueous Na₂SO₃ (2 x 35 mL). The combined aqueous layers were extracted with Et₂O (1 x 100 mL). Finally, the combined organic layers were washed with brine (1 x 50 mL), dried over MgSO₄, filtered, concentrated, and chromatographed on a 20.5 cm x 3 cm silica gel column (R_f = 0.10 in 96% hexanes/4% diethyl ether). Product **13** was obtained as a white solid (58.8 mg, 59% yield). Mp = 78.2-81.1 °C. ¹H NMR (700 MHz, CDCl₃): δ 8.78 (d, *J* = 4.9 Hz, 1H), 7.39 (t, *J* = 7.0 Hz, 1H), 7.33 (d, *J* = 7.7 Hz, 1H), 7.30-7.29 (multiple peaks, 2H), 7.14-7.13 (multiple peaks, 3H), 7.07 (s, 1H), 7.01-7.00 (multiple peaks, 2H), 2.21 (s, 3H). ¹³C{¹H} NMR (176 MHz, CDCl₃): δ 161.07, 149.75, 141.36, 141.04, 138.08, 137.87 (q, ²J_{C-F} = 34 Hz), 136.51, 129.63, 129.53, 128.61, 127.76, 127.66, 126.55, 122.61 (q, ¹J_{C-F} = 273 Hz), 121.62 (q, ³J_{C-F} = 4.0 Hz), 116.68 (q, ³J_{C-F} = 3.3 Hz), 20.45. ¹⁹F NMR (470 MHz, CDCl₃): δ -65.11 HRMS [M+H]⁺ Calcd for C₁₉H₁₅F₃N: 314.1151; Found: 314.1156.



Substrate **14** (75.0 mg, 0.35 mmol, 1.0 equiv), Ru(bpy)₃Cl₂•6H₂O (6.50 mg, 0.009 mmol, 0.025 equiv), and Pd(OAc)₂ (11.8 mg, 0.05 mmol, 0.15 equiv) were weighed into a 20 mL vial. The vial was taken into a glove box, and [PhN₂]BF₄ (334 mg, 1.75 mmol, 5.0 equiv) and MeOH (7.0 mL) were added. The vial was sealed with a Teflon lined cap, removed from the glove box, and placed on a stir plate with two 26 W compact fluorescent light bulbs (one on either side of the vial about 5 cm away). The reaction mixture was allowed to stir at room temperature for 9.5 h. The reaction was then quenched with brine (2 mL), 10% aqueous Na₂SO₃ (2 mL), and EtOAc (10 mL). The calibrated GC yield of the crude product was determined to be 51% (using hexadecane as the standard). The reaction mixture was then diluted with additional Et₂O (50 mL) and H₂O (25 mL), and extracted with 10% aqueous Na₂SO₃ (2 x 35 mL). The combined aqueous layers were extracted with Et₂O (1 x 100 mL). Finally, the combined organic layers were washed with brine (1 x 50 mL), dried over MgSO₄, filtered, concentrated, and chromatographed on a 20 cm x 3 cm silica gel column (R_f = 0.17 in 87.5% hexanes/12.5% diethyl ether). Product **15** was obtained as a clear viscous oil (47.8 mg, 47% yield). ¹H NMR (700 MHz, CDCl₃): δ 8.91 (d, *J* = 5.6 Hz, 1H), 7.81 (dd, *J* = 5.6, 2.1 Hz, 1H), 7.60 (d *J* = 2.1 Hz, 1H), 7.43 (t, *J* = 7.7 Hz, 1H), 7.34 (d, *J* = 7.4 Hz, 1H), 7.32 (d, *J* = 7.4 Hz, 1H), 7.15-7.12 (multiple peaks, 3H), 7.04-7.03 (multiple peaks, 2H), 2.20 (s, 3H). ¹³C{¹H} NMR (176 MHz, CDCl₃): δ 162.92, 153.44, 150.96, 141.49, 140.75, 137.46, 136.43, 129.69, 129.57, 128.94, 127.94, 127.83, 126.77, 118.23, 113.68, 20.43. IR (thin film, CH₂Cl₂): 2922, 1567, 1527, 1458, 1380, 1352, 1222 cm⁻¹. HRMS [M+H]⁺ Calcd for C₁₈H₁₅N₂O₂: 291.1128; Found: 291.1130.

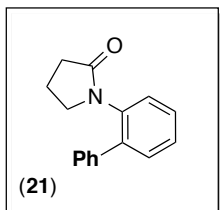


Ru(bpy)₃Cl₂•6H₂O (7.50 mg, 0.01 mmol, 0.025 equiv) and Pd(OAc)₂ (9.1 mg, 0.04 mmol, 0.1 equiv) were weighed into a 20 mL vial. The vial was taken into a glove box, and [PhN₂]BF₄ (309 mg, 1.62 mmol, 4.0 equiv) and MeOH (4.1 mL) were added. Substrate **16** (75.0 mg, 0.40 mmol, 1.0 equiv) was added to the reaction vial as a solution in MeOH (4.0 mL). The vial was sealed with a Teflon lined cap, removed from the glove box, and placed on a stir plate with two 26 W compact fluorescent light bulbs (one on either side of the vial about 5 cm away). The reaction mixture was allowed to stir at room temperature for 10 h. The reaction was then quenched with brine (2 mL), 10% aqueous Na₂SO₃ solution (2 mL) and EtOAc (10 mL). The reaction mixture was diluted with additional Et₂O (50 mL) and H₂O (25 mL), and extracted with 10% aqueous Na₂SO₃ (2 x 35 mL). The combined aqueous layers were extracted with Et₂O (1 x 100 mL). Finally, the combined organic layers were washed with brine (1 x 50 mL), dried over MgSO₄, filtered, and concentrated. The calibrated GC yield of the crude product was determined to be 77% (using undecane as the standard). The crude product was chromatographed on a 20 cm x 3 cm silica gel column (R_f = 0.10 in 60% hexanes/40% diethyl ether). Product **17** was obtained as a light yellow solid (73.3 mg, 69% yield). Mp = 77.7–85.4 °C. ¹H NMR (700 MHz, CDCl₃): δ 8.58–8.57 (m, 1H), 7.48 (td, *J* = 7.0, 1.4 Hz, 1H), 7.43 (t, *J* = 8.4 Hz, 1H), 7.15–7.11 (multiple peaks, 3H), 7.09–7.06 (multiple peaks, 4H), 7.02 (t, *J* = 6.8 Hz, 2H), 3.79 (s, 3H). ¹³C {¹H} NMR (176 MHz, CDCl₃): δ 157.22, 156.83, 148.80, 142.78, 141.04, 135.38, 129.53, 129.14, 129.07, 127.58, 126.31, 126.22, 122.48, 121.27, 110.02, 55.95. HRMS [M+H]⁺ Calcd for C₁₈H₁₆NO: 262.1226; Found: 262.1231.

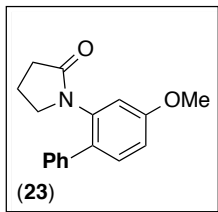


Ru(bpy)₃Cl₂•6H₂O (5.90 mg, 0.007 mmol, 0.025 equiv) and Pd(OAc)₂ (10.6 mg, 0.05 mmol, 0.15 equiv) were weighed into a 20 mL vial. The vial was taken into a glove box, and [PhN₂]BF₄ (302 mg, 1.57 mmol, 5.0 equiv) and MeOH (3.2 mL) were added. Substrate **18** (75.0 mg, 0.32 mmol, 1.0 equiv) was added to the reaction vial as a solution in MeOH (3.1 mL). The vial was sealed with a Teflon lined cap, removed from the glove box, and placed on a stir plate with two 26 W compact fluorescent light bulbs (one on either side of the vial about 5 cm away). The reaction mixture was allowed to stir at room temperature for 8 h. The reaction was then quenched with brine (2 mL), 10% aqueous Na₂SO₃ (2 mL), and EtOAc (10 mL). The calibrated GC yield of the crude product was determined to be 76% (using hexadecane as the standard). The reaction mixture was then diluted with an additional Et₂O (50 mL) and H₂O (25 mL), and extracted with 10% aqueous Na₂SO₃ (2 x 35 mL). The combined aqueous layers were extracted with Et₂O (1 x 100 mL). Finally, the combined organic layers were washed with brine (1 x 50 mL), dried over MgSO₄, filtered, concentrated, and chromatographed on a 21 cm x 3 cm silica gel column (R_f = 0.18 in 88% hexanes/12% diethyl ether). Product **19** was obtained as a clear viscous oil (59.2 mg, 60% yield). ¹H NMR (700 MHz, CD₂Cl₂): δ 8.47 (d, *J* = 4.9 Hz, 1H), 7.75 (s, 1H), 7.72 (d, *J* = 8.4 Hz, 1H), 7.52 (d, *J* = 7.7 Hz, 1H), 7.36 (d, *J* = 8.4 Hz, 1H), 7.24-7.19 (multiple peaks, 3H), 7.16-7.13 (multiple peaks, 3H), 1.78 (s, 3H). ¹³C{¹H} NMR (176 MHz, CD₂Cl₂): δ 158.47, 147.07, 143.67, 141.88, 140.14, 137.92, 131.88, 131.11, 130.61 (q, ²*J*_{C-F} = 32 Hz), 129.56, 128.40, 127.70, 127.02 (q, ³*J*_{C-F} = 3.8 Hz), 124.71 (q, ¹*J*_{C-F} = 272 Hz), 124.32 (q, ³*J*_{C-F} = 3.3 Hz), 122.97, 18.83. ¹⁹F NMR (377 MHz, CD₂Cl₂): δ -62.81 HRMS [M+H]⁺ Calcd for C₁₉H₁₅F₃N: 314.1151; Found: 314.1154.

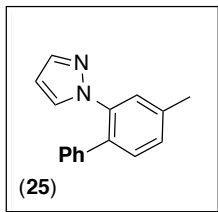
Synthesis of Products in Table 3.6



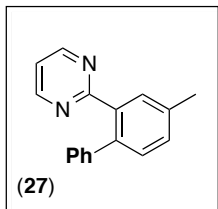
Substrate **20** (75.0 mg, 0.46 mmol, 1.0 equiv), Ru(bpy)₃Cl₂•6H₂O (8.70 mg, 0.01 mmol, 0.025 equiv), and Pd(OAc)₂ (10.4 mg, 0.05 mmol, 0.10 equiv) were weighed into a 20 mL vial. The vial was taken into the glove box, and [PhN₂]BF₄ (355 mg, 1.86 mmol, 4.0 equiv) and MeOH (4.6 mL) were added. The vial was sealed with a Teflon lined cap, removed from the glove box, and placed on a stir plate with two 26 W compact fluorescent light bulbs (one on either side of the vial about 5 cm away). The reaction mixture was allowed to stir at room temperature for 4 h. Then the reaction was quenched with brine (2 mL), 10% aqueous Na₂SO₃ (2 mL), and EtOAc (10 mL). The calibrated GC yield of the crude product was determined to be 85% (using hexadecane as the standard). The reaction mixture was then diluted with additional Et₂O (50 mL) and H₂O (25 mL), and extracted with 10% aqueous Na₂SO₃ (2 x 35 mL). The combined aqueous layers were extracted with Et₂O (1 x 100 mL). Finally, the combined organic layers were washed with brine (1 x 50 mL), dried over MgSO₄, filtered, concentrated, and chromatographed on a 17.5 cm x 3 cm silica gel column (R_f = 0.23 in 30% hexanes/70% diethyl ether). Product **21** was obtained as a clear viscous oil (79.1 mg, 72% yield). ¹H NMR (700 MHz, C₆D₆): δ 7.37 (d, *J* = 7.5 Hz, 2H), 7.32 (d, 1H), 7.20 (dd, *J* = 8.0, 1.2 Hz, 1H), 7.14-7.10 (multiple peaks, 3H), 7.09-7.03 (multiple peaks, 2H), 2.74 (t, *J* = 6.8 Hz, 2H), 2.01 (t, *J* = 8.0 Hz, 2H), 1.15 (quin, *J* = 7.5 Hz, 2H). ¹³C{¹H} NMR (125 MHz, CDCl₃): δ 175.66, 139.57, 139.05, 136.24, 130.80, 128.53, 128.39, 128.34, 128.31, 128.02, 127.55, 50.12, 31.16, 18.94. IR (thin film, CH₂Cl₂): 2926, 1692, 1482, 1436, 1404, 1302 cm⁻¹. HRMS [M+H]⁺ Calcd for C₁₆H₁₆NO: 238.1226; Found: 238.1230.



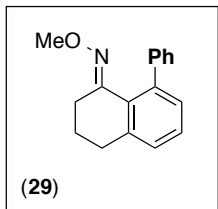
Substrate **22** (75.0 mg, 0.39 mmol, 1.0 equiv), Ru(bpy)₃Cl₂•6H₂O (14.6 mg, 0.02 mmol, 0.05 equiv), and Pd(OAc)₂ (8.8 mg, 0.04 mmol, 0.10 equiv) were weighed into a 20 mL vial. The vial was taken into a glove box, and [PhN₂]⁺BF₄⁻ (300 mg, 1.56 mmol, 4.0 equiv) and MeOH (3.9 mL) were added. The vial was sealed with a Teflon lined cap, removed from the glove box, and placed on a stir plate with two 26 W compact fluorescent light bulbs (one on either side of the vial about 5 cm away). The reaction mixture was allowed to stir at room temperature for 4 h. The reaction was then quenched with brine (2 mL), 10% aqueous Na₂SO₃ (2 mL), and EtOAc (10 mL). The calibrated GC yield of the crude product was determined to be 92% (using hexadecane as the standard). The reaction mixture was then diluted with additional Et₂O (50 mL) and H₂O (25 mL), and extracted with 10% aqueous Na₂SO₃ (2 x 35 mL). The combined aqueous layers were extracted with Et₂O (1 x 100 mL). Finally, the combined organic layers were washed with brine (1 x 50 mL), dried over MgSO₄, filtered, concentrated, and chromatographed on a 20.5 cm x 3 cm silica gel column (R_f = 0.12 in 20% hexanes/80% diethyl ether). Product **23** was obtained as a colorless viscous oil (82.9 mg, 79% yield). ¹H NMR (500 MHz, CDCl₃): δ 7.39-7.29 (multiple peaks, 6H), 6.93 (dd, *J* = 8.5, 3.0 Hz, 1H), 6.86 (d, *J* = 2.5 Hz, 1H), 3.84 (s, 3H), 3.20 (t, *J* = 7.0 Hz, 2H), 2.42 (t, *J* = 8.0 Hz, 2H), 1.86 (quin, *J* = 7.5 Hz, 2H). ¹³C{¹H} NMR (125 MHz, CDCl₃): δ 175.53, 159.62, 138.96, 137.16, 132.04, 131.59, 128.43, 128.36, 127.18, 114.19, 113.39, 55.46, 50.13, 31.20, 18.95. IR (thin film, neat): 2952, 1687, 1609, 1482, 1211, 1045 cm⁻¹. HRMS [M+H]⁺ Calcd for C₁₇H₁₈NO₂: 268.1332; Found: 268.1338.



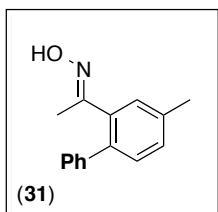
Ru(bpy)₃Cl₂•6H₂O (8.85 mg, 0.01 mmol, 0.025 equiv), Ag₂CO₃ (131 mg, 0.47 mmol, 1.0 equiv), and Pd(OAc)₂ (10.6 mg, 0.05 mmol, 0.10 equiv) were weighed into a 20 mL vial. The vial was taken into a glove box, and [PhN₂]⁺BF₄⁻ (362 mg, 1.89 mmol, 4.0 equiv) and MeOH (2.3 mL) were added. Substrate **24** (75.0 mg, 0.47 mmol, 1.0 equiv) was added to the reaction vial as a solution in MeOH (2.4 mL). The vial was sealed with a Teflon lined cap, removed from the glove box, and placed on a stir plate with two 26 W compact fluorescent light bulbs (one on either side of the vial about 5 cm away). The reaction mixture was allowed to stir at room temperature for 5 h. The reaction was quenched with brine (2 mL), 10% aqueous Na₂SO₃ (2 mL) and EtOAc (10 mL). The calibrated GC yield of the crude product was determined to be 53% (using hexadecane as the standard). The reaction mixture was then diluted with additional Et₂O (50 mL) and H₂O (25 mL), and extracted with 10% aqueous Na₂SO₃ (2 x 35 mL). The combined aqueous layers were extracted with Et₂O (1 x 100 mL). Finally, the combined organic layers were washed with brine (1 x 50 mL), dried over MgSO₄, filtered, concentrated, and chromatographed on a 20.5 cm x 3 cm silica gel column (R_f = 0.11 in 95% hexanes/5% diethyl ether). Product **25** was obtained as a clear viscous oil (59.1 mg, 53% yield). ¹H NMR (700 MHz, CDCl₃): δ 7.62 (d, *J* = 2.1 Hz, 1H), 7.44 (s, 1H), 7.35 (d *J* = 7.7 Hz, 1H), 7.28-7.24 (multiple peaks, 4H), 7.09-7.08 (multiple peaks, 2H), 7.04 (d, *J* = 2.1 Hz, 1H), 6.16 (t, *J* = 2.1 Hz, 1H), 2.43 (s, 3H). ¹³C{¹H} NMR (176 MHz, CDCl₃): δ 140.09, 138.51, 138.49, 138.24, 133.64, 131.27, 130.78, 128.96, 128.50, 128.35, 127.15, 126.98, 106.22, 20.89. HRMS [M+H]⁺ Calcd for C₁₆H₁₅N₂: 235.1230; Found: 235.1230.



Ru(bpy)₃Cl₂•6H₂O (8.20 mg, 0.01 mmol, 0.025 equiv) and Pd(OAc)₂ (9.9 mg, 0.04 mmol, 0.10 equiv) were weighed into a 20 mL vial. The vial was taken into a glove box, and [PhN₂]BF₄ (337 mg, 1.76 mmol, 4.0 equiv) and MeOH (2.2 mL) were added. Substrate **26** (75.0 mg, 0.44 mmol, 1.0 equiv) was added to the reaction vial as a solution in MeOH (2.2 mL). The vial was sealed with a Teflon lined cap, removed from the glove box, and placed on a stir plate with two 26 W compact fluorescent light bulbs (one on either side of the vial about 5 cm away). The reaction mixture was allowed to stir at room temperature for 5.0 h. The reaction was then quenched with brine (2 mL), 10% aqueous Na₂SO₃ (2 mL), and EtOAc (10 mL). The calibrated GC yield of the crude product was determined to be 47% (using hexadecane as the standard). The reaction mixture was then diluted with additional Et₂O (50 mL) and H₂O (25 mL), and extracted with 10% aqueous Na₂SO₃ (2 x 35 mL). The combined aqueous layers were extracted with Et₂O (1 x 100 mL). Finally, the combined organic layers were washed with brine (1 x 50 mL), dried over MgSO₄, filtered, concentrated, and chromatographed on a 21 cm x 3 cm silica gel column (R_f = 0.11 in 80% hexanes/20% diethyl ether). Product **27** was obtained as a clear viscous oil (47.5 mg, 44% yield). ¹H NMR (700 MHz, CDCl₃): δ 8.63 (dd, *J* = 5.2, 1.0 Hz, 2H), 7.61 (s, 1H), 7.37 (d, *J* = 7.7 Hz, 1H), 7.32 (d, *J* = 7.7 Hz, 1H), 7.22-7.18 (multiple peaks, 3H), 7.12-7.11 (multiple peaks, 2H), 7.09 (t, *J* = 4.9 Hz, 1H), 2.46 (s, 3H). ¹³C{¹H} NMR (176 MHz, CDCl₃): δ 168.22, 156.69, 141.52, 138.61, 137.97, 137.15, 131.04, 130.65, 130.15, 129.13, 127.90, 126.24, 118.35, 21.03. HRMS [M+H]⁺ Calcd for C₁₇H₁₅N₂: 247.1230; Found: 247.1236.

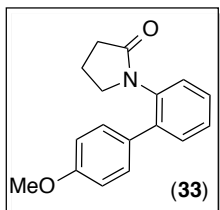


Ru(bpy)₃Cl₂•6H₂O (8.00 mg, 0.01 mmol, 0.025 equiv) and Pd(OAc)₂ (9.6 mg, 0.04 mmol, 0.10 equiv) were weighed into a 20 mL vial. The vial was taken into a glove box, and [PhN₂]BF₄ (286 mg, 1.50 mmol, 3.5 equiv) and MeOH (2.1 mL) were added. Substrate **28** (75.0 mg, 0.43 mmol, 1.0 equiv) was added to the reaction vial as a solution in MeOH (2.2 mL). The vial was sealed with a Teflon lined cap, removed from the glove box, and placed on a stir plate with two 26 W compact fluorescent light bulbs (one on either side of the vial about 5 cm away). The reaction mixture was allowed to stir at room temperature for 4 h. The reaction was then quenched with brine (2 mL), 10% aqueous Na₂SO₃ solution (2 mL), and EtOAc (10 mL). The calibrated GC yield of the crude product was determined to be 58% (using hexadecane as the standard). The reaction mixture was then diluted with additional Et₂O (50 mL) and H₂O (25 mL), and extracted with 10% aqueous Na₂SO₃ (2 x 35 mL). The combined aqueous layers were extracted with Et₂O (1 x 100 mL). Finally, the combined organic layers were washed with brine (1 x 50 mL), dried over MgSO₄, filtered, concentrated, and chromatographed on a 21 cm x 3 cm silica gel column (R_f = 0.21 in 99% hexanes/1% diethyl ether). Product **29** was obtained as a light orange solid (52.5 mg, 49% yield). The ¹H NMR and ¹³C NMR spectroscopic data were identical to that reported previously in the literature.²⁵

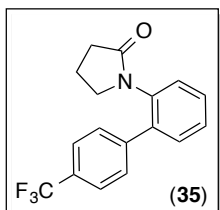


Substrate **30** (100 mg, 0.67 mmol, 1.0 equiv), Ru(bpy)₃Cl₂•6H₂O (12.5 mg, 0.02 mmol, 0.025 equiv), and Pd(OAc)₂ (30.0 mg, 0.13 mmol, 0.20 equiv) were weighed into a 20 mL vial. The vial was taken into a glove box, and [PhN₂]BF₄ (512 mg, 2.68 mmol, 4.0 equiv) and MeOH (3.3 mL) were added. The vial was sealed with a Teflon lined cap, removed from the glove box, and placed on a stir plate with two 26 W compact fluorescent light bulbs (one on either side of the vial about 5 cm away). The reaction mixture was allowed to stir at room temperature for 5.5 h. The reaction was then quenched with brine (2 mL), 10% aqueous Na₂SO₃ (2 mL), and EtOAc (10 mL). The calibrated GC yield of the crude product was determined to be 66% (using hexadecane as the standard). The reaction mixture was then diluted with additional Et₂O (50 mL) and H₂O (25 mL) and extracted with 10% aqueous Na₂SO₃ (2 x 35 mL). The combined aqueous layers were extracted with Et₂O (1 x 100 mL). Finally, the combined organic layers were washed with brine (1 x 50 mL), dried over MgSO₄, filtered, concentrated, and chromatographed on a 20.5 cm x 3 cm silica gel column (R_f = 0.12 in 87.5% hexanes/12.5% diethyl ether). Product **31** was obtained as a white solid (75.7 mg, 50% yield). Mp = 117.5-118.2 °C. ¹H NMR (700 MHz, C₆D₆): δ 9.58 (br s, 1H), 7.33 (d, *J* = 7.0 Hz, 2H), 7.27 (s, 1H), 7.10 (d, *J* = 7.7 Hz, 1H), 7.04 (t, *J* = 7.7 Hz, 2H), 7.01-6.99 (m, 1H), 6.90 (d, *J* = 7.7 Hz, 1H), 2.03 (s, 3H), 1.73 (s, 3H). ¹³C{¹H} NMR (125 MHz, CDCl₃): δ 159.33, 140.94, 137.73, 137.15, 136.56, 130.22, 129.74, 129.69, 128.94, 128.38, 127.09, 20.96, 15.96. IR (thin film, CH₂Cl₂): 3212 (br), 2921, 1602, 1479, 1443, 1363, 1306 cm⁻¹. HRMS [M+H]⁺ Calcd for C₁₅H₁₆NO: 226.1226; Found: 226.1227.

Synthesis of Products in Table 3.8 & Scheme 3.12

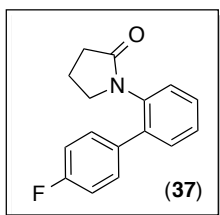


Substrate **20** (100 mg, 0.62 mmol, 1.0 equiv), Ru(bpy)₃Cl₂•6H₂O (11.6 mg, 0.02 mmol, 0.025 equiv), and Pd(OAc)₂ (13.9 mg, 0.06 mmol, 0.10 equiv) were weighed into a 20 mL vial. The vial was taken into a glove box, and [p-MeOC₆H₄N₂]₂BF₄ (**32**) (550 mg, 2.5 mmol, 4.0 equiv) and MeOH (6.2 mL) were added. The vial was sealed with a Teflon lined cap, removed from the glove box and placed on a stir plate with two 26 W compact fluorescent light bulbs (one on either side of the vial about 5 cm away). The reaction mixture was allowed to stir at room temperature for 6 h. The reaction was then quenched with brine (2 mL), 10% aqueous Na₂SO₃ (2 mL), and Et₂O (10 mL). The calibrated GC yield of the crude product was determined to be 76% (using hexadecane as the standard). The reaction mixture was then diluted with additional Et₂O (50 mL) and H₂O (25 mL), and extracted with 10% aqueous Na₂SO₃ (2 x 35 mL). The combined aqueous layers were extracted with Et₂O (1 x 100 mL). Finally, the combined organic layers were washed with brine (1 x 50 mL), dried over MgSO₄, filtered, concentrated, and chromatographed on a 20 cm x 3 cm silica gel column (R_f = 0.11 in 30% hexanes/70% diethyl ether). Product **33** was obtained as an orange viscous oil (116 mg, 76% yield). The ¹H NMR and ¹³C NMR spectroscopic data were identical to that reported previously in the literature.²⁶



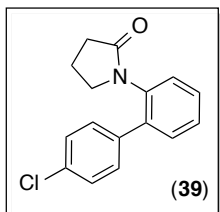
Substrate **20** (100 mg, 0.62 mmol, 1.0 equiv), Ru(bpy)₃Cl₂•6H₂O (11.6 mg, 0.02 mmol, 0.025 equiv), and Pd(OAc)₂ (13.9 mg, 0.06 mmol, 0.10 equiv) were weighed into a 20

mL vial. The vial was taken into a glove box, and [*p*-CF₃C₆H₄N₂]BF₄ (**34**) (545 mg, 2.1 mmol, 3.4 equiv), and MeOH (6.2 mL) were added. The vial was sealed with a Teflon lined cap, removed from the glove box, and placed on a stir plate with two 26 W compact fluorescent light bulbs (one on either side of the vial about 5 cm away). The reaction mixture was allowed to stir at room temperature for 4 h. The reaction was then quenched with brine (2 mL), 10% aqueous Na₂SO₃ solution (2 mL), and Et₂O (10 mL). The calibrated GC yield of the crude product was determined to be 92% (using hexadecane as the standard). The reaction mixture was then diluted with an additional Et₂O (50 mL) and H₂O (25 mL), and extracted with 10% aqueous Na₂SO₃ (2 x 35 mL). The combined aqueous layers were extracted with Et₂O (1 x 100 mL). Finally, the combined organic layers were washed with brine (1 x 50 mL), dried over MgSO₄, filtered, concentrated, and chromatographed on a 19 cm x 3 cm silica gel column (R_f = 0.16 in 30% hexanes/70% diethyl ether). Product **35** was obtained as a white solid (165 mg, 87% yield); Mp = 86.1-88.0 °C. ¹H NMR (700 MHz, CDCl₃): δ 7.67 (d, *J* = 8.4 Hz, 2H), 7.50 (d, *J* = 7.7 Hz, 2H), 7.46 (td, *J* = 7.7, 0.7 Hz, 1H), 7.41 (t, *J* = 7.7 Hz, 1H), 7.38 (d, *J* = 7.7 Hz, 1H), 7.33 (d, *J* = 7.7 Hz, 1H), 3.28 (t, *J* = 7.0 Hz, 2H), 2.42 (t, *J* = 8.1 Hz, 2H), 1.92 (quin, *J* = 7.5 Hz, 2H). ¹³C{¹H} NMR (175 MHz, CDCl₃): δ 175.51, 142.88, 138.42, 136.37, 130.70, 129.77 (q, ²*J*_{C-F} = 33 Hz), 129.36, 128.75, 128.39, 128.24, 125.34 (q, ³*J*_{C-F} = 4.0 Hz), 124.14 (q, ¹*J*_{C-F} = 270 Hz), 50.43, 31.06, 18.96. ¹⁹F NMR (376 MHz, CDCl₃): δ -62.51 (s). IR (thin film, CH₂Cl₂): 2978, 2880, 1692, 1616, 1488, 1324, 1108 cm⁻¹. HRMS [M+H]⁺ Calcd for C₁₇H₁₅F₃NO: 306.1100; Found: 306.1106.



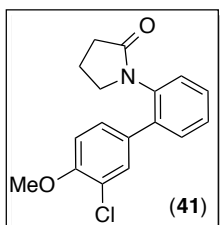
Substrate **20** (100 mg, 0.62 mmol, 1.0 equiv), Ru(bpy)₃Cl₂•6H₂O (11.6 mg, 0.02 mmol, 0.025 equiv), and Pd(OAc)₂ (13.9 mg, 0.06 mmol, 0.10 equiv) were weighed into a 20 mL vial. The vial was taken into a glove box, and [*p*-FC₆H₄N₂]BF₄ (**36**) (521 mg, 2.5 mmol, 4.0 equiv) and MeOH (6.2 mL) were added. The vial was sealed with a Teflon lined cap, removed from the glove box, and placed on a stir plate with two 26 W compact

fluorescent light bulbs (one on either side of the vial about 5 cm away). The reaction mixture was allowed to stir at room temperature for 4 h. The reaction was quenched with brine (2 mL), 10% aqueous Na₂SO₃ (2 mL), and Et₂O (10 mL). The calibrated GC yield of the crude product was determined to be 86% (using hexadecane as the standard). The reaction mixture was then diluted with additional Et₂O (50 mL) and H₂O (25 mL), and extracted with 10% aqueous Na₂SO₃ (2 x 35 mL). The combined aqueous layers were extracted with Et₂O (1 x 100 mL). Finally, the combined organic layers were washed with brine (1 x 50 mL), dried over MgSO₄, filtered, concentrated, and chromatographed on a 20 cm x 3 cm silica gel column (R_f = 0.16 in 30% hexanes/70% diethyl ether). Product **37** was obtained as a clear viscous oil (122 mg, 76% yield). ¹H NMR (700 MHz, CDCl₃): δ 7.41-7.34 (multiple peaks, 5H), 7.31 (d, *J* = 7.7 Hz, 1H), 7.09 (t, *J* = 8.4 Hz, 2H), 3.24 (t, *J* = 7.0 Hz, 2H), 2.42 (t, *J* = 8.1 Hz, 2H), 1.90 (quin, *J* = 7.4 Hz, 2H). ¹³C{¹H} NMR (125 MHz, CDCl₃): δ 173.07, 159.84 (d, ¹*J*_{C-F} = 247 Hz), 136.21, 133.80, 132.52 (d, ⁴*J*_{C-F} = 3.5 Hz), 128.22, 127.47 (d, ³*J*_{C-F} = 8.3 Hz), 126.18, 125.83, 125.57, 112.79 (d, ²*J*_{C-F} = 21 Hz), 47.69, 28.56, 16.39. ¹⁹F NMR (470 MHz, C₆D₆): δ -114.82 to -114.85 (m). IR (thin film, neat): 3059, 2974, 2880, 1688, 1484, 1405, 1217 cm⁻¹. HRMS [M+H]⁺ Calcd for C₁₆H₁₅FNO: 256.1132; Found: 256.1135.



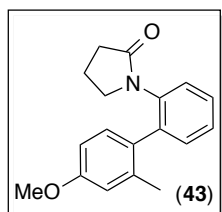
Substrate **20** (100 mg, 0.62 mmol, 1.0 equiv), Ru(bpy)₃Cl₂•6H₂O (11.6 mg, 0.02 mmol, 0.025 equiv), and Pd(OAc)₂ (13.9 mg, 0.06 mmol, 0.10 equiv) were weighed into a 20 mL vial. The vial was taken into a glove box, and [*p*-ClC₆H₄N₂]BF₄ (**38**) (561 mg, 2.5 mmol, 4.0 equiv) and MeOH (6.2 mL) were added. The vial was sealed with a Teflon lined cap, removed from the glove box, and placed on a stir plate with two 26 W compact fluorescent light bulbs (one on either side of the vial about 5 cm away). The reaction mixture was allowed to stir at room temperature for 4 h. The reaction was then quenched with brine (2 mL), 10% aqueous Na₂SO₃ (2 mL), and Et₂O (10 mL). The calibrated GC yield of the crude product was determined to be 99% (using hexadecane as the standard).

The reaction mixture was then diluted with additional Et₂O (50 mL) and H₂O (25 mL), and extracted with 10% aqueous Na₂SO₃ (2 x 35 mL). The combined aqueous layers were extracted with Et₂O (1 x 100 mL). Finally, the combined organic layers were washed with brine (1 x 50 mL), dried over MgSO₄, filtered, concentrated, and chromatographed on a 14 cm x 3 cm silica gel column (*R_f* = 0.19 in 20% hexanes/80% diethyl ether). Product **39** was obtained as a light yellow solid (131 mg, 78% yield); Mp = 93.9-96.0 °C. ¹H NMR (500 MHz, C₆D₆): δ 7.23 (dd, *J* = 8.0, 1.0 Hz, 1H), 7.11-7.04 (multiple peaks, 7H), 2.69 (t, *J* = 7.0 Hz, 2H), 1.97 (t, *J* = 8.3 Hz, 2H), 1.13 (quin, *J* = 7.5 Hz, 2H). ¹³C{¹H} NMR (125 MHz, CDCl₃): δ 175.61, 138.52, 137.57, 136.28, 133.70, 130.69, 129.70, 128.94, 128.63, 128.40, 128.17, 50.28, 31.11, 18.96. IR (thin film, CH₂Cl₂): 3063, 2978, 2876, 1692, 1476, 1403 cm⁻¹. HRMS [M+H]⁺ Calcd for C₁₆H₁₅ClNO: 272.0837; Found: 272.0837.



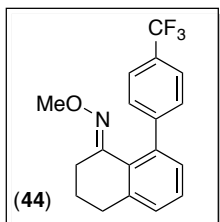
Substrate **20** (100 mg, 0.62 mmol, 1.0 equiv), Ru(bpy)₃Cl₂•6H₂O (23.1 mg, 0.03 mmol, 0.05 equiv), and Pd(OAc)₂ (13.9 mg, 0.06 mmol, 0.10 equiv) were weighed into a 20 mL vial. The vial was taken into a glove box, and [3-Cl-4-MeO-C₆H₃N₂]⁺BF₄⁻ (**40**) (636 mg, 2.5 mmol, 4.0 equiv) and MeOH (6.2 mL) were added. The vial was sealed with a Teflon lined cap, removed from the glove box, and placed on a stir plate with two 26 W compact fluorescent light bulbs (one on either side of the vial about 5 cm away). The reaction mixture was allowed to stir at room temperature for 4 h. The reaction was then quenched with brine (2 mL), 10% aqueous Na₂SO₃ (2 mL), and Et₂O (10 mL). The calibrated GC yield of the crude product was determined to be 81% (using hexadecane as the standard). The reaction mixture was then diluted with additional Et₂O (50 mL) and H₂O (25 mL), and extracted with 10% aqueous Na₂SO₃ (2 x 35 mL). The combined aqueous layers were extracted with Et₂O (1 x 100 mL). Finally, the combined organic layers were washed with brine (1 x 50 mL), dried over MgSO₄, filtered, concentrated, and chromatographed on a 20 cm x 3 cm silica gel column (*R_f* = 0.18 in 15% hexanes/85%

diethyl ether). Product **41** was obtained as a yellow viscous oil (147 mg, 79% yield). ^1H NMR (500 MHz, CDCl_3): δ 7.41-7.35 (multiple peaks, 4H), 7.31-7.29 (m, 1H), 7.26 (dd, $J = 8.5, 2.0$ Hz, 1H), 6.96 (d, $J = 9.0$ Hz, 1H), 3.94 (s, 3H), 3.28 (t, $J = 7.0$ Hz, 2H), 2.44 (t, $J = 8.0$ Hz, 2H), 1.94 (quin, $J = 7.5$ Hz, 2H). $^{13}\text{C}\{^1\text{H}\}$ NMR (100 MHz, CDCl_3): δ 175.59, 154.51, 138.00, 136.29, 132.35, 130.71, 129.98, 128.68, 128.39, 128.13, 127.82, 122.36, 111.93, 56.16, 50.23, 31.15, 19.01. IR (thin film, neat): 2970, 2888, 1688, 1482, 1255 cm^{-1} . HRMS $[\text{M}+\text{H}]^+$ Calcd for $\text{C}_{17}\text{H}_{17}\text{ClNO}_2$: 302.0942; Found: 302.0948.



Substrate **20** (100 mg, 0.62 mmol, 1.0 equiv), $\text{Ru}(\text{bpy})_3\text{Cl}_2 \cdot 6\text{H}_2\text{O}$ (23.1 mg, 0.03 mmol, 0.05 equiv), and $\text{Pd}(\text{OAc})_2$ (13.9 mg, 0.06 mmol, 0.10 equiv) were weighed into a 20 mL vial. The vial was taken into a glove box, and $[\text{2-CH}_3\text{-4-MeO-C}_6\text{H}_3\text{N}_2]\text{BF}_4$ (**42**) (585 mg, 2.5 mmol, 4.0 equiv) and MeOH (3.1 mL) were added. The vial was sealed with a Teflon lined cap, removed from the glove box, and placed on a stir plate with two 26 W compact fluorescent light bulbs (one on either side of the vial about 5 cm away). The reaction mixture was allowed to stir at room temperature for 10 h. The reaction was then quenched with brine (2 mL), 10% aqueous Na_2SO_3 (2 mL), and Et_2O (10 mL). The calibrated GC yield of the crude product was determined to be 55% (using hexadecane as the standard). The reaction mixture was then diluted with additional Et_2O (50 mL) and H_2O (25 mL), and extracted with 10% aqueous Na_2SO_3 (2 x 35 mL). The combined aqueous layers were extracted with Et_2O (1 x 100 mL). Finally, the combined organic layers were washed with brine (1 x 50 mL), dried over MgSO_4 , filtered, concentrated, and chromatographed on a 19 cm x 3 cm silica gel column ($R_f = 0.13$ in 20% hexanes/80% diethyl ether). Product **43** was obtained as a yellow viscous oil (98.7 mg, 57% yield). ^1H NMR (400 MHz, CDCl_3): δ 7.41-7.31 (multiple peaks, 3H), 7.26-7.24 (m, 1H), 7.08 (d, $J = 8.4$ Hz, 1H), 6.81 (d, $J = 2.8$ Hz, 1H), 6.75 (dd, $J = 8.4, 2.8$ Hz, 1H), 3.83 (s, 3H), 3.24 (m, 1H), 3.11 (m, 1H), 2.35 (m, 2H), 2.14 (s, 3H), 1.83 (m, 2H). $^{13}\text{C}\{^1\text{H}\}$ NMR (100 MHz, CDCl_3): δ 175.19, 158.96, 138.58, 137.35, 137.23, 131.56, 131.06, 130.46, 128.23,

128.02, 127.28, 115.37 110.95, 55.15, 49.91, 31.19, 20.25, 19.05. IR (thin film, neat): 2949, 1692, 1605, 1482, 1233 cm^{-1} . HRMS $[\text{M}+\text{H}]^+$ Calcd for $\text{C}_{18}\text{H}_{20}\text{NO}_2$: 282.1489; Found: 282.1495.



$\text{Ru}(\text{bpy})_3\text{Cl}_2 \cdot 6\text{H}_2\text{O}$ (8.00 mg, 0.01 mmol, 0.025 equiv), and $\text{Pd}(\text{OAc})_2$ (9.6 mg, 0.04 mmol, 0.10 equiv) were weighed into a 20 mL vial. The vial was taken into a glove box, and $[\textit{p}\text{-CF}_3\text{C}_6\text{H}_4\text{N}_2]\text{BF}_4$ (**34**) (445 mg, 1.7 mmol, 4.0 equiv) and MeOH (2.1 mL) were added. Substrate **28** (75.0 mg, 0.43 mmol, 1.0 equiv) was added to the reaction vial as a solution in MeOH (2.2 mL). The vial was sealed with a Teflon lined cap, removed from the glove box, and placed on a stir plate with two 26 W compact fluorescent light bulbs (one on either side of the vial about 5 cm away). The reaction mixture was allowed to stir at room temperature for 4 h. The reaction was then quenched with brine (2 mL), 10% aqueous Na_2SO_3 (2 mL), and Et_2O (10 mL). The calibrated GC yield of the crude product was determined to be 64% (using hexadecane as the standard). The reaction mixture was then diluted with additional Et_2O (50 mL) and H_2O (25 mL), and extracted with 10% aqueous Na_2SO_3 (2 x 35 mL). The combined aqueous layers were extracted with Et_2O (1 x 100 mL). Finally, the combined organic layers were washed with brine (1 x 50 mL), dried over MgSO_4 , filtered, concentrated, and chromatographed on a 19 cm x 3 cm silica gel column ($R_f = 0.13$ in 99% hexanes/1% diethyl ether). Product **44** was obtained as a light pink solid (71.3 mg, 52% yield); Mp = 54.1-55.6 $^\circ\text{C}$. ^1H NMR (700 MHz, CDCl_3): δ 7.58 (d, $J = 8.4$ Hz, 2H), 7.35 (d, $J = 8.4$ Hz, 2H), 7.28 (t, $J = 7.7$ Hz, 1H), 7.18 (d, $J = 7.7$ Hz, 1H), 7.13 (d, $J = 7.0$ Hz, 1H), 3.36 (s, 3H), 2.72 (t, $J = 6.0$ Hz, 2H), 2.68 (t, $J = 7.0$ Hz, 2H), 1.84 (quin, $J = 6.3$ Hz, 2H). $^{13}\text{C}\{^1\text{H}\}$ NMR (175 MHz, CDCl_3): δ 152.80, 147.84, 142.23, 139.93, 129.26, 129.21, 128.21, 128.14, 128.12 (q, $^2J_{\text{C-F}} = 32$ Hz), 127.81, 124.56 (q, $^1J_{\text{C-F}} = 270$ Hz), 124.49 (q, $^3J_{\text{C-F}} = 4.0$ Hz), 61.40, 30.78, 24.96, 21.26. ^{19}F NMR (376 MHz, CDCl_3): δ -62.06 (s). IR (thin film, CH_2Cl_2): 2937, 1616, 1326, 1122 cm^{-1} . HRMS $[\text{M}+\text{H}]^+$ Calcd for $\text{C}_{18}\text{H}_{17}\text{F}_3\text{NO}$: 320.1257; Found: 320.1257.

3.10 References

- ¹ Hassan, J.; Sevignon, M.; Gozzi, C.; Schulz, E.; Lemaire, M. *Chem. Rev.* **2002**, *102*, 1359.
- ² Horton, D. A.; Bourne, G. T.; Smythe, M. L. *Chem. Rev.* **2003**, *103*, 893.
- ³ For representative reviews of C–H arylation, see: (a) Alberico, D.; Scott, M. E.; Lautens, M. *Chem. Rev.* **2007**, *107*, 174. (b) Kakiuchi, F.; Kochi, T. *Synthesis* **2008**, 3013. (c) McGlacken, G. P.; Bateman, L. *Chem. Soc. Rev.* **2009**, *38*, 2447. (d) Chen, X.; Engle, K. M.; Wang, D.-H.; Yu, J.-Q. *Angew. Chem., Int. Ed.* **2009**, *48*, 5094. (e) Lyons, T. W.; Sanford, M. S. *Chem. Rev.* **2010**, *110*, 1147. (f) Daugulis, O. *Top. Curr. Chem.* **2010**, *292*, 57. (g) Chiusoli, G. P.; Catellani, M.; Costa, M.; Motti, E.; Ca', N. D.; Maestri, G. *Coord. Chem. Rev.* **2010**, *254*, 456.
- ⁴ (a) Ames, D. E.; Opalko, A. *Synthesis*, **1983**, 234. (b) Ames, D. E.; Opalko, A. *Tetrahedron* **1984**, *40*, 1919.
- ⁵ Satoh, T.; Kawamura, Y.; Miura, M.; Nomura, M. *Angew. Chem. Int. Ed.* **1997**, *36*, 1740.
- ⁶ Wencel-Delord, J.; Droge, T.; Liu, F.; Glorius, F. *Chem. Soc. Rev.* **2011**, *40*, 4740.
- ⁷ For isolated examples of room-temperature Pd-catalyzed C–H arylation, see: (a) Hull, K. L.; Lanni, E. L.; Sanford, M. S. *J. Am. Chem. Soc.* **2006**, *128*, 14047. (b) Xiao, B.; Fu, Y.; Xu, J.; Gong, T.-J.; Dai, J.-J.; Yi, J.; Liu, L. *J. Am. Chem. Soc.* **2010**, *132*, 468. (c) Nishikata, T.; Abela, A. R.; Huang, S.; Lipshutz, B. H. *J. Am. Chem. Soc.* **2010**, *132*, 4978. (d) Nishikata, T.; Abela, A. R.; Lipshutz, B. H. *Angew. Chem., Int. Ed.* **2010**, *49*, 781. (e) Haffemayer, B.; Gulias, M.; Gaunt, M. *J. Chem. Sci.* **2011**, *2*, 312. (f) Tredwell, M. J.; Gulias, M.; Bremeyer, N.; Johansson, C. C. C.; Collins, B. S. L.; Gaunt, M. J. *Angew. Chem., Int. Ed.* **2011**, *50*, 1076.
- ⁸ Kalyani, D.; Deprez, N. R.; Desai, L. V.; Sanford, M. S. *J. Am. Chem. Soc.* **2005**, *127*, 7330.
- ⁹ (a) Deprez, N. R.; Sanford, M. S. *J. Am. Chem. Soc.* **2009**, *131*, 11234. (b) Ariaifard, A.; Hyland, C. J. T.; Canty, A. J.; Sharma, M.; Yates, B. F. *Inorg. Chem.* **2011**, *50*, 6449.
- ¹⁰ Yu, W.-Y.; Sit, W.; Zhou, Z.; Chan, A. S. C. *Org. Lett.* **2009**, *11*, 3174.
- ¹¹ (a) Cano-Yelo, H.; Deronzier, A. *J. Chem. Soc., Perkin Trans. 2* **1984**, 1093. (b) Cano-Yelo, H.; Deronzier, A. *J. Chem. Soc., Faraday Trans. 1* **1984**, 3011. (c) Cano-Yelo, H.; Deronzier, A. *Tetrahedron Lett.* **1984**, *25*, 5517. (d) Cano-Yelo, H.; Deronzier, A. *J. Photochem.* **1987**, *37*, 315. (e) Cano-Yelo, H.; Deronzier, A. *New J. Chem.* **1987**, *11*, 479. (f) Lalevee, J.; Blanchard, N.; Tehfe, M.-A.; Peter, M.; Morlet-Savary, F.; Fouassier, J. P. *Macromol. Rapid Commun.* **2011**, *32*, 917.

- ¹² Kalyani, D; McMurtrey, K. B.; Neufeldt, S. R.; Sanford, M. S. *J. Am. Chem. Soc.* **2011**, *133*, 18566.
- ¹³ (a) Desai, L. V.; Hull, K. L.; Sanford, M. S. *J. Am. Chem. Soc.* **2004**, *126*, 9542. (b) Neufeldt, S. R.; Sanford, M. S. *Org. Lett.* **2010**, *12*, 532.
- ¹⁴ Hanson, P.; Jones, J. R.; Taylor, A. B.; Walton, P. H.; Timms, A. W. *J. Chem. Soc., Perkin Trans. 2*, **2002**, 1135.
- ¹⁵ Maas, G., Tanaka, M. and Sakakura, T. *Benzenediazonium Tetrafluoroborate, e-EROS Encyclopedia of Reagents for Organic Synthesis*, **2001**.
- ¹⁶ (a) Igarashi, T.; Konishi, K.; Aida, T. *Chem. Lett.* **1998**, 1039. (b) Nguyen, J. D.; Tucker, J. W.; Konieczynska, M. D.; Stephenson, C. R. J. *J. Am. Chem. Soc.* **2011**, *133*, 4160.
- ¹⁷ (a) Ye, Y., Sanford, M. S. *J. Am. Chem. Soc.*, **2012**, *134*, 9034. (b) Neufeldt, S. R.; Sanford, M. S. *Adv. Synth. Catal.* **2012**, *354*, 3517. (c) Tellis, J. C.; Primer, D. N.; Molander, G. A. *Science*: 10.1126/science.1253647. (d) Zuo, Z.; Ahneman, D.; Chu, L.; Terrett, J.; Doyle, A. G.; MacMillan, D. W. C. *Science*: 10.1126/science.1255525.
- ¹⁸ Stowers K. J.; Sanford, M. S. *Org. Lett.* **2009**, *11*, 4584.
- ¹⁹ Ewing, W. R. *et. al.* PCT Int. Appl. 2006014287 **2006**.
- ²⁰ Shakespeare, W. C. *Tetrahedron Lett.* **1999**, *40*, 2035.
- ²¹ Cristau, H.-J.; Cellier, P. P.; Spindler, J.-F.; Taillefer, M. *Eur. J. Org. Chem.* **2004**, 695.
- ²² Zheng, X.; Song, B.; Xu, B. *Eur. J. Org. Chem.* **2010**, 4376.
- ²³ Neufeldt, S. R.; Sanford, M. S. *Org. Lett.* **2010**, *12*, 532.
- ²⁴ Hanson, P.; Jones, J. R.; Taylor, A. B.; Walton, P. H.; Timms, A. W. *J. Chem. Soc., Perkin Trans. 2* **2002**, 1135.
- ²⁵ Sun, C.-L.; Liu, N.; Li, B.-J.; Yu, D.-G.; Wang, Y.; Shi, Z.-J. *Org. Lett.* **2010**, *12*, 184.
- ²⁶ Yeung, C. S.; Zhao, X.; Borduas, N.; Dong, V. M. *Chem. Sci.* **2010**, *1*, 331.

CHAPTER 4

Mechanistic Investigation of C–H Arylation with Diaryliodonium Salts by Palladium-Catalysis and Visible-Light Photocatalysis

4.1 Background and Significance

Visible-light photoredox catalysis has grown exponentially over the past six years as a strategy for achieving synthetically useful organic reactions.¹ This environmentally friendly approach utilizes a photocatalyst in combination with visible light (ideally from the sun) to access excited states of the photocatalyst. Using energy from light frequently results in milder conditions for these transformations. Most organic molecules do not absorb visible light and are therefore unaffected by the initial photochemical step. Once the photocatalyst is in its excited state, it is chemically more reactive and can proceed to react with organic substrate(s), often through a single-electron-transfer (SET).² Most photocatalysts can operate through two mechanistic pathways: reductive or oxidative quenching (Figure 4.1). Both routes are comprised of a quenching and regenerative step. This mechanistic manifold presents many opportunities for achieving existing chemical transformations under milder conditions as well as for developing novel reactions.

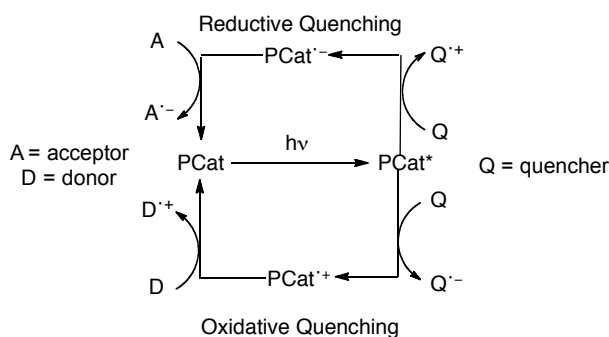


Figure 4.1. General Reductive and Oxidative Quenching Cycles for Photocatalyst

Due to our interest in these transformations, we next sought to study the mechanism of a photocatalytic system. In particular, we investigated the details of the mechanism of a similar transformation to the Pd-/Ru-catalyzed C–H arylation method discussed in Chapter 3. We were interested in studying the mechanism of the arylation method using diazonium salts. However, as described in detail below, a related Pd-/Ir-catalyzed C–H arylation method using diaryliodonium salts³ ultimately proved to be a more tractable alternative. An understanding of the mechanism of this reaction would help address challenges for this methodology. These challenges include: (1) the requirement for relatively high catalyst loadings, (2) the requirement for relatively large equivalents of oxidant, and (3) a limited set of effective directing groups. Arguably more important than how we could improve this transformation however, would be studying the mechanism with the goal of applying this type of dual catalytic system using photocatalysis to other functionalization reactions. Additionally, we were interested in assessing mechanistic differences between analogous thermal and photocatalytic transformations to explore advantages of both systems.

The Pd-/Ir-catalyzed C–H arylation method using diaryliodonium salts was an advantageous system to study for a number of reasons. First, the mechanism of the analogous thermal transformation has been studied in extensive detail in our group.⁴ This would thus allow us to directly compare the two systems mechanistically. Second, the oxidant in the Pd-/Ir-catalyzed system, $[\text{Ph}_2\text{I}]\text{BF}_4$, is more stable and easier to use than $[\text{PhN}_2]\text{BF}_4$. Additionally we found $[\text{Ph}_2\text{I}]\text{BF}_4$ to be more stable in MeOH than $[\text{PhN}_2]\text{BF}_4$. This decomposition made Stern-Volmer quenching studies (see section 4.5) with $[\text{PhN}_2]\text{BF}_4$ difficult to conduct. Third, $[\text{Ph}_2\text{I}]\text{BF}_4$ proved to be more soluble in MeOH than $[\text{PhN}_2]\text{BF}_4$, which is important in measuring reaction rates. For all of these reasons, this method was the clear choice for mechanistic study; however, there was still a major challenge in investigating this transformation. In particular, the photocatalyst $[\text{Ir}(\text{ppy})_2(\text{dtbbpy})]^+$ has not been studied as thoroughly as the well-known $[\text{Ru}(\text{bpy})_3]^{2+}$.⁵ This challenge was overcome through additional studies, and the details of the [Ir] catalyst are addressed in section 4.5.

Our initial working mechanism for this transformation involves the following steps (Figure 4.2). First, there is photoexcitation of the Ir catalyst to generate $[\text{Ir}^{\text{III}}(\text{ppy})_2(\text{dtbbpy})]^{+*}$ (step *i*), followed by reduction of the diaryliodonium salt to Ar^\bullet and concomitant oxidation of the Ir center to $[\text{Ir}^{\text{IV}}(\text{ppy})_2(\text{dtbbpy})]^{2+}$ (step *ii*). The reaction of Ar^\bullet with palladacycle **1**, which was generated by C–H activation of the substrate, could then occur to afford the Pd^{III} intermediate **2** (step *iii*). Next, the one-electron oxidation of **2** by $[\text{Ir}^{\text{IV}}(\text{ppy})_2(\text{dtbbpy})]^{2+}$ would regenerate the photocatalyst and form Pd^{IV} intermediate **3** (step *iv*). The final step would be C–C bond-forming reductive elimination to release the arylated product and regenerate the Pd^{II} catalyst (step *v*).

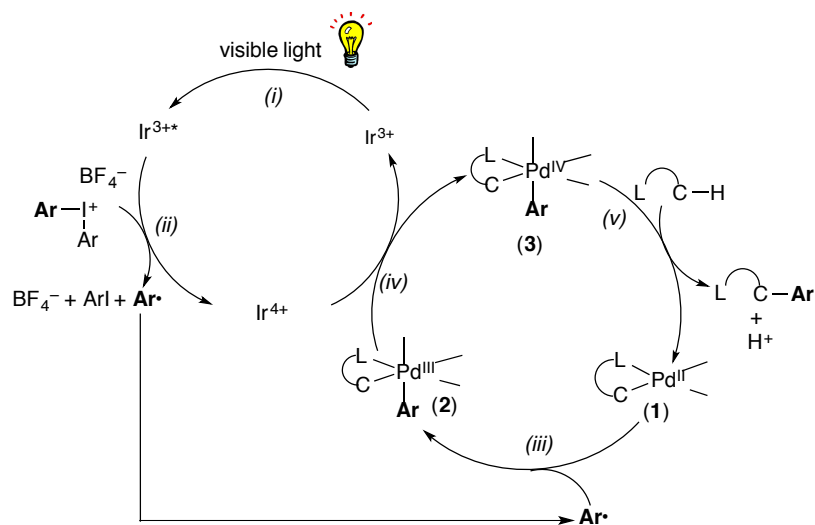


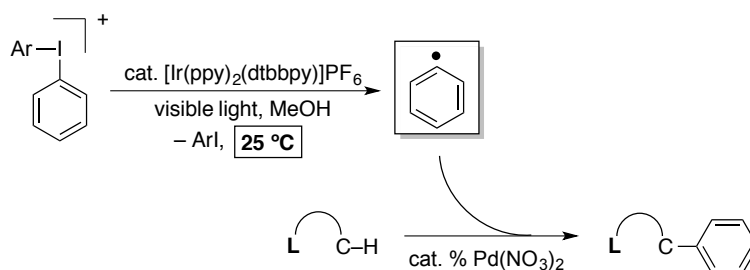
Figure 4.2. Proposed Catalytic Cycle for the Pd-/Ir-Catalyzed C–H Arylation Reaction

We chose to utilize a variety of experiments to investigate the mechanism of the reaction. We first probed the intermediacy of radicals by examining the effects of radical scavengers and by determining if a radical chain mechanism was operating. Second, we performed a number of kinetic studies including Hammett investigations and kinetic isotope effect studies. Lastly, Stern-Volmer quenching studies were conducted in collaboration with Dr. James McCusker’s group at Michigan State University to analyze the photochemical portion of the mechanism.

4.2 Methodology and Comparison

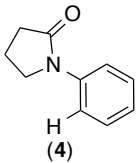
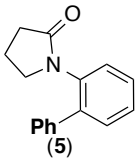
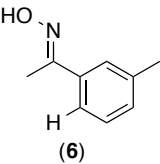
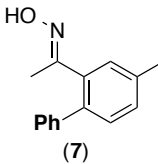
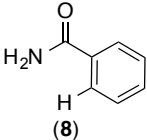
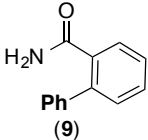
As discussed above, we chose to study the mechanism of the Pd-Ir-catalyzed C–H arylation with diaryliodonium salts, which was reported from by Dr. Sharon Neufeldt.³ This transformation is similar to the one described in Chapter 3 in several ways. Once again room-temperature arylation was possible by the use of putative aryl radical chemistry (Scheme 4.1).³ However in this system diaryliodonium salts were reduced by the excited photocatalyst rather than aryldiazonium derivatives. An iridium catalyst ($[\text{Ir}(\text{ppy})_2(\text{dtbbpy})]\text{PF}_6$) was used to form the putative aryl radical intermediate rather than $\text{Ru}(\text{bpy})_3^{2+}$. Two lamps were used with 26 W light bulbs. Additionally, similar to our system in Chapter 3, a non-acid solvent (MeOH) and a palladium catalyst ($\text{Pd}(\text{NO}_3)_2$) were utilized. Silver salts were not required to enhance the yield in the Pd/Ir/ Ph_2I^+ method. A major advantage of this method is the use of diaryliodonium salts instead of aryl diazonium salts. The iodonium salts are more stable, thus easily stored, and are not an explosion hazard like the diazonium salts. However, diaryliodonium salts produce a stoichiometric equivalent of aryl iodine, which is less favorable than the innocuous N_2 released from diazonium salts.

Scheme 4.1. Pd-Catalyzed C–H Arylation with Diaryliodonium Salts via Photocatalysis



Several of the same substrates were successfully arylated in both systems; however Table 4.1 shows some of the differences.³ Substrate **4** was compatible in both transformations, though oxime **6** was only able to be arylated in the Pd/Ru/ PhN_2^+ system. Conversely, benzamide **9** was formed in higher yields from **8** using the Pd/Ir/ Ph_2I^+ protocol than the diazonium salt system. The complete substrate scope for the Pd/Ir/ Ph_2I^+ transformation is shown in Table 4.2.³

Table 4.1. Comparison of Pd/Ir-Catalyzed C–H Phenylation with Ph_2I^+ vs Pd/Ru-Catalyzed C–H Phenylation with PhN_2^+

entry	substrate	product	yield ^{a,b} (Ph_2I^+)(%)	yield ^{a,c} (PhN_2^+)(%)
1	 (4)	 (5)	89	91
2	 (6)	 (7)	<1 ^d	66
3	 (8)	 (9)	54	25

^a Calibrated yields determined by gas chromatographic analysis of the crude reaction mixtures. ^b General procedure: Substrate (1.0 equiv), $\text{Pd}(\text{NO}_3)_2$ (0.1 equiv), $[\text{Ir}(\text{ppy})_2(\text{dtbbpy})]\text{PF}_6$ (0.05 equiv), $[\text{Ph}_2\text{I}]\text{OTf}$ (2.0 equiv), MeOH (0.2 M in substrate), rt, 15 h, 26 W compact fluorescent light bulb, degassed by sparging with N_2 . ^c General procedure: Substrate (1.0 equiv), $\text{Pd}(\text{OAc})_2$ (0.1 equiv), $\text{Ru}(\text{bpy})_3\text{Cl}_2 \cdot 6\text{H}_2\text{O}$ (0.025 equiv), $[\text{PhN}_2]\text{BF}_4$ (4.0 equiv), MeOH (0.1 M in substrate), rt, 15 h, 26 W compact fluorescent light bulb, degassed by sparging with N_2 . ^d Product **7** was not detected by GC, and only traces of **6** and 3-methylacetophenone were observed.

Table 4.2. Substrate Scope for the Pd-/Ir-Catalyzed C-H Phenylation Reaction with Ph₂I⁺

entry ^a	substrate	product	isolated yield (%)	entry ^a	substrate	product	isolated yield (%)
1			81	7			9
2			94	8			62
3 ^b			72	9			67
4 ^{b,c,d}			44	10			60
5			40	11			57
6			54				

^a General procedure: Substrate (1.0 equiv), Pd(NO₃)₂ (0.1 equiv), [Ir(ppy)₂(dtbbpy)]PF₆ (0.05 equiv), [Ph₂]OTf (2.0 equiv), MeOH (0.2 M in substrate), rt, 15 h, 26 W compact fluorescent light bulb, degassed by sparging with N₂. ^b [Ph₂]BF₄ was used as the oxidant. ^c Addition of 1 equiv MgO. ^d 0.20 equiv Pd(NO₃)₂ was used.

Similar to our arylation system using diazonium salts, the Pd/Ir/Ar₂I⁺ method can be used to arylate amide substrates such as **4**. As shown in Table 4.3, electron rich and electron deficient diaryliodonium salts were effective for this method. However,

relatively electron neutral diaryliodonium salts afforded the highest yield of product (Table 4.3, entry 3-6). Iodonium salts bearing *ortho*-substitution on the aromatic ring were also tolerated in this reaction, although they generally afforded lower yields (entry 2).

Table 4.3. Scope of Ar₂I⁺ Salts for the Pd-/Ir-Catalyzed C–H Arylation of **4**

10 mol % Pd(NO₃)₂
5 mol % [Ir(ppy)₂(dtbbpy)]PF₆
26 W light bulb
MeOH, 25 °C, 15 h

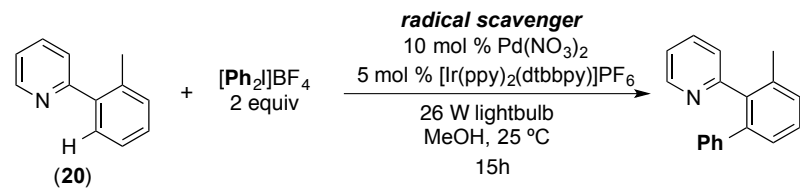
entry ^a	[Ar ₂ I]BF ₄	product	isolated yield (%)
1			41
2 ^b			11
3			85
4			87
5			79
6			77
7			69

^a General procedure: Substrate **4** (1.0 equiv), Pd(NO₃)₂ (0.1 equiv), [Ir(ppy)₂(dtbbpy)]PF₆ (0.05 equiv), [Ar₂I]OTf (2.0 equiv), MeOH (0.2 M in substrate), rt, 15 h, 26 W compact fluorescent light bulb, degassed by sparging with N₂. ^b OTf salt of oxidant used.

4.3 Radical Mechanism

As presented in the paper reporting this transformation, Dr. Sharon Neufeldt conducted experiments to investigate the intermediacy of radicals in this reaction. She found that the addition of radical scavengers inhibited the reaction. In the phenylation of **20** under otherwise standard reaction conditions, the addition of either galvinoxyl or TEMPO afforded low yields of the product in a dose-dependent manner. These results are consistent with the presence of radicals in the course of the reaction.

Table 4.4. Addition of Radical Scavengers on the Pd-/Ir-Catalyzed C–H Arylation of **20**



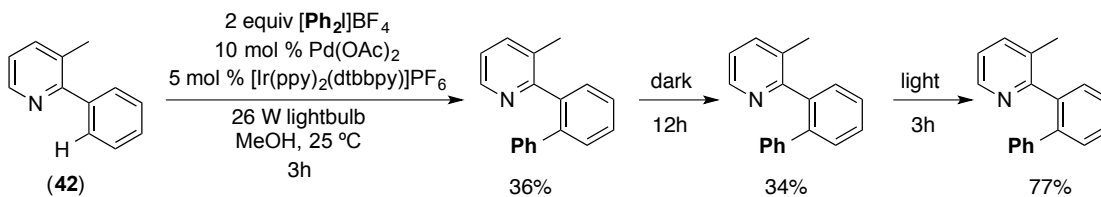
entry ^a	scavenger	mol %	yield (%) ^b
1	none	--	52 ± 4
2	galvinoxyl	10	42 ± 2
3	galvinoxyl	25	20 ± 9
4	TEMPO	50	34 ± 14
5	TEMPO	100	6 ± 2

^a General conditions: **20** (1 equiv), Pd(NO₃)₂ (0.1 equiv), [Ir(ppy)₂(dtbbpy)]PF₆ (0.05 equiv), [Ph₂]BF₄ (2.0 equiv), MeOH (0.2 M in **20**), rt, 15 h, two 26 W compact fluorescent light bulbs, degassed by sparging with N₂. ^b Calibrated yields determined by gas chromatographic analysis reported as % yield ± standard deviation.

In section 3.7 we discussed an experiment that would probe for the possibility of a mechanism involving long-lived radical chains. We were interesting in performing the same experiment, which has also been used by others,⁶ for this system to determine if a radical chain mechanism was contributing to the overall mechanism. As previously outlined, the experiment was constructed of periods of time alternating between light and dark for an otherwise analogous reaction set up. As shown in Scheme 4.2, **42** was submitted to the standard conditions, and the reaction yielded 36% of product after 3 hours. Upon subjecting the reaction to the dark for 12 hours, the yield of product, within error, did not change. Resubmitting the reaction to the light for 3 hours led to a 77%

yield, which is a typical yield for this set of substrates. These experiments suggest that if a radical chain pathway is operating, the chains terminate rapidly in the absence of light. Thus we hypothesize that the proposed photocatalyzed mechanism is likely the major pathway for this C–H arylation reaction.

Scheme 4.2. Experiment to Probe for Radical Chain Mechanism



4.4 Kinetic Studies

We conducted rate studies in order to gain insight into the mechanism including the rate-determining step and order in reagents. In designing experiments, a number of potential reaction pathways were considered. Although a $\text{Pd}^{\text{II/IV}}$ /Ir mechanism was proposed, it is equally important to explore the possibility of alternative routes such as a $\text{Pd}^{\text{I/III}}$ /Ir mechanism as well as many other possibilities.

For all of the rate studies, the appropriate choice of model substrate was important. As mentioned in section 4.1, one reason for studying this Pd/Ir-catalyzed arylation reaction was because it was analogous to the Pd-catalyzed arylation with diaryliodonium salts under thermal conditions. The substrate 3-methyl-2-phenylpyridine (**42**) was the model substrate used for rate studies for the thermal system, and therefore for direct comparison we chose to use the same substrate.

4.4.1 Hammett Studies

First, we performed a competition study to investigate the effect that oxidant electronics had on the reaction. A 1:1 ratio of two electronically different oxidants were added, and the reaction was run to low conversion in order to assess the competition product ratio. This approach allowed us to gain information about the first irreversible

step that oxidant participates in, regardless of its place in the catalytic cycle (*i.e.* at or after the rate-determining step). The product distributions of these reactions were analyzed and a ratio was taken from the yields of the two products.

In these experiments 1 equiv of 3-methyl-2-phenylpyridine (**42**) was combined with 2 equiv $[\text{Ph}_2\text{I}]\text{BF}_4$, 2 equiv of $[\text{Ar}_2\text{I}]\text{BF}_4$, 10 mol % of $\text{Pd}(\text{OAc})_2$, and 5 mol % $[\text{Ir}(\text{ppy})_2(\text{dtbbpy})]\text{PF}_6$ in MeOH. The reaction was placed between two lamps with 26 W light bulbs for 30-70 minutes (Figure 4.3). (Reaction time was determined by the length of time needed to reach approximately 15% yield from the sum of the two products.) The value for P_X/P_H was determined from the ratio of Ar- ($p\text{-XC}_6\text{H}_4\text{-}$) to Ph- products based on calibrated GC yields. A Hammett plot was created by plotting $\log(P_X/P_H)$ versus σ^+ , and the data fit well to a straight line ($R^2=0.77$) with $\rho = +1.0$. The data best fits σ^+ constants, as opposed to σ or σ^- .

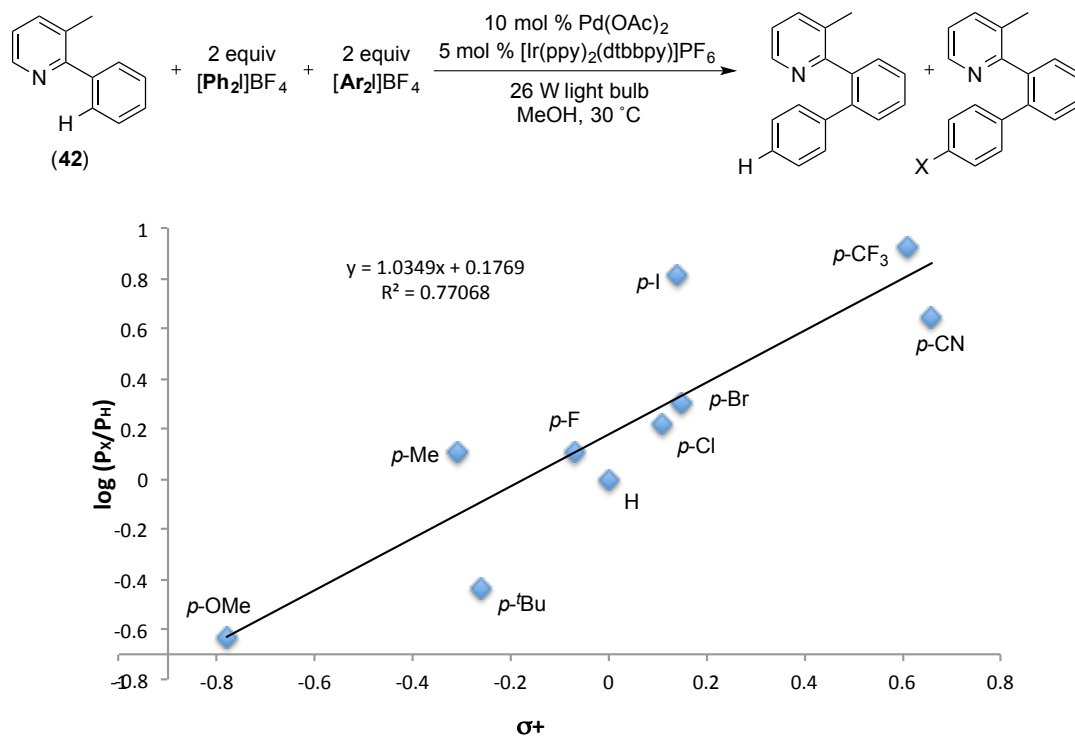


Figure 4.3. Hammett Plot of Competition Study with $[\text{Ph}_2\text{I}]\text{BF}_4$ and $[\text{Ar}_2\text{I}]\text{BF}_4$

This plot indicates that electron-poor oxidants react faster than electron-rich oxidants. This is consistent with what would be expected for reduction of the oxidant by

methyl-2-(*ds*)-phenylpyridine (**44**) (Scheme 4.4). The k_H/k_D was determined to be 1.6 (initial rate for **42** = 22×10^{-5} M/min; initial rate for **44** = 14×10^{-5} M/min) (Figure 4.4 and Figure 4.5). We compared our k_H/k_D to that of the analogous thermal system. Interestingly, using the same substrates, under their thermal conditions, they obtained a k_H/k_D of 1. Importantly, the presence of a kinetic isotope effect in our system suggests a substantial difference in the two mechanisms. A kinetic isotope effect of 1.6 suggests that C–H activation is occurring between the catalyst resting state and the rate-determining step of the catalytic cycle. Investigation of the catalyst resting state could help verify C–H activation as the rate-determining step.

Scheme 4.4. Rates Kinetic Isotope Effect Study of **42**

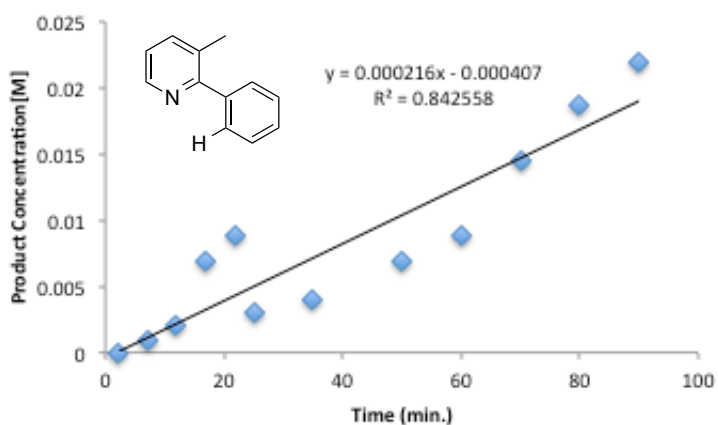
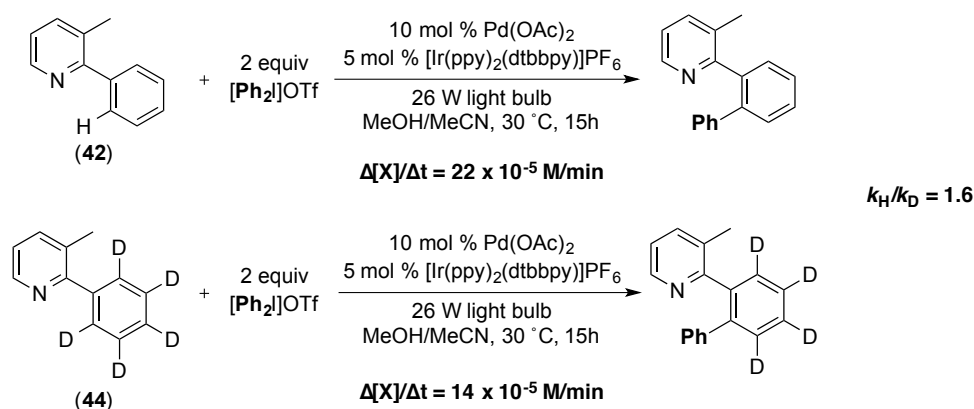


Figure 4.4. Rate Plot for Substrate **42**

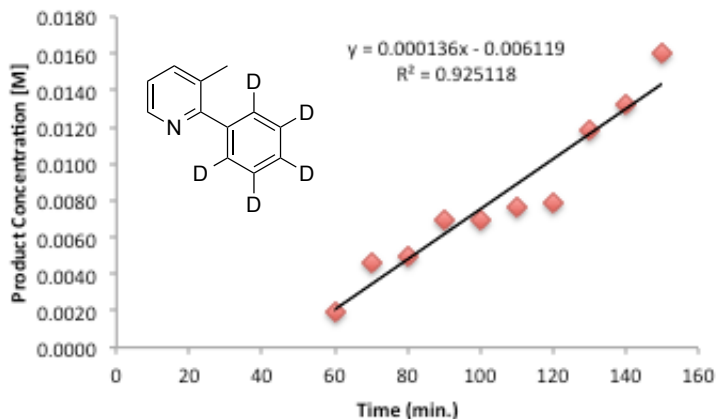


Figure 4.5. Rate Plot for Substrate **44**

4.5 Stern-Volmer Quenching Studies

In order to gain a better mechanistic understanding of both catalytic cycles and their interaction, we hoped to investigate the photochemical portion of the reaction by examining those steps in our proposed mechanistic cycle. To do this, we sought the expertise of Dr. James McCusker and his group at Michigan State University. Their experimental work focuses on the physical and photophysical properties of transition metal complexes. The data presented in the following subsections (4.5.1-4.5.4) outlines the experiments conducted at their facilities.

Through this collaboration, we sought to answer a number of questions that would assist in our understanding of the mechanism. The questions are the following: (1) Is the oxidant ($[\text{Ph}_2\text{I}]\text{BF}_4$) quenching the excited state of the photocatalyst ($[\text{Ir}(\text{ppy})_2(\text{dtbbpy})]^{+*}$)? (2) How does the rate of quenching of $[\text{Ir}(\text{ppy})_2(\text{dtbbpy})]^{+*}$ by other electronically diverse oxidants compare with $[\text{Ph}_2\text{I}]\text{BF}_4$? (3) Are there other reaction components that are quenching the excited state? (4) Are we going through a reductive or oxidative quenching cycle? Throughout this chapter, quenching is described as a decrease in excited state luminescence.

Before investigating these questions, we were interested in understanding the photophysical properties of our photocatalyst ($[\text{Ir}(\text{ppy})_2(\text{dtbbpy})]\text{PF}_6$). We obtained the absorption and emission spectra for $[\text{Ir}(\text{ppy})_2(\text{dtbbpy})]\text{PF}_6$, which are shown in Figure

4.6. The λ_{max} for this catalyst is approximately 270 nm, which is denoted on the absorption curve (red line). The emission spectrum (blue line), on the right, is at higher wavelengths, and has a λ_{max} around 580 nm. These wavelengths were important for the quenching experiments. Additionally, we made note of the redox potentials for our catalyst of study as both a reductive and oxidative quenching cycle are feasible for $[\text{Ir}(\text{ppy})_2(\text{dtbbpy})]\text{PF}_6$ (Figure 4.7).^{1d}

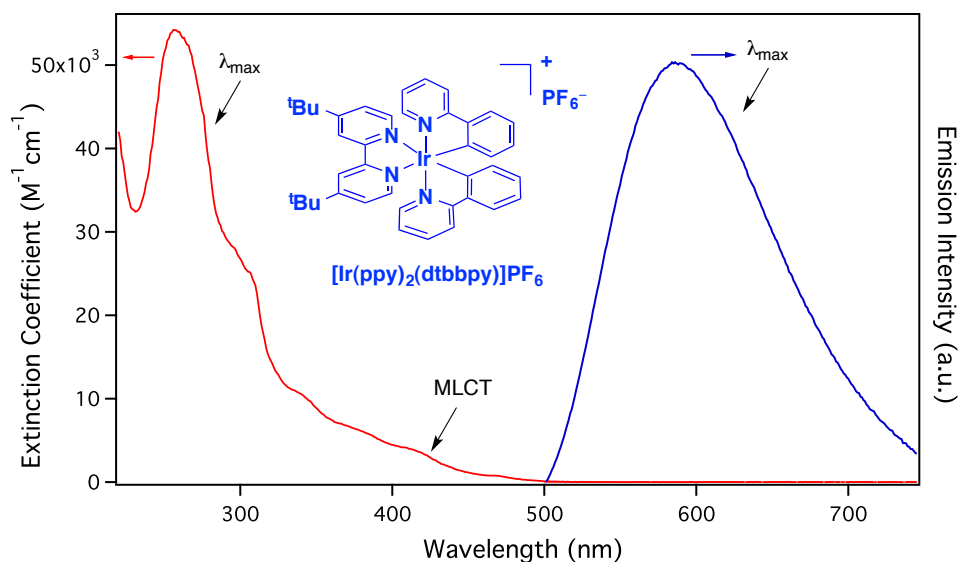
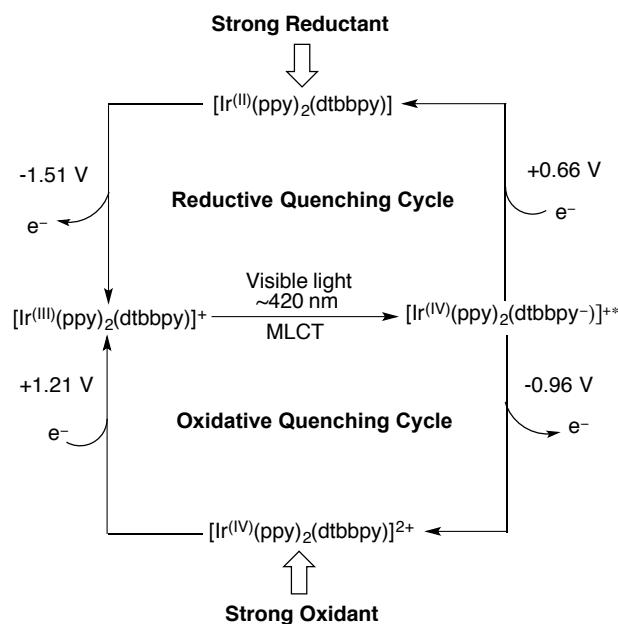


Figure 4.6. Absorption and Emission Spectra of $[\text{Ir}(\text{ppy})_2(\text{dtbbpy})]\text{PF}_6$



^a Potentials are given in volts versus the saturated calomel electrode (SCE).

Figure 4.7. Oxidative and Reductive Quenching Cycles for $[\text{Ir}^{\text{III}}(\text{ppy})_2(\text{dtbbpy})]^+$ ^a

An important process by which excitation occurs and a charge-separated state is formed for $[\text{Ir}(\text{ppy})_2(\text{dtbbpy})]\text{PF}_6$, and other photocatalysts such as the well-known $[\text{Ru}(\text{bpy})_3]^{2+}$, is by metal-to-ligand charge-transfer (MLCT). An electron on the metal is excited from the singlet ground state by absorption of visible light (around 420 nm for $[\text{Ir}(\text{ppy})_2(\text{dtbbpy})]\text{PF}_6$) to an excited state in a ligand-based orbital. This forms the ¹MLCT (Figure 4.8). Thus, the MLCT can be thought of as a simultaneous reduction of the ligand and oxidation of the metal. However, the overall charge and electron count of the complex remains the same. Therefore a more informative depiction of the excited state of our [Ir] catalyst ($[\text{Ir}^{\text{III}}(\text{ppy})_2(\text{dtbbpy})]^{+*}$) is $[\text{Ir}^{\text{IV}}(\text{ppy})_2(\text{dtbbpy}^-)]^{+*}$, as used in Figure 4.7. To continue with the excitation and decay process, rapid intersystem crossing occurs to form the triplet excited state from which emission can occur, returning the complex to the ground state (Figure 4.8). The excited state can also relax back to the ground state via non-radiative decay, where heat is released.

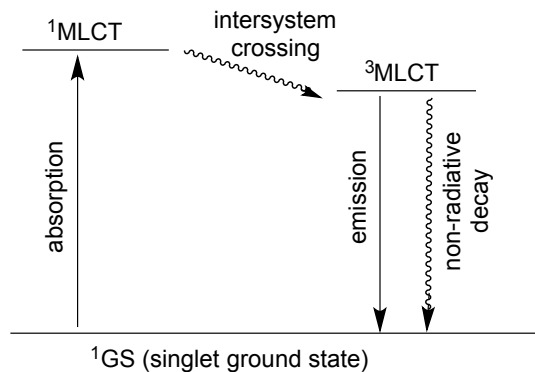


Figure 4.8. Jablonski Diagram for Transition Metal Complexes

One type of experiment of interest to us was Stern-Volmer quenching studies.⁹ These studies allow us to select a potential quencher and study the kinetics of a photophysical system in which the deactivation of an excited species occurs. In these studies, the emission lifetime is measured in the presence of a suspected quencher. In the absence of a quencher, photocatalysts decay through a combination of emission and non-radiative decay back to the ground state. However, in the presence of a quencher, the emission will be diminished, and the lifetime shortened, because some of the excited state is being quenched, or rerouted, potentially by electron transfer. Often this results in new [Ir] intermediates, either oxidized or reduced. Figure 4.9 shows the specifics of this process for our [Ir] catalyst. Therefore, in the Stern-Volmer quenching studies for $[\text{Ir}(\text{ppy})_2(\text{dtbbpy})]^+$, a decrease in emission intensity at 585 nm would indicate the species present, or suspected quencher, is quenching the excited state ($[\text{Ir}(\text{ppy})_2(\text{dtbbpy})]^{+*}$).

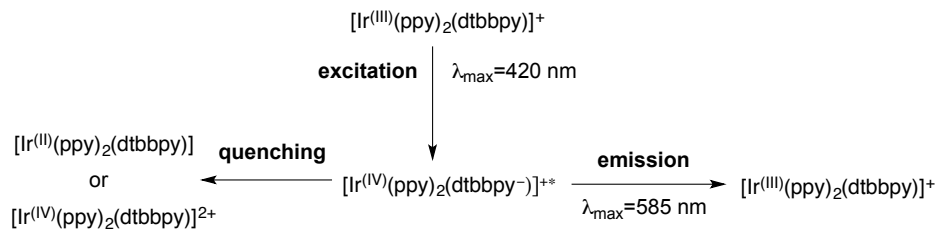


Figure 4.9. Possible Decay Routes for $[\text{Ir}(\text{ppy})_2(\text{dtbbpy})]^{+*}$

4.5.1 Time-Resolved Emission of [Ir] with [Ph₂I]BF₄

The main technique we used for the Stern-Volmer quenching studies was time-resolved emission spectroscopy.¹⁰ A rudimentary sketch of the layout of the experiment is shown in Figure 4.10, with the emission from the sample being detected 90° from the laser light. The sample is composed of the photocatalyst and the suspected quencher in the reaction solvent under pseudo-first order conditions ($[Q] \gg [PC]$). The laser is set to excite at one wavelength, and we probe, or detect, at another. The absorption and emission spectra from Figure 4.6 lead us to appropriate values for those wavelengths (420 nm for excitation and 585 nm for detection). The data collected is obtained as a kinetic trace because the emission is recorded over time (Figure 4.11). From these emission traces we can obtain the lifetime of the excited state and from the Stern-Volmer plot (Figure 4.13) we find the rate constant for quenching (k_q).

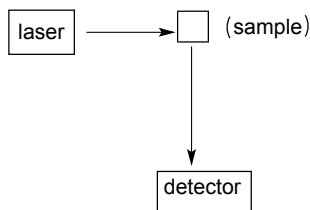


Figure 4.10. Basic Layout for Time-Resolved Emission Spectroscopy

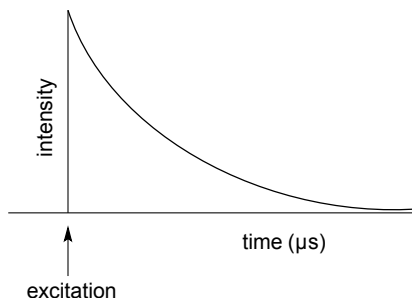


Figure 4.11. Example of Kinetic Trace as Collected by Time-Resolved Emission

We expected and proposed that the oxidant [Ph₂I]BF₄ would quench the excited state of our [Ir] catalyst in the Pd-/Ir-catalyzed arylation reaction. Therefore, using a drybox to ensure the exclusion of O₂ (because O₂ quenches the MLCT of these compounds), a series of MeOH solutions of [Ph₂I]BF₄ and [Ir(ppy)₂(dtbbpy)]PF₆ were

prepared in airtight cuvettes. These solutions had a constant concentration of Ir, but varied concentrations of $[\text{Ph}_2\text{I}]\text{BF}_4$, in order to probe the impact of this putative quencher on the intensity of emission. Figure 4.12 shows an overlay of a trace with the photocatalyst (red line) and a trace with both the photocatalyst and quencher (blue line). The results show that there is a faster decrease in the emission in the presence of the iodonium salt. Additionally, the excited state lifetimes for both curves were calculated.⁹ The sample containing the quencher displays a shorter lifetime of 356 ns compared to the 477 ns lifetime of $[\text{Ir}(\text{ppy})_2(\text{dtbbpy})]^{+\ast}$.

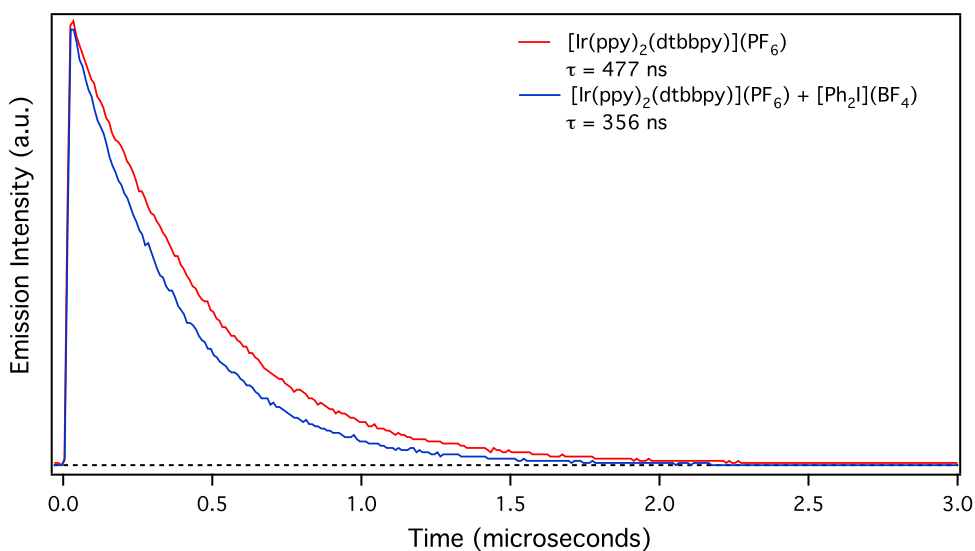


Figure 4.12. Time-Resolved Emission Traces of $[\text{Ir}(\text{ppy})_2(\text{dtbbpy})]\text{PF}_6$ with and without $[\text{Ph}_2\text{I}]\text{BF}_4$ in MeOH

The samples with other concentrations of $[\text{Ph}_2\text{I}]\text{BF}_4$ were subjected to the same experiment. From the data, a Stern-Volmer plot was constructed (Figure 4.13). The data fit well to a line, indicating that $[\text{Ph}_2\text{I}]\text{BF}_4$ is quenching $[\text{Ir}(\text{ppy})_2(\text{dtbbpy})]^{+\ast}$. This supports our proposed mechanism in that the diphenyliodonium salt reacts with $[\text{Ir}(\text{ppy})_2(\text{dtbbpy})]^{+\ast}$. However, these data do not provide information as to the type of quenching that is taking place (reductive versus oxidative). Since diphenyliodonium salts are known to be oxidants, we believe this data supports our mechanism that $[\text{Ph}_2\text{I}]\text{BF}_4$ is receiving an electron from $[\text{Ir}]^*$. To verify this proposal, transient absorption

spectroscopy was conducted (see section 4.5.4). Additionally, a quenching rate of $4.6 \times 10^7 \text{ M}^{-1} \text{ s}^{-1}$ is observed.

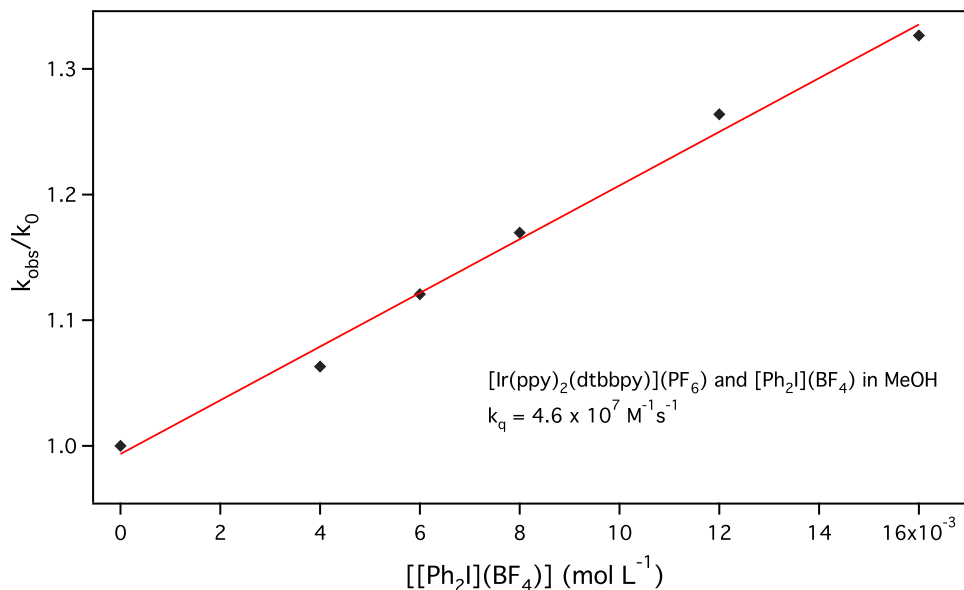


Figure 4.13. Stern-Volmer Plot for the Quenching of the Excited State of $[\text{Ir}(\text{ppy})_2(\text{dtbbpy})]\text{PF}_6$ with $[\text{Ph}_2\text{I}]\text{BF}_4$

4.5.2 Time-Resolved Emission of [Ir] with $[\text{Ar}_2\text{I}]\text{BF}_4$

Once we had confirmed that $[\text{Ph}_2\text{I}]\text{BF}_4$ was quenching the excited state of $[\text{Ir}(\text{ppy})_2(\text{dtbbpy})]\text{PF}_6$ and established a rate of quenching, we next explored the quenching rates of other diaryliodonium salts. Using the same experimental setup as described in section 4.5.1, we studied a number of electronically diverse $[\text{Ar}_2\text{I}]\text{BF}_4$ with *para*-substitution. These included *p*-MeO-, *p*-Cl-, *p*-CF₃- as shown by the Stern-Volmer quenching plots in Figure 4.14, Figure 4.15, and Figure 4.16 respectively. The data at various concentrations had a linear fit for all oxidants.

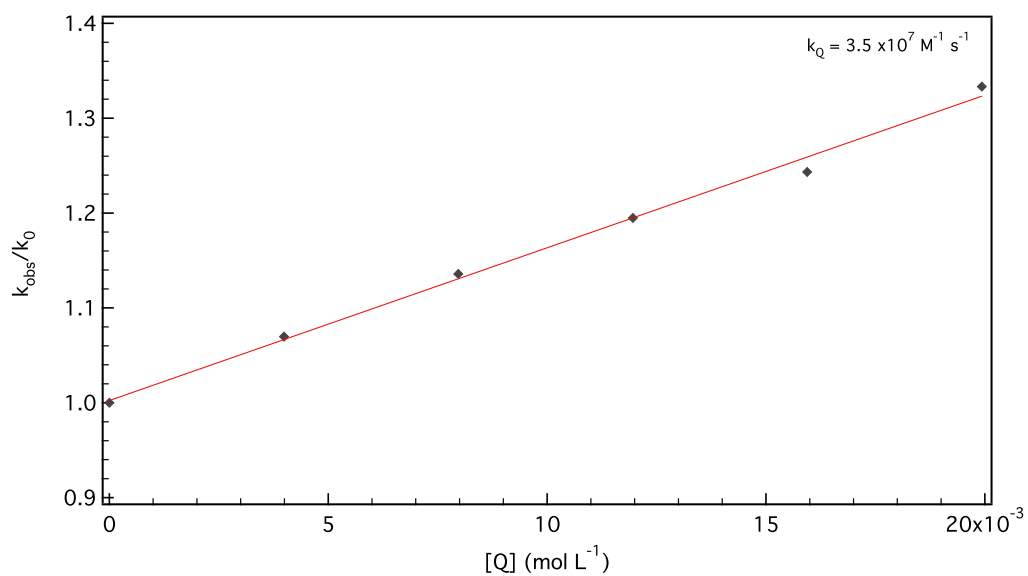


Figure 4.14. Stern-Volmer Plot for the Quenching of the Excited State of $[\text{Ir}(\text{ppy})_2(\text{dtbbpy})]\text{PF}_6$ with $[(p\text{-MeOC}_6\text{H}_4)_2\text{I}]\text{BF}_4$

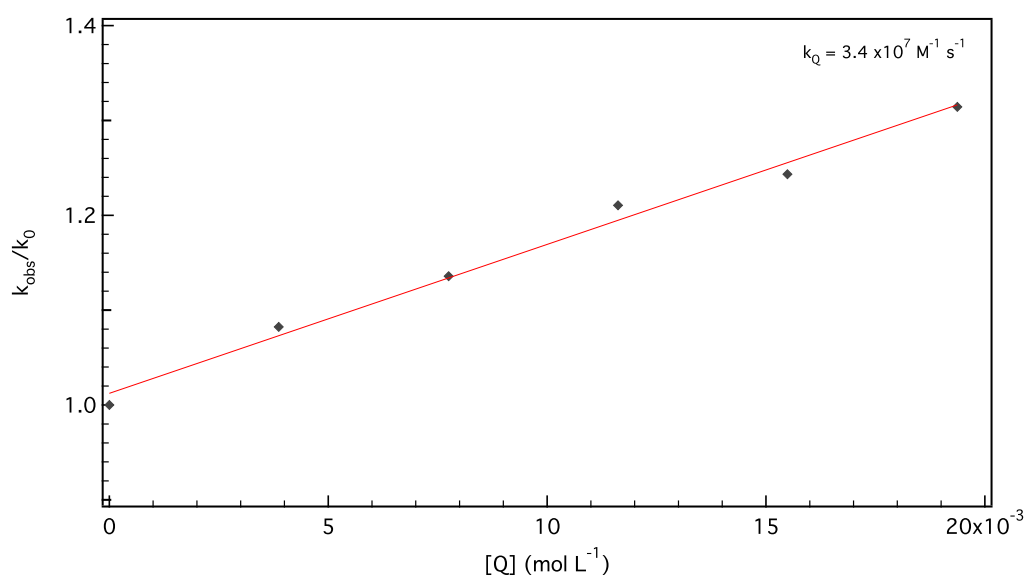


Figure 4.15. Stern-Volmer Plot for the Quenching of the Excited State of $[\text{Ir}(\text{ppy})_2(\text{dtbbpy})]\text{PF}_6$ with $[(p\text{-ClC}_6\text{H}_4)_2\text{I}]\text{BF}_4$

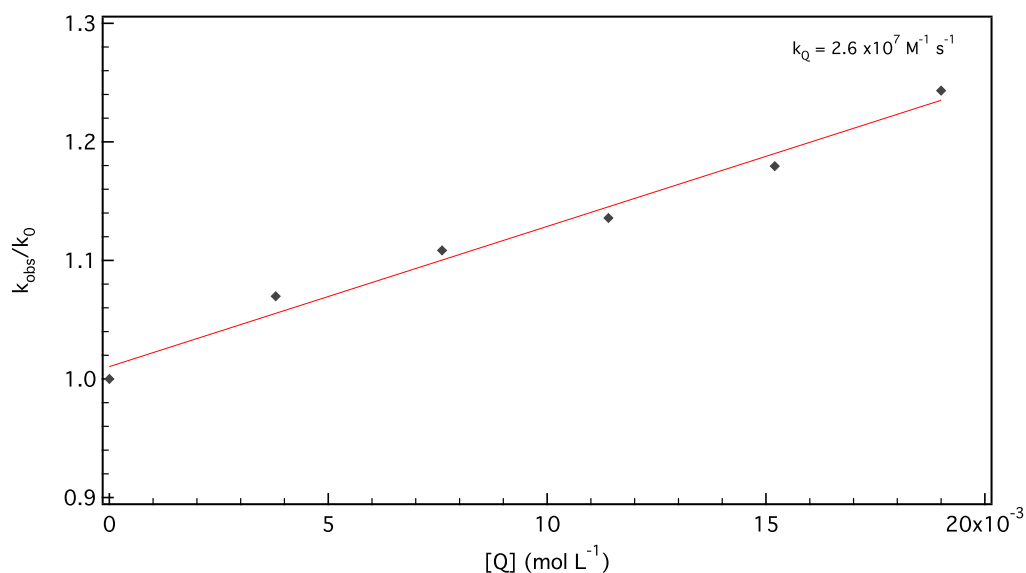


Figure 4.16. Stern-Volmer Plot for the Quenching of the Excited State of $[\text{Ir}(\text{ppy})_2(\text{dtbbpy})]\text{PF}_6$ with $[(p\text{-CF}_3\text{C}_6\text{H}_4)_2\text{I}]\text{BF}_4$

Quenching rates were obtained for each case, with $[(p\text{-MeOC}_6\text{H}_4)_2\text{I}]\text{BF}_4$ showing a rate of $3.5 \times 10^7 \text{ M}^{-1} \text{ s}^{-1}$ and $[(p\text{-CF}_3\text{C}_6\text{H}_4)_2\text{I}]\text{BF}_4$ with the slowest rate of $2.6 \times 10^7 \text{ M}^{-1} \text{ s}^{-1}$. In addition to these results we included $[\text{Ph}_2\text{I}]\text{BF}_4$ from section 4.5.1 as the H point in the construction of a Hammett plot (Figure 4.17). However, this point from $[\text{Ph}_2\text{I}]\text{BF}_4$ does not fit linearly with the other data as it displays the highest rate of quenching. Additionally, we expected to see a positive ρ value for this Hammett plot, as we believe the Hammett plot from section 4.4.1, is also measuring the quenching step. Therefore, this data appears to be inconsistent with our previous Hammett study. Additional substrates need to be tested in order to make firm conclusions about the effect of electronics on the rate of quenching.

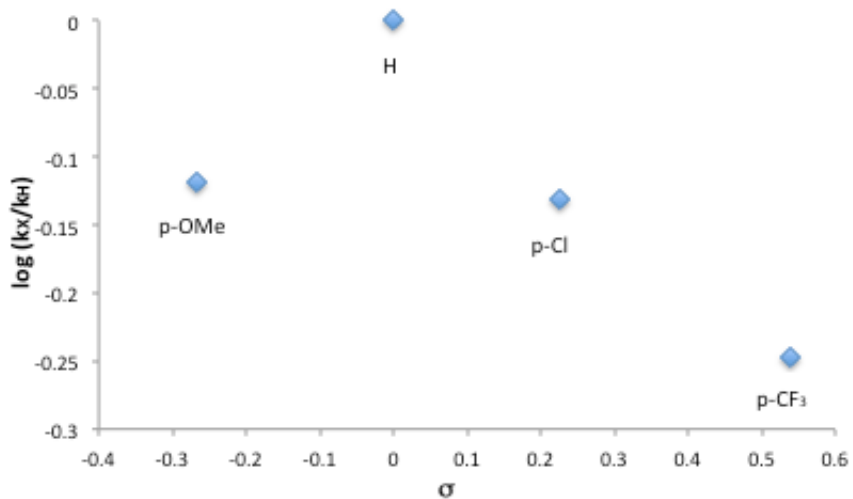


Figure 4.17. Hammett Plot of k_q of Diaryliodonium Salts

4.5.3 Time-Resolved Emission of [Ir] with Other Reaction Components

In order to fully investigate the photochemistry occurring in this transformation, we sought to probe other reaction components for quenching using time-resolved emission. The two that we were most interested in testing were the Pd catalyst, Pd(OAc)₂, and a Pd-dimer **45** which closely resembles the C–H activated intermediate **1** (Figure 4.18). With these compounds in hand, a time-resolved emission experiment was run on each compound. As a quick initial investigation of these compounds, one concentration of the potential quenchers, with roughly 1:100 catalyst-to-quencher ratio, was analyzed for quenching.

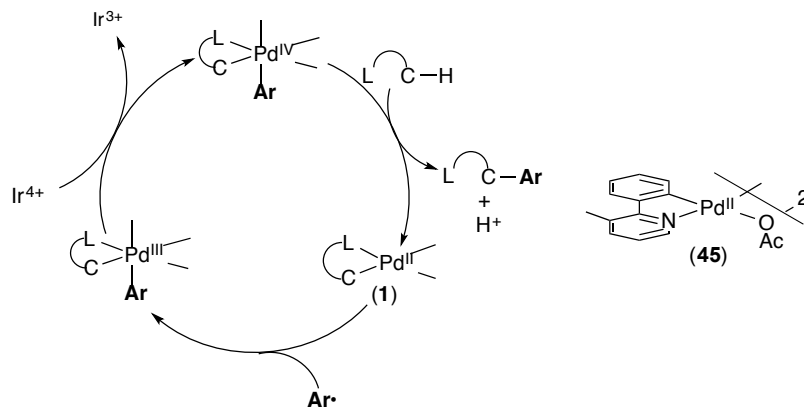


Figure 4.18. Pd-Dimer **45** as a Substitute for C-H Activated Intermediate **1**

Interestingly, the emission traces collected for both compounds indicated a decrease in excited state lifetime, suggesting some sort of electron or energy transfer from $[\text{Ir}]^*$ to the Pd complexes. Figure 4.19 shows a greatly decreased $[\text{Ir}]$ excited state lifetime of 105 ns when $\text{Pd}(\text{OAc})_2$ is present. Thus, this indicates $\text{Pd}(\text{OAc})_2$ is quenching the $[\text{Ir}(\text{ppy})_2(\text{dtbbpy})]^{+*}$. Likewise, Pd-dimer **45** produces similar results, with an $[\text{Ir}]$ excited state lifetime of 245 ns (Figure 4.20). Further experiments, such as transient absorption (see section 4.5.4), would be needed to determine if the $[\text{Pd}]$ species are being reduced or oxidized. Additionally, conducting a full set of experiments for a Stern-Volmer plot would allow us to compare the extend of quenching of $\text{Pd}(\text{OAc})_2$ and Pd-dimer **45** to $[\text{Ph}_2\text{I}]\text{BF}_4$. Furthermore, experiments to probe the outcome of these species, especially if side reactions are inhibiting or aiding in the desired transformation, remain to be studied.

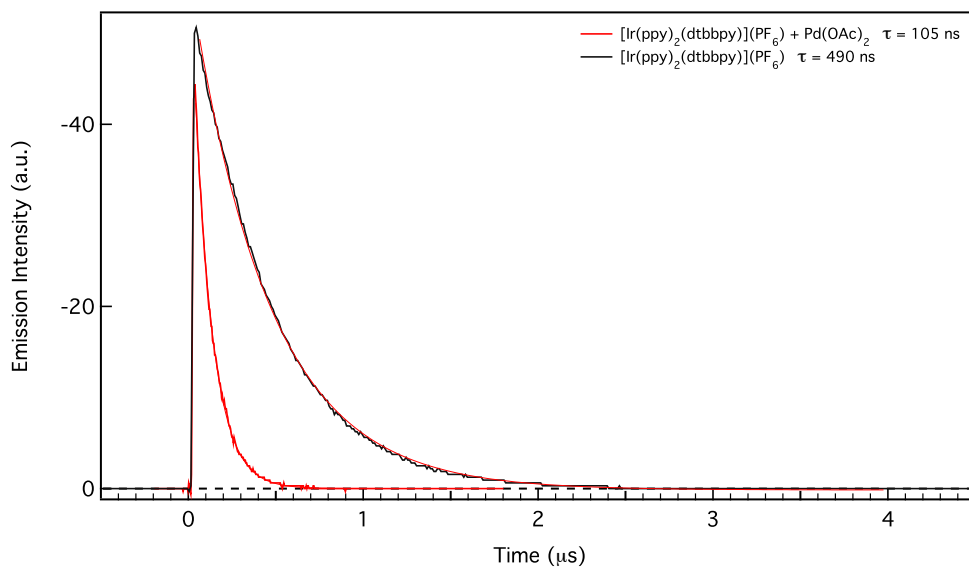


Figure 4.19. Time-Resolved Emission Traces of $[\text{Ir}(\text{ppy})_2(\text{dtbbpy})]\text{PF}_6$ with and without $\text{Pd}(\text{OAc})_2$ in MeOH

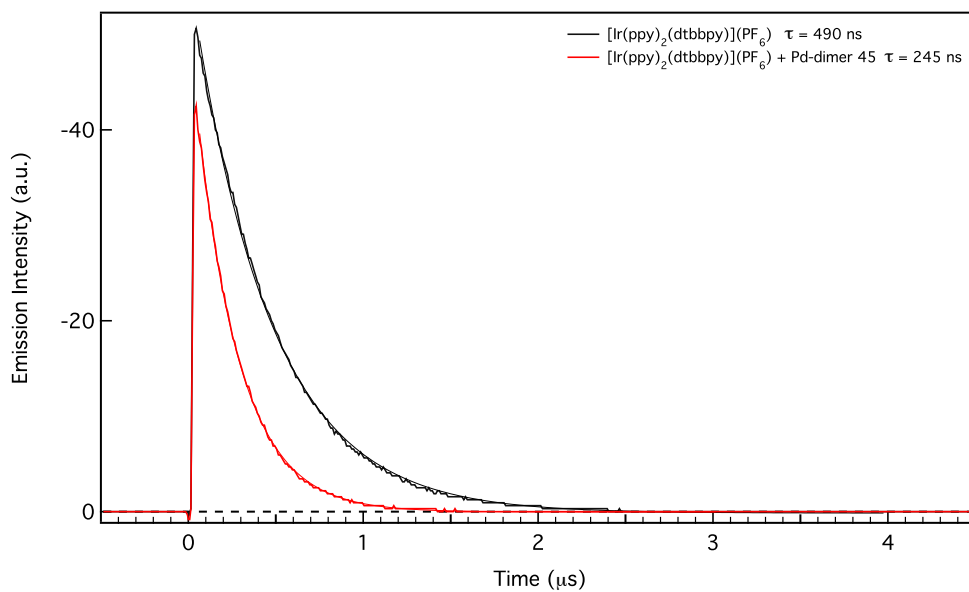


Figure 4.20. Time-Resolved Emission Traces of $[\text{Ir}(\text{ppy})_2(\text{dtbbpy})]\text{PF}_6$ with and without Pd-Dimer **45** in MeOH

4.5.4 Transient Absorption

One important topic of interest to us was if the reaction was proceeding through a reductive or oxidative quenching cycle. To address this question we used a technique called transient absorption spectroscopy (TA), which allows us to take an ultraviolet-visible spectrum (UV-visible) of the excited state of a compound.¹⁰ The general setup for this technique is shown in Figure 4.21, with the typical configuration for UV-visible spectroscopy with the addition of a laser at 90° to excite at the appropriate wavelength. We are probing the step in the mechanism shown in Scheme 4.5, from the excited state to the proposed oxidized species, to determine if the oxidized species is indeed formed.

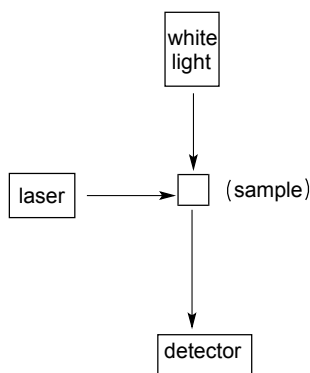
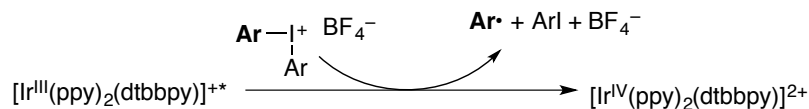


Figure 4.21. General Setup for Transient Absorption Spectroscopy

Scheme 4.5. Proposed Mechanistic Step Studied using Transient Absorption Spectroscopy



Before conducting the TA experiments, another technique is required to inform us of peaks to probe for in the actual TA experiment. Spectroelectrochemistry allows us to obtain the UV-visible absorption spectrum of both the reduced and oxidized photocatalyst, which in our case are $[\text{Ir}^{\text{II}}(\text{ppy})_2(\text{dtbbpy})]$ and $[\text{Ir}^{\text{IV}}(\text{ppy})_2(\text{dtbbpy})]^{2+}$, respectively. The two spectra obtained are shown in Figure 4.22, with the red line showing the reduced species and the green the oxidized species. Importantly, the spectra are portrayed as a change in absorbance, as shown on the y-axis, from the ground state.

Therefore, there are both positive and negative (bleach) features present, as they show differences from the ground state.

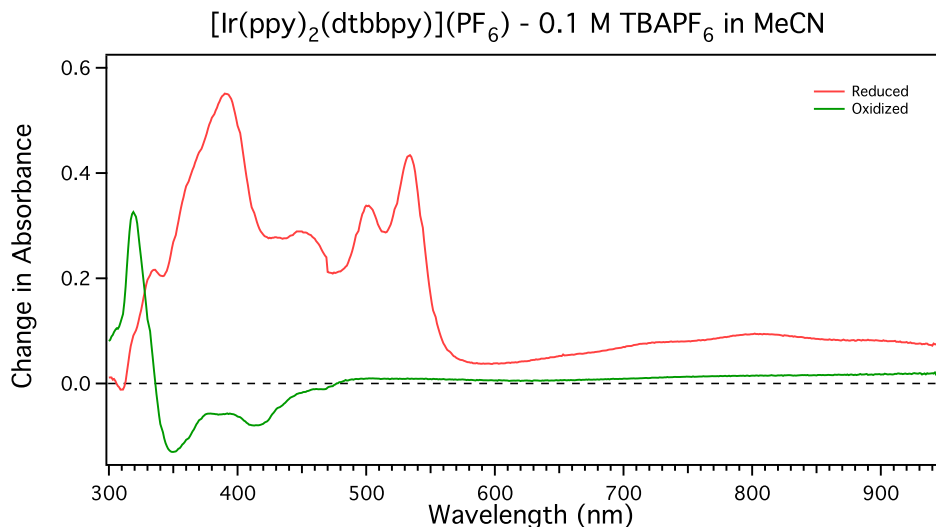


Figure 4.22. Spectroelectrochemistry of $[\text{Ir}(\text{ppy})_2(\text{dtbbpy})]\text{PF}_6$

In TA spectroscopy we excite the sample at one wavelength (410 nm for $[\text{Ir}(\text{ppy})_2(\text{dtbbpy})]\text{PF}_6$ because it is in the MLCT band) and probe at another wavelength. We expect to see spectral signatures of either the reduced or oxidized species as shown in Figure 4.22 from the spectroelectrochemistry. The resulting spectra will indicate if a reductive or oxidative quenching step is taking place based on which spectral signature is observed. Therefore if oxidative quenching takes place between $[\text{Ir}(\text{ppy})_2(\text{dtbbpy})]\text{PF}_6$ and $[\text{Ph}_2\text{I}]\text{BF}_4$, we would expect to observe the oxidized photocatalyst, as shown by the green line above (Figure 4.22).

The quenching is the reaction between $[\text{Ir}(\text{ppy})_2(\text{dtbbpy})]^{+*}$ and $[\text{Ph}_2\text{I}]\text{BF}_4$; however not every [Ir] photocatalyst molecule undergoes this reaction. As a consequence, the TA traces show a signal that corresponds to the excited photocatalyst, $[\text{Ir}(\text{ppy})_2(\text{dtbbpy})]^{+*}$ as well as a signal for the $[\text{Ir}^{\text{IV}}(\text{ppy})_2(\text{dtbbpy})]^{2+}$, if oxidative quenching is taking place. The excited photocatalyst has a lifetime of about 300 ns in the presence of the quencher and thus any spectral features due to $[\text{Ir}(\text{ppy})_2(\text{dtbbpy})]^{+*}$ will disappear after about 1.5 μs . Spectral features corresponding to either the reduced or

oxidized species will remain for a longer time. Therefore the important part of the spectra is the portion after about 1.5–2 μs .

The first wavelength that was probed was 385 nm. In the absence of the quencher, the signal goes back to zero after about 2 μs (the excited state lifetime is about 500 ns) (Figure 4.23). As zero is indicating the ground state, this is normal decay, as we would expect in the absence of a quencher.

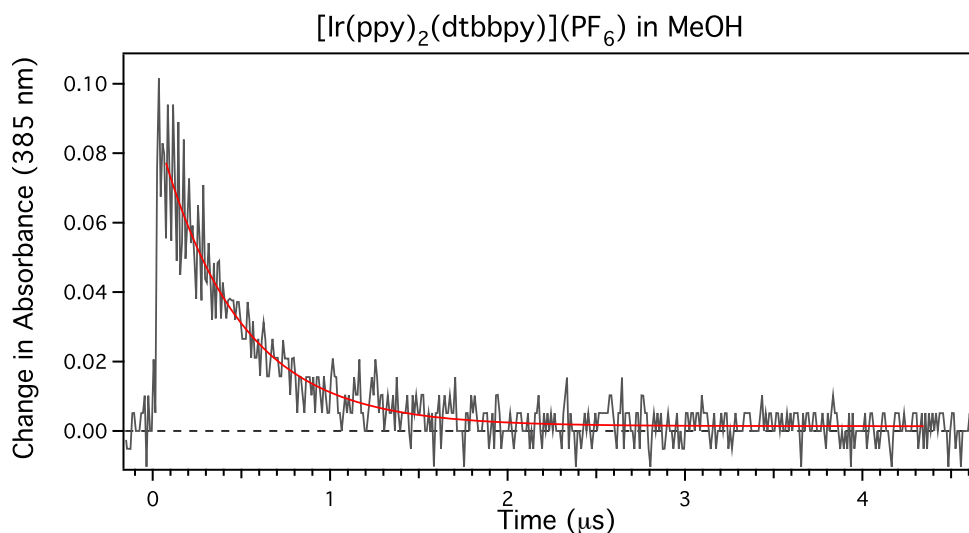


Figure 4.23. Transient Absorption of $[\text{Ir}(\text{ppy})_2(\text{dtbbpy})]\text{PF}_6$ probing at 385 nm

While probing at 385 nm, when the quencher is present, the signal becomes negative after about 2 μs (Figure 4.24). Based on our observations from the spectroelectrochemistry (Figure 4.22) at 385 nm, the oxidized species is negative and the reduced species is positive. Therefore, this TA result suggests that $[\text{Ir}(\text{ppy})_2(\text{dtbbpy})]^{2+}$ is formed by oxidative quenching and this species remains after the excited [Ir] photocatalyst has gone back to the ground state.

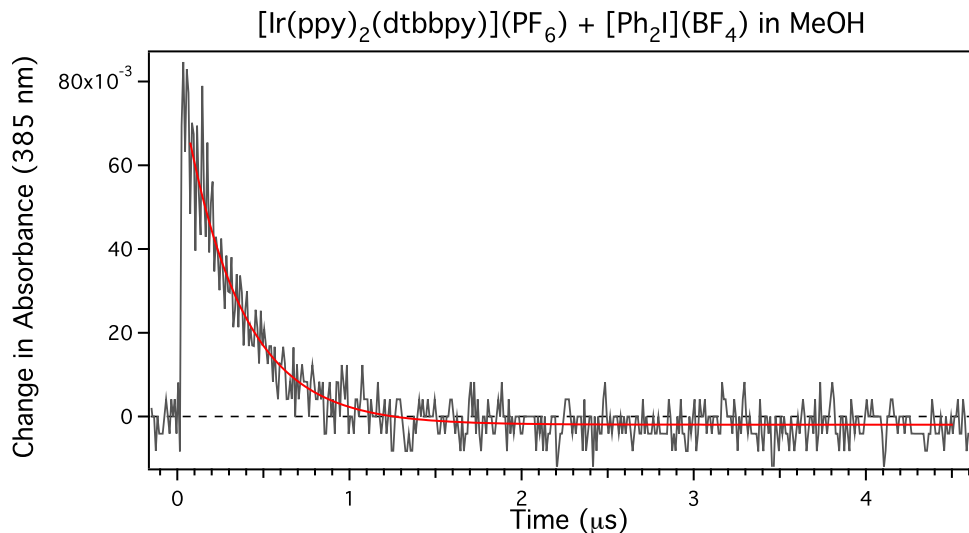


Figure 4.24. Transient Absorption of $[\text{Ir}(\text{ppy})_2(\text{dtbbpy})]\text{PF}_6$ with $[\text{Ph}_2\text{I}]\text{BF}_4$ probing at 385 nm

The second wavelength we chose to probe was 460 nm. Again as a control we observed that in the absence of quencher the signal returns to zero (Figure 4.25). However, when the quencher is present, a residual positive signal can be seen in Figure 4.26. At first glance this data may appear to be supporting the reductive quenching pathway. However, we believe the isosbestic point (~ 475 nm, where the oxidized species and the Ir photocatalyst have the same absorption or otherwise stated as $\Delta\text{Abs} = 0$) is shifted. The spectroelectrochemistry experiment was conducted in acetonitrile, as methanol is not suitable for electrochemistry due to its narrow potential window, whereas the TA experiments were carried out in methanol, which is the reaction solvent. The wavelength of the isosbestic point may change from one solvent to the other.⁵ Therefore we believe the oxidative species has a positive change in absorption feature at 460 nm. If this were true, then the data observed in Figure 4.26 could support either a reductive or oxidative quenching cycle. Therefore, the data at 385 nm is more clear and conclusive.

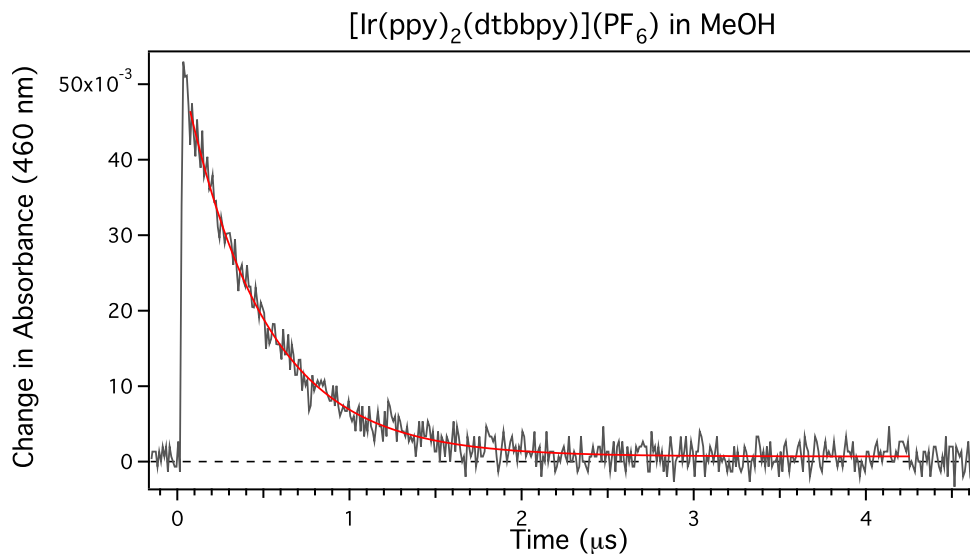


Figure 4.25. Transient Absorption of $[\text{Ir}(\text{ppy})_2(\text{dtbbpy})]\text{PF}_6$ probing at 460 nm

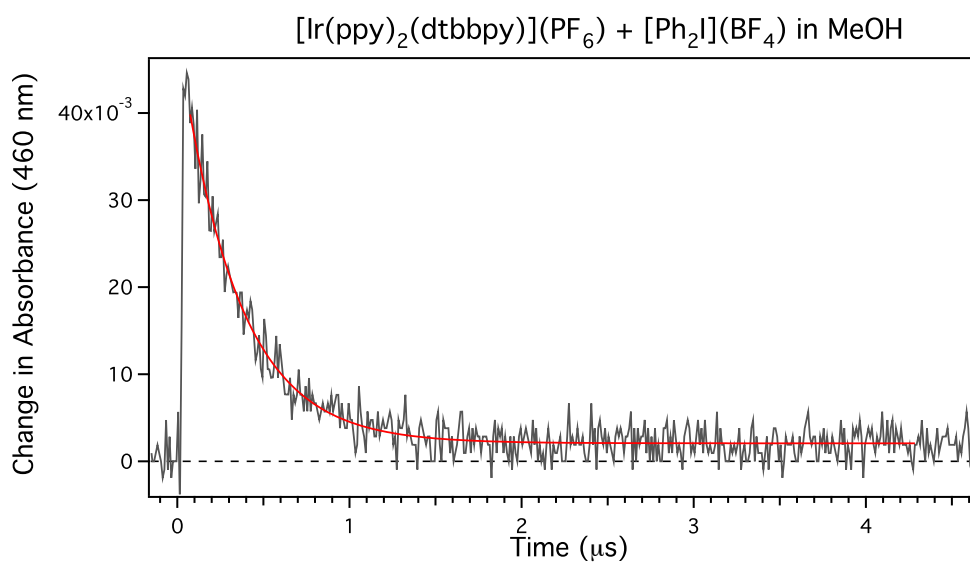


Figure 4.26. Transient Absorption of $[\text{Ir}(\text{ppy})_2(\text{dtbbpy})]\text{PF}_6$ with $[\text{Ph}_2\text{I}]\text{BF}_4$ probing at 460 nm

Additionally, the driving force for both the reductive and oxidative quenching for this transformation was calculated. For oxidative quenching $\Delta G_{\text{et}}^0 = -0.17$ eV and for reductive quenching $\Delta G_{\text{et}}^0 = 1.37$ eV. This negative ΔG for oxidative quenching and high positive value for reductive quenching supports our findings.

4.6 Conclusions

In summary, we have investigated the mechanism of the Pd-/Ir-catalyzed arylation reaction with $[\text{Ar}_2\text{I}]\text{BF}_4$. We probed the radical nature of the reaction as well as utilized kinetic experiments and Stern-Volmer quenching studies. The radical experiments suggested that a radical mechanism is in operation, however a radical chain mechanism is not a major pathway. A kinetic isotope effect of 1.6 from the rates of parallel reactions suggest the C–H activation is before or during the rate-determining step. Additionally, a competition Hammett plot had a positive ρ value, indicating that the electronics of the oxidant impact the first irreversible reaction of the oxidant. However, the full implications of these experiments on the catalytic cycle are not yet known. Additional kinetic experiments, as outlined below, would need to be conducted to draw further conclusions. The Stern-Volmer quenching studies and transient absorption experiments conducted agreed with the proposed catalytic cycle in which $[\text{Ph}_2\text{I}]\text{BF}_4$ is quenching the excited state of $[\text{Ir}]$ and that is taking place by an oxidative quenching cycle. Additionally other reaction components including $\text{Pd}(\text{OAc})_2$ and a Pd-dimer species representing the C–H activated palladacycle were shown to also quench the excited state of our Ir catalyst. Further experiments would be needed to determine the fate of these species and if they are being reduced or oxidized.

With these initial mechanistic findings, we have not made any changes to our original mechanistic picture (Figure 4.27). However, a full understanding of the mechanism is far from complete. Other mechanisms should be considered as further investigations are discovered such as those shown in Figure 4.28 and Figure 4.29.¹¹ Our mechanistic findings have strongly supported the Ir-catalytic cycle. Therefore, the majority of additional experiments should focus on the Pd-cycle and the interactions of the whole transformation.

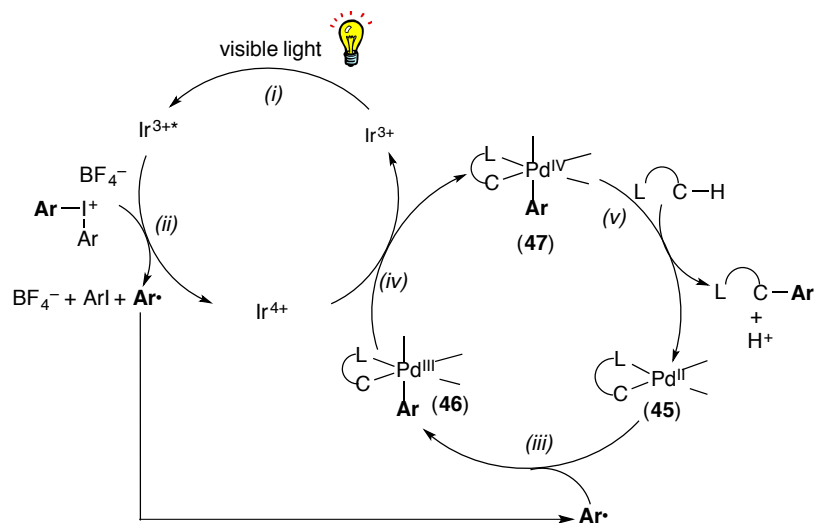


Figure 4.27. Proposed Catalytic Cycle for the Pd-/Ir-Catalyzed C-H Arylation Reaction

Future work on the elucidation of this arylation mechanism should focus on kinetic experiments. These should include (1) a Hammett plot using rates of individual reactions with a variety of [Ar₂I]BF₄, (2) order studies for catalysts, oxidant, and substrate, and (3) the investigation of catalyst and oxidant resting states. Additional Stern-Volmer quenching studies could aid in a more complete understanding of the transformation including uncovering any possible side reactions. These findings could lead us to further optimize the reaction conditions as well as increased knowledge for better designs for other transformation. Additionally we hope these findings, once complete, can contribute to the library of knowledge about the growing field of visible-light photoredox catalysis.

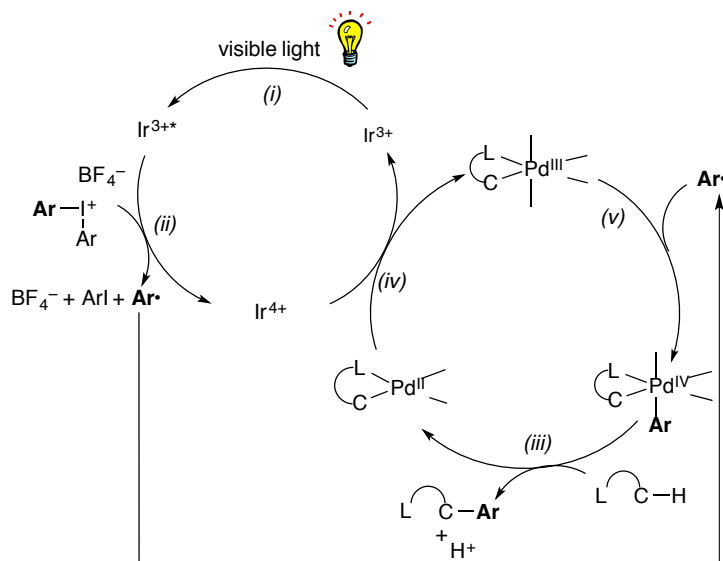


Figure 4.28. Alternative Pd^{II/IV} Mechanism for the Pd/Ir-Catalyzed C–H Arylation Reaction

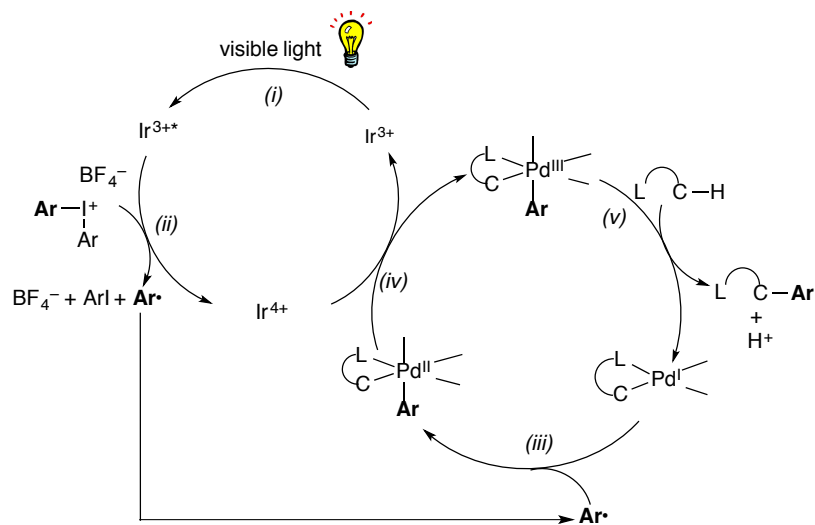


Figure 4.29. Alternative Pd^{I/III} Mechanism for the Pd/Ir-Catalyzed C–H Arylation Reaction

4.7 Experimental Procedures and Characterization of Data

General Procedures

NMR spectra were obtained on a Varian vnmrs 700 (699.76 MHz for ¹H; 175.95 MHz for ¹³C), Varian vnmrs 500 (500.10 MHz for ¹H; 125.75 MHz for ¹³C, 470.56 MHz for ¹⁹F),

Varian Inova 500 (499.90 MHz for ^1H ; 125.70 MHz for ^{13}C), Varian MR400 (400.52 MHz for ^1H ; 100.71 for ^{13}C , 376.87 MHz for ^{19}F), or a Varian Inova 400 (399.96 MHz for ^1H ; 100.57 MHz for ^{13}C ; 376.34 MHz for ^{19}F) spectrometer. ^1H NMR chemical shifts are reported in parts per million (ppm) relative to TMS, with the residual solvent peak used as an internal reference. Multiplicities are reported as follows: singlet (s), doublet (d), doublet of doublets (dd), doublet of doublets of doublets (ddd), doublet of triplets (dt), triplet (t), quartet (q), quintet (quin), multiplet (m), and broad resonance (br). HRMS data were obtained on a Micromass AutoSpec Ultima Magnetic Sector mass spectrometer. Gas chromatography was carried out on a Shimadzu 17A using a Restek Rtx®-5 (Crossbond 5% diphenyl – 95% dimethyl polysiloxane; 15 m, 0.25 mm ID, 0.25 μm df) column. UV-visible absorption spectra were recorded using a Hewlett-Packard 8452A diode array spectrophotometer. Steady-state emission spectra were acquired using a SpexFluoroMax fluorimeter. Emission spectra were corrected for instrumental response by using a NIST standard of spectral irradiance (Optronic Laboratories, Inc., OL220M tungsten quartz lamp).

Time-resolved measurements on the nanosecond time scale were carried out with an OPOTEK optical parametric oscillator-based spectrometer. The emitted light is collected at 90° to the excitation via matched back-to-back plano-convex lenses ($f_o = 200$ mm, $\phi = 90$ mm) and coupled into a McPherson Model 272 200 mm $f/2$ monochromator equipped with a 100 mm diameter holographic grating (1140 G/mm). Typical slit settings are 0.5 mm for both the entrance and exit slits. Detection is achieved by using a negatively-biased Hamamatsu R928 photomultiplier tube operated at a voltage of -650 Vdc. The tube is housed in a RF and magnetically shielded PMT housing (Thorn EMI Electron Tubes). The PMT signal is terminated through a 50 Ω resistor to a LeCroy Model 9360 Digitizing Oscilloscope. Linearity of the PMT signal is checked, using neutral density filters, with the signal intensity adjusted if necessary via attenuation of the excitation beam. The data from the scope, representing a 300-shot signal average collected at a repetition rate of 10 Hz, is transferred to a computer and processed by using programs of local origin.

The time-resolved absorption measurements use the output from the OPO directly. The beam is cylindrically focused onto the sample at 90° to the probe beam. Excitation

energies used are typically in the range of 1-3 mJ/pulse. The probe consists of a current-intensified pulsed Xe arc lamp (Applied Photophysics, Ltd.). Detection is achieved by using a negatively-biased Hamamatsu R446 photomultiplier tube operating at -650 Vdc and housed in a Products for Research PMT housing. As with the emission experiment, the signal from the R446 is terminated through a 50 Ω resistor to the LeCroy scope. The entire experiment is synchronized by using a timing circuit of local design. The data, consisting of a 30-shot average of both the signal and the baseline at a repetition rate of 1 Hz, is transferred to a computer for analysis with programs of local origin.

Materials and Methods

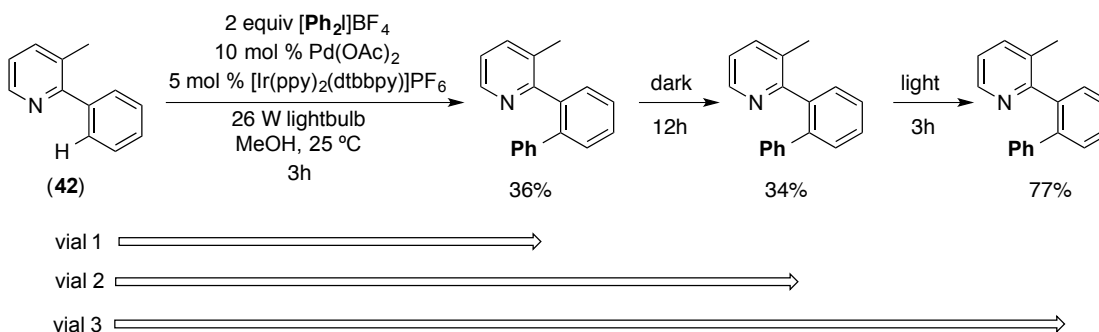
Substrate **42** was prepared according to the literature procedure.¹² Aryl diazonium tetrafluoroborate salts were prepared according to a literature procedure.¹³ Pd(OAc)₂ was obtained from Pressure Chemical and used as received. [Ir(ppy)₂(dtbbpy)]PF₆ was synthesized in a two-step procedure, first forming the dimer [Ir(ppy)₂Cl]₂¹⁴ and then the final catalyst.¹⁵ MeOH was dried over sodium and distilled under N₂ prior to use. Flash chromatography was performed on EM Science silica gel 60 (0.040–0.063 mm particle size, 230–400 mesh) and thin layer chromatography was performed on Merck TLC plates pre-coated with silica gel 60 F₂₅₄.

Experimental Details

Synthesis of Products in Table 4.1 through Table 4.4

The data in section 4.2 and the first part of section 4.3 was collected by Dr. Sharon Neufeldt and is reported in her graduate dissertation.¹⁶

Radical Chain Mechanism Experiment



Three reactions were set up identically in three separate vials. Each vial was run under the light and dark scheme according to the scheme above to obtain. The vials were equipped with a stir bar and 2 mg of Pd(OAc)₂ (10 mol %) was added via 200 μL of a 0.4 M stock solution in CH₂Cl₂. The CH₂Cl₂ was allowed to evaporate by stirring open to the air until dry. The vial was pumped into the glovebox for further reaction setup. [Ph₂I]BF₄ (2 equiv) was weighed into a vial along with 4.2 mg of [Ir(ppy)₂(dtbbpy)]PF₆ (5 mol %) and 0.45 mL of MeOH (0.05 M). Finally, **42** (13.4 mg, 0.089 mmol, 1 equiv) was added neat outside of the glovebox through a septum screw cap top via a 25 μL syringe. The reactions were placed in front of two 26 W fluorescent compact light bulbs in a 30 °C water bath for the appropriate amount of time. The reactions were quenched by freezing in a liquid N₂ bath followed by addition of a saturated aqueous solution of K₂CO₃ (2 mL). The resulting mixture was warmed slowly to room temperature and transferred to a 20 mL vial for work up with the addition of EtOAc (6 mL) and H₂O (3 mL). Neopentylbenzene (15.4 μL) was added as a standard via a 25 μL syringe and the vial was shaken vigorously. A sample of the organic layer was collected and the reaction was analyzed by gas chromatography. The yield of product for each vial was determined versus neopentylbenzene as the internal standard.

Kinetic Experiments

Methods

Kinetics experiments were run in 4 mL vials sealed with Teflon-lined caps. Each data point within a kinetics experiment represents an average of at least two experiments, with each vial containing a constant concentration of oxidant, catalyst, and substrate. For the Hammett competition studies, reactions were run to between 14-16% yield from the sum of the two products. For the KIE experiments, reactions were run to between 1-10% conversion.

General Procedure

For each experiment, vials were equipped with a stir bar and 2 mg of Pd(OAc)₂ (10 mol %) was added via 200 μL of a 0.4 M stock solution in CH₂Cl₂. The CH₂Cl₂ was allowed to evaporate by stirring open to the air until dry. The vial was pumped into the glovebox for further reaction setup. The arylating reagent [Ar₂I]BF₄ (2 equiv) was weighed into a vial along with 4.2 mg of [Ir(ppy)₂(dtbbpy)]PF₆ (5 mol %) and 0.45 mL of MeOH (0.05 M). Finally, the substrate (1 equiv) was added neat outside of the glovebox through a septum screw cap top via a 25 μL syringe. The reactions were placed in front of two 26 W fluorescent compact light bulbs in a 30 °C water bath for the appropriate amount of time. The reactions were quenched by freezing in a liquid N₂ bath followed by addition of a saturated aqueous solution of K₂CO₃ (2 mL). The resulting mixture was warmed slowly to room temperature and transferred to a 20 mL vial for work up with the addition of EtOAc (6 mL) and H₂O (3 mL). Neopentylbenzene (15.4 μL) was added as a standard via a 25 μL syringe and the vial was shaken vigorously. A sample of the organic layer was collected and the reaction was analyzed by gas chromatography. The yield of product for each time point was determined versus neopentylbenzene as the internal standard.

Competition Hammett Plot

As outlined in the general procedure, substrate **42** (13.4 mg, 0.089 mmol, 1 equiv), [Ph₂I]BF₄ (65.5 mg, 0.178 mmol, 2.0 equiv), [Ar₂I]BF₄ (0.178 mmol, 2.0 equiv), Pd(OAc)₂ (2.0 mg, 0.0089 mmol, 10 mol %), and [Ir(ppy)₂(dtbbpy)]PF₆ (4.2 mg, 0.0045 mmol, 5 mol %) were combined in MeOH (0.45 mL) in a 4 mL vial equipped with a small magnetic stir bar. The vials were placed in front of two 26 W fluorescent compact light bulbs in a 30 °C water bath for the length of time needed to reach 14-17% yield from the sum of the two products (see table below). The reaction was quenched, and standard added, as outlined in the General Procedure and analyzed by gas chromatography to give a calibrated yield of each product. The value for P_X/P_H was determined by % yield Ar divided by % yield Ph and plotted against σ₊.

entry	oxidant X ([<i>p</i> -XC ₆ H ₄) ₂ I]BF ₄)	time (min)	yield (%)	
			X	H
1	MeO	60	3	13
2	^t Bu	70	4	11
3	Me	40	9.5	7.5
4	F	50	9	7
5	Cl	70	9	5.5
6	Br	50	10	5
7	I	70	13	2
8	CN	60	11	2.5
9	CF ₃	30	12.5	1.5

Intramolecular Kinetic Isotope Effect

The intramolecular kinetic isotope effect was obtained using substrate **43**, which was synthesized via a three step sequence involving: (i) Suzuki-Miyaura coupling of 2-bromo-3-methylpyridine with C₆D₅B(OH)₂,¹⁷ (ii) palladium-catalyzed ligand directed bromination,¹⁸ and (iii) lithium/halogen exchange with n-BuLi, followed by a quench with deionized H₂O. Substrate **43** was measured to be 99% pure as synthesized. As outlined in the general procedure, substrate **43** (13.8 mg, 0.089 mmol, 1 equiv), [Ph₂I]BF₄ (65.5 mg, 0.178 mmol, 2.0 equiv), Pd(OAc)₂ (2.0 mg, 0.0089 mmol, 10 mol %), and [Ir(ppy)₂(dtbbpy)]PF₆ (4.2 mg, 0.0045 mmol, 5 mol %) were combined in MeOH (0.45 mL) in a 4 mL vial and equipped with a small magnetic stir bar. The vials were placed in front of two 26 W fluorescent compact light bulbs in a 30 °C water bath for 16 h. The reaction was quenched, and standard added, as outlined in the general procedure and then concentrated under vacuum. The resulting crude oil was purified by chromatography on silica gel (R_f = 0.1 in 90% hexanes/10% diethyl ether). The isotope effect was determined using electrospray ionization mass spectrometry (ESI-MS). The percentages of products labeled with three (P_D) and four (P_H) deuterium atoms were determined to be 13.8% and 84.7%, respectively. A ratio of the two provided the P_H/P_D of 6.1.

Intermolecular Kinetic Isotope Effect

The intermolecular kinetic isotope effect was determined by studying the initial rate of reactions with 3-methyl-2-(*d*5-phenyl)pyridine (**44**) and 3-methyl-2-(H5-phenyl)pyridine (**42**) (section 4.4.2). The general procedure was used with [Ph₂I]BF₄ (65.5 mg, 0.178 mmol, 2.0 equiv), 3-methyl-2-(*d*5-phenyl)pyridine (13.8 mg, 0.089 mmol, 1 equiv) or 3-

methyl-2-(H5-phenyl)pyridine (13.4 mg, 0.089 mmol, 1 equiv), Pd(OAc)₂ (2.0 mg, 0.0089 mmol, 10 mol %), and [Ir(ppy)₂(dtbbpy)]PF₆ (4.2 mg, 0.0045 mmol, 5 mol %) were combined in MeOH (0.45 mL). The reactions were placed in front of two 26 W fluorescent compact light bulbs in a 30 °C water bath. The k_H/k_D was determined to be 1.6 (initial rate for **42** = 22 x 10⁻⁵ M/min; initial rate for **44** = 14 x 10⁻⁵ M/min).

Stern-Volmer Quenching Experiments

Procedure for Time-Resolved Emission of [Ir] with [Ph₂I]BF₄

Stock solutions and sample preparation was conducted in the glovebox. A stock solution (solution A) of about 30 mL was prepared of 0.075M tetrabutylammonium hexafluorophosphate (TBAPF₆), which was used as a supporting electrolyte, in dry, degases MeOH. [Ir(ppy)₂(dtbbpy)]PF₆ was added to the solution until an absorbance between 0.1–0.2 AU at 425 nm was obtained. A second solution (solution B) of 25 mL was prepared of 0.4M [Ph₂I]BF₄ (367.9 mg, 1.0 mmol) in dry, degases MeOH. From these two stock solutions five samples were prepared based on the table below. For example, Q1 was prepared by adding 500 μL of solution B to a 5 mL volumetric flask and filling the rest of the volume with solution A. This 5 mL solution was used to fill airtight cells.

sample	amount from solution B	mmol [Ph ₂ I]BF ₄	concentration of [Ph ₂ I]BF ₄ in cell
Q1	500 μL	0.02	0.004M
Q2	750 μL	0.03	0.006M
Q3	1000 μL	0.04	0.008M
Q4	1500 μL	0.06	0.012M
Q5	2000 μL	0.08	0.016M

Procedure for Time-Resolved Emission of [Ir] with [Ar₂I]BF₄

The procedure for the TRE with various diaryliodonium salts is analogous to the procedure with [Ph₂I]BF₄ shown above. The following are the amounts of each [Ar₂I]BF₄ used: [(*p*-MeOC₆H₄)₂I]BF₄ (428.0 mg, 1.0 mmol), [(*p*-ClC₆H₄)₂I]BF₄ (436.8 mg, 1.0 mmol), and [(*p*-CF₃C₆H₄)₂I]BF₄ (503.9 mg, 1.0 mmol). Otherwise the procedure is the same.

Procedure for Time-Resolved Emission of [Ir] with Pd(OAc)₂ and Pd-dimer 45

The procedure for the TRE with Pd(OAc)₂ and Pd-dimer **45** is similar to the procedure with [Ph₂I]BF₄ shown above. However, only one sample of each potential quencher was prepared and tested. Approximately a 1:100 [Ir(ppy)₂(dtbbpy)]PF₆ to quencher ratio used.

Procedure for Transient Absorption of [Ir] with [Ph₂I]BF₄

In the glovebox, one sample was prepared for TA with TBAPF₆ (290 mg, 0.749 mmol), [Ph₂I]BF₄ (59.0 mg, 0.160 mmol) in MeOH (10 mL). [Ir(ppy)₂(dtbbpy)]PF₆ was added to the solution until an absorbance between 0.4–0.6 AU at 425 nm was obtained. This solution was used to fill an airtight cell.

4.8 References

- ¹ (a) Yoon, T. P.; Ischay, M. A.; Du, J. *Nature Chem.* **2010**, *2*, 527. (b) Narayanam, J. M. R.; Stephenson, C. R. J. *Chem. Soc. Rev.* **2011**, *40*, 102. (c) Tucker, J. W.; Stephenson, C. R. J. *J. Org. Chem.* **2012**, *77*, 1617. (d) Prier, C. K.; Rankic, D. A.; MacMillan, D. W. C. *Chem. Rev.* **2013**, *113*, 5322.
- ² Prier, C. K.; Rankic, D. A.; MacMillan, D. W. C. *Chem. Rev.* **2013**, *113*, 5322.
- ³ Neufeldt, S. R.; Sanford, M. S. *Adv. Synth. Catal.* **2012**, *354*, 3517.
- ⁴ Deprez, N. R.; Sanford, M. S. *J. Am. Chem. Soc.* **2009**, *131*, 11234.
- ⁵ Juris, A.; Balzani, V.; Barigelletti, F.; Campagna, S.; Belser, P.; Von Zelewsky, A. *Coord. Chem. Rev.* **1988**, *84*, 85.
- ⁶ (a) Igarashi, T.; Konishi, K.; Aida, T. *Chem. Lett.* **1998**, 1039. (b) Nguyen, J. D.; Tucker, J. W.; Konieczynska, M. D.; Stephenson, C. R. J. *J. Am. Chem. Soc.* **2011**, *133*, 4160.
- ⁷ Heinrich, M. R. *Chem. Eur. J.* **2009**, *15*, 820.
- ⁸ (a) Cai, G.; Fu, Y.; Li, Y.; Wan, X.; Shi, Z. *J. Am. Chem. Soc.* **2007**, *129*, 7666. (b) Shi, Z.; Li, B.; Wan, X.; Cheng, J.; Fang, Z.; Cao, B.; Qin, C.; Wang, Y. *Angew. Chem., Int. Ed.* **2007**, *46*, 5554. (c) Chiong, H. A.; Pham, Q.-N.; Daugulis, O. *J. Am. Chem. Soc.* **2007**, *129*, 9879-9884. (d) Li, J.-J.; Giri, R.; Yu, J.-Q. *Tetrahedron* **2008**, *64*, 6979. (e) Kirchberg, S.; Vogler, T.; Studer, A. *Synlett* **2008**, 2841.
- ⁹ Arnaut, L.; Formosinho, S.; Burrows, H. *Chemical Kinetics: From Molecular Structure to Chemical Reactivity*. Elsevier, Amsterdam **2007**.
- ¹⁰ McCusker, C. E. *Doctoral Thesis at the Michigan State University* **2010**.
- ¹¹ Maestri, G.; Malacria, M.; Derat, E. *Chem. Commun.* **2013**, *49*, 10424.
- ¹² Stowers K. J.; Sanford, M. S. *Org. Lett.* **2009**, *11*, 4584.
- ¹³ Hanson, P.; Jones, J. R.; Taylor, A. B.; Walton, P. H.; Timms, A. W. *J. Chem. Soc., Perkin Trans. 2* **2002**, 1135.
- ¹⁴ Sprouse, S.; King, K. A.; Spellane, P. J.; Watts, R. J. *J. Am. Chem. Soc.* **1984**, *106*, 6647.
- ¹⁵ Lowry, M. S.; Hudson, W. R.; Pascal Jr., R. A.; Bernhard, S. *J. Am. Chem. Soc.* **2004**, *126*, 14129.
- ¹⁶ Neufeldt, S. R. *Doctoral Thesis at the University of Michigan* **2013**.

¹⁷ Littke, A. F.; Dai, C.; Fu, G. C. *J. Am. Chem. Soc.* **2000**, *122*, 4020.

¹⁸ Kalyani, D.; Dick, A. R.; Anani, W. Q.; Sanford, M. S. *Tetrahedron* **2006**, *62*, 11483.